HOKKAIDO UNIVERSITY

| | |
|---|---|
| Title | Analysis of four giant inhibitory neurons projecting to the input sites of mushroom body in the cockroach brain |
| Author(s) | 髙橋, 直美 |
| Degree Grantor | 北海道大学 |
| Degree Name | 博士(生命科学) |
| Dissertation Number | 甲第13168号 |
| Issue Date | 2018-03-22 |
| DOI | https://doi.org/10.14943/doctoral.k13168 |
| Doc URL | https://hdl.handle.net/2115/75541 |
| Type | doctoral thesis |
| File Information | Naomi_Takahashi.pdf |

Hokkaido University Collection of Scholarly and Academic Papers : HUSCAP

博士学位論文

# Analysis of four giant inhibitory neurons projecting to the input sites of mushroom body in the cockroach brain

（ゴキブリ高次嗅覚中枢に入力する巨大抑制性ニューロンに関する研究）

髙橋直美

北海道大学大学院生命科学院

２０１８年３月

# Contents

**Abbreviations**.....3

**General introduction**.....4

**Chapter 1:**

Identification of four giant interneurons supplying mushroom body calyces in the cockroach brain .....7

**Chapter 2:**

Investigation of the mushroom body feedback circuit formed by calycal giants in the cockroach brain .....58

**General discussion**.....90

**Acknowledgements**.....94

**Literature cited**.....95

## Abbreviations

CG: calycal giant interneuron

EPSP: excitatory postsynaptic potential

GABA: gamma-aminobutyric acid

JON: junction output neuron

KC: Kenyon cell

IPSP: inhibitory postsynaptic potential

lALT: lateral antennal lobe tract

LH: lateral horn

mALT: medial antennal lobe tract

MB: mushroom body

MBON: mushroom body output neuron

ML: medial lobe

MLON: medial lobe output neuron

NS: nonspiking

PN: projection neuron

VL: vertical lobe

VLON: vertical lobe output neuron

## General introduction

Olfactory system of terrestrial animals must deal with not only a large ensemble of odors but also complex spatio-temporal distribution patterns of odor, because an odor plume, spreading into the air, is broken up into concentrated filaments separated by pockets of very low odor concentration (Huston et al., 2015). Although how olfactory system accomplishes those highly complex tasks has been unknown, terrestrial animals such as mammals and insects have evolved similar nervous systems at the circuitry level (Hildebrand and Shepherd, 1997; Kay and Stopfer, 2006), perhaps to perform sophisticated olfactory processing with a limited number of neurons. A remarkable example of convergent evolution is spherical neuropils called "glomeruli" seen in the first-order olfactory center, the olfactory bulb in mammals and the antennal lobe in insects. In insects, each glomerulus offers a site where incoming axons of olfactory sensory neurons expressing cognate receptors converge upon dendrites of projection neurons (PNs; functional homolog of mammalian mitral/tufted cells) that relay information to the protocerebrum. These glomeruli are laterally interconnected by excitatory circuits (Shang et al., 2007; Olsen et al., 2007; Huang et al., 2010) and inhibitory circuits (e.g., Wilson and Mainen, 2006) formed by local interneurons, equivalent to granule cells in mammals (Hildebrand and Shepherd, 1997; Kay and Stopfer, 2006). Odor-driven circuit interactions mediated by local interneurons coordinate PNs into widespread oscillatory synchrony and transform representations of any odor into specific and temporally complex patterns of action potentials. PNs are, therefore, generally more broadly tuned to odors than are olfactory sensory neurons (Wilson et al. 2004; Wilson and Laurent, 2005; Olsen and Wilson, 2008).

Growing evidence now suggests that the circuitry similarity is extended to higher-order centers. In both the mammalian piriform cortex (olfactory cortex) and insect mushroom bodies (MBs), odor representation is sparse (Perez-Orive et al., 2002; Szyszka et al., 2005; Ito et al., 2008; Poo and Isaacson, 2009; Lin et al., 2014). In MBs, several hundred PNs synapse onto 2500 intrinsic neurons (Kenyon cells, KCs) in fruit flies (Balling et al., 1987) and approximately 170,000 intrinsic neurons in honey bees (Witthöft, 1967). Despite apparent divergence from PNs to KCs, their synaptic connections are generally convergent: multiple PNs make synaptic connections with single KCs (Jortner et al., 2007; Turner et al.,

2008). KCs act as coincidence detectors to summate subthreshold, synchronized synaptic input (Perez-Orive et al., 2002, 2004). The sparse odor representation in KCs results from intrinsic membrane properties that show a high input threshold (Turner et al., 2008; Denmar and Kloppenburg, 2009; Froese et al., 2014). This situation is similar to that in the rat olfactory cortex in which odors evoke spiking activity that is sparse across the cortical population (Poo and Isaacson, 2009).

Sparse codes enable neural representation with a high degree of specificity, conversely expanding memory capacity (Olshausen and Field, 2004). Therefore, the higher order olfactory center is equipped with neural mechanisms to maintain its sparse activities in addition to intrinsic membrane properties of neurons. One example is widespread and broadly tuned inhibition. In the MB of insect brain, large MB extrinsic neurons are responsible for that inhibition (Papadopoulou et al., 2011; Lin et al., 2014). In the locust *Schistocerca americana,* for example, a single giant gamma-aminobutyric acid (GABA)-ergic nonspiking neuron (GGN) interconnects between MB output sites (lobes) and input sites (calyces), and provides powerful feedback inhibition to KCs (Papadopoulou et al., 2011; Gupta and Stopfer, 2014); this inhibition prevents lengthy temporal integration to help KCs to detect coincident spikes from the PN population (Assisi et al., 2007; Kee et al., 2015). The functional analogue of this MB feedback neuron identified in the fruit fly (anterior paired lateral neuron: APL, Tanaka et al., 2008) exhibits decreased activity to trained odor but not to control odor, thereby facilitating formation of "memory trace" in the MB (Liu and Davis, 2009; Pitman et al., 2011; Wu et al., 2012). In insects with larger and more complex MBs (Farris, 2005), there are multiple feedback neurons per hemisphere: *ca.* 60 neurons in honey bee (Grünewald, 1999b; Haehnel and Menzel, 2010; Boitard et al., 2015) and *ca.* 150 neurons in tobacco hawk moth (Bicker et al., 1985; Homberg et al., 1987). Roles of those multiple feedback neurons appear not confined to the functions described above. However, detailed study on functional segregation of individual feedback neurons has not been performed.

The American cockroach *Periplaneta americana,* with well-developed MB comparable to those of social hymenoptera (Farris, 2005), has four giant GABA-immunoreactive neurons in the hemibrain. Those neurons, termed "calycal giants (CGs)," are among the largest neurons in the cockroach brain (Weiss, 1974; Yamazaki et al., 1998). Because CGs widely innervate the MB calyces,

they were assumed to provide inhibitory feedback onto MB calyces (Nishino and Mizunami, 1998; Strausfeld and Li, 1999a). Consistent with extensive innervation of CGs to the entire MB calyces, both $GABA_A$ and $GABA_B$ receptors expressed intensely in the entire MB calyces of *P. americana* (Sattelle et al., 2000; Blankenburg et al., 2015).

CGs have been classified into at least two subtypes according to their termination areas in the calyces (Strausfeld and Li, 1999a; Nishino et al., 2012). Interestingly, these two distinct termination areas well correspond to those of two distinct population of uniglomerular PNs, type 1 and type 2 PNs (Strausfeld and Li, 1999a; Nishino et al., 2012). Recently, Watanabe et al. (2017) proposed that type 1 and type 2 PNs of *P. americana* code different odor aspects: the former codes odor identity and the latter codes spatio-temporal odor distribution and concentration. Thus, clarifying the functional segregation among four CGs in the cockroach brain will lead to understand how different kinds of olfactory inputs are processed in the MB, providing valuable insights in the neural mechanisms of the olfactory system. Unfortunately, the lack of information on morphology and identity of individual CGs has interfered with in-depth analysis. Further, CGs, different from MB feedback neurons in other insects, do not have dendrites in the lobes of the MB. Rather, it has been speculated that CGs receive signals from MB extrinsic (output) neurons, which have dendrites in the lobes of MB, but no studies have been performed to confirm it.

The purpose of this study is to clarify detailed features of putative MB feedback circuits in the cockroach brain in terms of morphological and physiological properties of individual CGs to establish the foundation of further analysis on functional segregation of each feedback circuit. In Chapter 1, I first unambiguously identified four CGs based on their morphologies and physiologies by intracellular recording and staining of individual CGs. In addition, differential staining of a CG and a MB extrinsic (output) neuron showed potent synaptic connection between them. In Chapter 2, I investigated synaptic connections between CGs and MB extrinsic (output) neurons by paired intracellular recording of these neurons. The results of this study demonstrated parallel feedback circuits of the MB corresponding well to parallel olfactory inputs from two populations of PNs, which is important first step to further clarify parallel odor processing in the MB.

# Chapter 1: Identification of four giant interneurons supplying mushroom body calyces in the cockroach brain.

## Introduction

The American cockroach *Periplaneta americana* has been traditionally favored for investigation of olfactory processing (Boeckh and Ernst, 1987). The cockroach retains simplicity of the nervous system as an evolutionally basal neopteran but exhibits excellent odor discrimination (Sakura et al., 2002) and associative learning (Watanabe and Mizunami, 2007) due to heavy reliance on olfaction to search for resources. In fact, the cockroach is equipped with a pair of well-developed mushroom bodies (MBs) comparable to social insects (Fig. 1A; Farris, 2005), and the principal input to the MB is olfactory (Strausfeld and Li, 1999a; Nishino et al., 2012), although there is evidence that the MB also participates in multisensory processing (Li and Strausfeld, 1997; Mizunami et al., 1998c, 1998d; Okada et al., 1999).

The overall olfactory circuits of cockroaches resemble those of other insects (Fig. 1A,B; Galizia and Rössler, 2010; Martin et al., 2011). Olfactory signals are processed in 205 readily identifiable glomeruli in the antennal lobe (Watanabe et al., 2010). Usually one uniglomerular projection neuron (PN) exits from a single sexually isomorphic glomerulus, relaying olfactory signals ipsilaterally to the concentric MB calyces and the lateral horn (LH) in the protocerebrum (Ernst and Boeckh, 1983; Malun et al., 1993). Each MB of *P. americana* contains about 175,000 Kenyon cells (KCs; Neder, 1959), the dendrites of which receive direct input from PNs, and axons bifurcate into the vertical lobe (VL) and the medial lobe (ML; Mizunami et al., 1998b; Strausfeld and Li, 1999b). More than one hundred MB extrinsic neurons with dendrites in particular regions of the lobes project primarily to neuropils surrounding the LH in the lateral protocerebrum, which are thought to participate in the formation of innately meaningful signals for behavioral control (Li and Strausfeld, 1997, 1999).

Putative feedback neurons, calycal giants (CGs) are assumed to receive signal inputs from those MB extrinsic neurons and provide feedback inhibition to KCs in the MB calyces. In this chapter, with the use of single/multiple intracellular recordings and stainings from different combinations of CGs, I succeeded in unambiguous identification of the four CGs. All CGs supply axon terminals to the MB calyces and usually exhibited robust and dynamic responses to every odor tested, which provide basis to discuss functional roles of feedback inhibition in olfactory processing.

## Materials and methods

### Animals

Adult male cockroaches (*Periplaneta americana*) raised in the laboratory colony under a 12 h-12 h (light-dark) cycle at 27 ºC were used. Physiological recordings were performed in the subjective night (during the 12-hour dark cycle). More than 370 cockroaches were used for the experiments. Morphological and physiological data are based on results from 70 type 1 CGs, 22 nonspiking CGs, 17 type 2a CGs and 11 type 2b CGs which are successfully recorded and stained, though data for a much smaller number of neurons were used in figures.

### Intracellular recordings and sensory stimuli

The procedures for dissection of animals, intracellular recordings, and odor stimulation were almost the same as those described by Nishino et al. (2003). Briefly, a glass microelectrode was filled with either 8% Lucifer Yellow (LY, Sigma-Aldrich, St. Louis, MO) dissolved in 1 M LiCl or 2% Alexa Fluor 568 hydrazide dissolved in 400 mM KCl. Unless otherwise stated, the electrode was inserted into the junction of the MB calyces in the right hemisphere of the brain to record from individual axons of CGs. Odor stimuli were delivered through a glass wind tunnel (ID: 2 cm) covering the right antenna. I used four categories of odors: 1) organic alcohol: 1-hexanol (Wako, Osaka, Japan), 2) fatty alcohol: 1-octanol (Wako), 3) fatty acid: n-caproic acid (Sigma-Aldrich), and 4) food odors: orange essence (John Wagner and Sons, Ivyland, PA) and green apple essence (Mikoya Kosyo, Tokyo, Japan). An air current (0.125 l/min) was passed through a cartridge containing a filter paper (5 × 40 mm) soaked with 5 µl of n-caproic acid or 20 µl of other odorant solutions. The flow speed in the wind tunnel was adjusted to be 20 cm/s. The residual air in the recording cage was continuously removed with a vacuum. Due to the distance of the wind tunnel and the odor-containing cartridge, there was a delay between the onset of odor stimulation monitored by the solenoid valve and time the odor reached the antenna. The latency and the rise-time of odor (apple) delivery after the opening of the valve was measured by a photo-ionization detector (Model 200B, Aurora Scientific Inc., ON, Canada) in the center of the wind tunnel, at which the antenna is situated. The latency that the odor reached the antenna was approximately 85 ms

(the half value of the peak concentration) and the time that the odor concentration reached the peak was 158 ms from the onset of valve opening.

A visual stimulus was applied by illuminating the compound eyes with a light guide. Tactile stimuli to the ipsilateral antenna were applied with a wooden needle. Timing of tactile and light stimuli was monitored by narration into a microphone connected to the DAT recorder.

### Morphological observation of recorded neurons

Immediately after physiological recordings, a constant hyperpolarizing current (–1 to –5 nA) was applied for 5–60 minutes to stain neurons. The decapitated head was incubated in a humidified chamber at 5 ºC for 5–10 h to let dye diffuse throughout the neurons. In some specimens in which a CG had been labeled with LY, micro-Ruby (dextran, tetramethylrhodamine, and biotin, 3000 MW, ThermoFisher Scientific, MA) was injected into the antennal lobe or VL to label PNs and KCs/CGs, respectively. The head was incubated in a humidified chamber at 5 ºC for 12-16 h to facilitate dye diffusion. The brain was dissected out and fixed in 4% formaldehyde in phosphate buffer (pH = 7.4) at 4 ºC for 6–12 h, dehydrated in an ascending ethanol series (from 50% to 100%), and cleared in methyl salicylate.

The cleared brain was observed under a confocal laser scanning microscope (LSM 5 Pascal; Carl Zeiss, Jena, Germany) equipped with argon and helium-neon lasers. Single neurons labeled with LY were visualized with an argon laser (458 nm), whereas those labeled with Alexa Fluor 568 were visualized with a helium-neon laser (543 nm). Specimens in which neurons were differentially labeled with LY and Alexa Fluor 568 (or micro-Ruby) were visualized with an argon laser with a 505–530-nm bandpass filter and a helium-neon laser with a longpass filter (>560 nm), respectively. Images were obtained using three objective lenses: Plan-Apochromat 10×/0.75 and Plan-Apochromat 20×/0.8 for low-magnification images and oil-immersion Plan-Neofluar 40×/1.3 for high-magnification images. The thicknesses of optical sections were 5–11-μm intervals for low-magnification images and 1.0–1.2 for high-magnification images. The resolution of optical sections was at 1024 × 1024 pixels. Optical sections were reconstructed two-dimensionally using image-processing software incorporated in the

confocal microscope (LSM Image Browser; Carl Zeiss). Reconstructed images were processed in Photoshop CS3 (Adobe Systems, San Jose, CA) to adjust their brightness and contrast.

For three-dimensional reconstruction, optical sections were converted to TIFF-formatted files using the LSM Image Browser (Carl Zeiss). TIFF images were processed with image processing software (Amira ver. 3.1, Visage imaging, Berlin, Germany). Surface rendering of MB neuropils was achieved by outlining each optical section manually. Volume rendering was applied for 3D reconstruction of neuronal branches.

### Antibody characterization

To label putative GABAergic neurons in the brain of *P. americana*, I used a commercially available polyclonal antibody (Table 1, A2052, Sigma) that was raised against a GABA-bovine serum albumin conjugate in rabbits. The resulting staining pattern was identical to that obtained in previous immunocytochemical studies in the protocerebrum (Yamazaki et al., 1998) and in the antennal lobe of *P. americana* (Distler, 1990; Fusca et al., 2013). According to the manufacturer's data sheet, the antibody showed positive binding with GABA and GABA-KLH in a dot blot assay, and negative binding with BSA. To check the specificity of the GABA antibody, I double-checked control experiments made by Fusca et al. (2013). First, the antibody was preincubated with several doses of GABA (A5835; Sigma), and dose-dependent elimination of the antibody was observed. The GABA immunoreactivity was abolished when the antibody was preincubated with 50 mM GABA. There were no signals when the primary antibody was omitted.

For synapsin immunohistochemistry, I used a commercially available monoclonal antibody directed against *Drosophila* synapsin I isoform (SYNORF1, Table 1, 3C11, DSHB, Iowa). The antibody was generated against a fusion protein consisting of glutathione-S-transferase and synapsin protein in the mouse. Its cross-reactivity with synapsin in *P. americana* has been identified by Western blots of the cockroach brains and salivary glands (Baumann et al., 2004). It has been shown that the anti-synapsin detects a broad band of proteins of ≈ 80 kDa in cockroach brain homogenates, which corresponds to 70, 74, and 80 kDa of *D. melanogaster* synapsin isoforms and suggests that an orthologous synapsin protein

is expressed in the cockroach. Baumann et al. (2004) also revealed that anti-synapsin immunoreactivity was highly concentrated at presynaptic sites, varicosities, in *P. americana*. In the cockroach brain, the staining patterns in this study were identical to those obtained in previous immunohistochemical studies using the same anti-synapsin antibody (Wei et al., 2010; Groh and Rössler, 2011). There were no signals when the anti-synapsin antibody was omitted.

### Immunohistochemical stainings

Immediately after a brief morphological check of intracellularly stained CGs, the brain was rehydrated in a descending ethanol series (from 100% to 50%) and then kept in phosphate-buffered saline (PBS: 0.14 M NaCl in 0.01 M sodium phosphate buffer, pH 7.4). Immunohistochemistry was modified from that performed in a previous study using *P. americana* (Watanabe et al., 2014). After washing the brain in PBS, each specimen was embedded in 7.5% aqueous solution of agarose. Each brain was cut into 80-µm-thick slices with a vibrating blade microtome (Linearslicer PRO 7; DSK, Kyoto, Japan). Sections were then washed with PBS containing 1% Triton X-100 (X100RS, Sigma; PBST) and blocked for 1 hour using 2% normal goat serum (S26, Chemicon, Temecula, CA) in PBST with 0.25% bovine serum albumin (PBST-BSA). The sections were then incubated with a mixture of anti-synapsin monoclonal antibody generated in a mouse (Table 1, 3C11, DSHB; diluted 1:50 in PBST-BSA) and anti-GABA polyclonal antibody generated in a rabbit (Table 1, A2052, Sigma; diluted 1:1000 in PBST-BSA) at 4 ˚C for 4 days. On the following day, the sections were washed again in PBST-BSA and then incubated with a mixture of Alexa Fluor 555-labeled secondary anti-mouse IgG antibody (A21422, ThermoFisher Scientific; diluted 1:1000 in PBST-BSA) and Alexa Fluor 647-labeled secondary anti-rabbit IgG antibody generated in a goat (A21245, Invitrogen; diluted 1:1000 in PBST-BSA) at 4 ˚C for 4 days. Then the sections were finally washed in PBST-BSA, and cleared in a mounting medium (Vectashield, VECTOR, Burlingame, CA).

To identify the distribution patterns of GABAergic neurons in the lateral protocerebrum (Fig. 2), immunohistochemistry was performed using the wholemount brain after PNs had been stained by micro-Ruby injection into the AL. To facilitate antibody penetration, the brains were treated with

collagenase/dispase (10269638001, Roche; diluted 1 mg/ml in 0.05M Tris buffer) at 40 ˚C for 10 min. The brains were then washed and blocked by the standard protocol described above and incubated with a rabbit anti-GABA antibody (1:1000) in PBS with 5% Triton X-100 containing 2% normal goat serum at 4 ˚C for 7 days. On the following day, the brains were washed again in PBST-BSA and then incubated with an Alexa Fluor 488-labeled secondary anti-rabbit IgG antibody generated in a goat (A11034, ThermoFisher Scientific; diluted 1:1000 in PBS with 5% Triton X-100) at 4 ˚C for 7 days. Then the brains were finally washed in PBST-BSA, dehydrated in an ascending ethanol series (from 50% to 100%), and cleared in methyl salicylate.

The cleared specimens were observed with a confocal laser scanning microscope (LSM-510; Carl Zeiss) equipped with argon and helium-neon lasers. Neurons labeled by Lucifer yellow or Alexa Fluor 488 secondary antibody were visualized using an argon laser (458 nm) with a band-pass emission filter (505-550 nm), whereas neurons labeled by Alexa Fluor 647 secondary antibody were visualized by a helium-neon laser (633 nm) with a long-pass emission filter (>650 nm). In addition, neuropils labeled by Alexa Fluor 555 secondary antibody were visualized by a different helium-neon laser (543 nm) with a band-pass emission filter (560-615 nm). Images were obtained using three different objective lenses: a Plan-Apochromat 20×/0.8 for low-magnification images and oil-immersion Plan-Neofluar 40×/1.3 and Plan-Apochromat 63×/1.4 objectives for high magnification images. Optical sections were captured at 0.5–2.0-µm intervals with a resolution of 1024 ×1024 pixels.

### Analysis of physiological data

Physiological data and odor stimulus timings stored on DAT tapes were digitized at 10 kHz using the CED micro 1401 mkII interface (Cambridge Electronic Design Ltd., Cambridge, UK) and Spike2 ver. 6.0–6.18 software (CED). The digitized data were exported as text format to the free programming software R ver. 2.15.1 (R Foundation for Statistical Computing, Vienna, Austria) and then plotted as PDF format using ggplot2 package ver. 0.9.3.1 in R. The plots were processed in Illustrator CS3 (Adobe Systems) to edit document size, line width, and letterings.

To compare the shape of action potentials between CG types, linear mixed models were

constructed, in which a response variable was (i) peak amplitude of action potential or (ii) falling voltage change (mV/ms) from the peak to the half value of action potential recorded at the junction of MB calyces. CG types and individual differences were used as fixed effect and random effect, respectively. The constructed model was compared to the null model, which ignores fixed effect, by likelihood ratio chi-square test with one degree of freedom. The result was considered to be significant when $P < 0.05$.

### Terminology

I referred to Strausfeld and Li (1999a) for the naming of projection neurons and to Ito et al. (2014) for the naming of neuropils and tracts in the brain. Dendrites and axon terminals were defined on the basis of morphological, physiological, and immunocytochemical criteria. Morphologically, branches that exhibit spiny processes and those that exhibit swollen, varicosity-rich processes were assumed to be dendrites and axon terminals, respectively (Okada et al., 2003). The physiological criterion is based on the shape of action potentials because dendritic spikes exhibit small amplitude (30–40 mv) accompanied by higher excitatory postsynaptic potentials (EPSPs), whereas axonal spikes exhibit higher amplitude (50–60 mv) followed by undershoots (Nishino and Mizunami, 1998). Finally, co-localization of synapsin-immunoreactive vesicles in a CG intracellularly stained was checked to define axon terminals. In this study, defined branches fulfilled all three criteria.

The LH is compartmentalized into three regions: triangular-shaped antero-dorsal (a-d) LH, oval-shaped antero-ventral (a-v) LH and triangular-shaped posterior (p) LH (Nishino et al., 2003). The “calycal neuropil” of the MB is defined as dendritic fields of KCs (Weiss, 1974; Strausfeld and Li, 1999b). The calycal neuropil has been divided into four zones (I–III, IIIA) from the periphery to the base (Strausfeld and Li, 1999a). Since MB extrinsic neurons projecting to the LH have typical spiny processes in lobes and varicose processes in the LH, I term them “mushroom body output neurons (MBON)” to facilitate understanding. Anatomical features of neurons are given with reference to the body axis (Strausfeld and Li, 1999a; Nishino et al., 2012).

# Results

## Distribution of GABA-immunoreactive neurons in the lateral protocerebrum

When I performed intracellular recording and staining of CGs, I used two criteria to identify CGs: (i) wide innervation in the MB calyces and (ii) location and large size of the cell body in the lateral protocerebrum following previous reports (Yamazaki et al., 1998; Strausfeld and Li, 1999a). To confirm the validity of the criteria (ii), I examined the GABA-immunoreactive cell clusters in the neighborhood of four CG cell bodies located in postero-ventral region of the lateral protocerebrum.

GABA-immunoreactive neurons in wholemount preparations revealed five GABA-immunoreactive neuronal clusters in the cell body rind of the anterior to posterior lateral protocerebrum (1–5 encircled by white lines in Fig. 2A–C; number of cell bodies in each cluster is summarized in table 2). Cell cluster 1 is located in the anterior surface of the lateral protocerebrum (Fig. 2A). This cluster contains the large cell body (diameter > 30 µm) of "the type 1 olfactory input neuron" with dendrites in part of the LH and axon terminals in the base of MB calyces (see Fig. 5 in Nishino et al., 2012). Cell cluster 3 is located in the antero-dorsal region of the optic lobe (OL) base, comprising small- and middle-sized neurons (diameter < 30 µm; Fig. 2C). Cell cluster 4 is located in the posterior surface just beneath the lateral calyx, comprising small- and middle-sized neurons (diameter < 30 µm; Fig. 2C). Cell clusters 2 and 5 are located in the antero-ventral region (Fig. 2B) and postero-ventral region of the OL base, respectively (Fig. 2C). The former contains large and middle cell bodies (diameter > 15 µm) of "type 2 olfactory input neurons" with dendrites throughout the LH and axon terminals in the entire MB calyces (see Fig. 6 in Nishino et al., 2012) and the latter contains four conspicuously large cell bodies of CGs (outlined by white lines in Fig. 2C; diameter > 30 µm; Yamazaki et al., 1998; Strausfeld and Li, 1999a). The four CG cell bodies are so large that there are some gaps between them, and the gaps are occupied by smaller GABA-immunoreactive cell bodies (diameter < 30 µm). Since the four large cell bodies of CGs were so far away from other GABA-immunoreactive large cell bodies that I concluded the validity of defining a neuron as CG by its cell body size and location.

GABA-immunolabeling in wholemount preparations further revealed neurites of the four CGs dissociating antero-posteriorly in the base of MB calyces (arrowheads, Fig. 2F) different from tightly

bundled neurites in the a-v LH and a satellite neuropil around the VL (arrowheads, Fig. 2D,E). By pinpointing the recording sites to those dissociating branches instead of the bundle in the lateral protocerebrum, I succeeded in recording and staining of individual CGs.

### Gross morphology of the four CGs

Intracellular staining of individual CGs and subsequent GABA-immunoreactive neuronal staining revealed that the four CGs are indeed GABA-immunoreactive (Figs. 3-6D–F). Moreover, Intracellular staining of individual CGs and subsequent synapsin immunolabeling in wholemount specimens showed that synapsin-immunoreactive vesicles are localized in branches in the MB calyces but not in other areas (Figs. 3-6C), suggesting that the four CGs supply axon terminals almost exclusively to MB calyces.

The trajectories of primary dendrites and axonal branches are conserved among the four CGs (Figs. 3-6A,B,G–J). I concluded that the LH and the satellite neuropil around the VL are the input regions of CGs because the dendritic branches with spiny processes typical of dendrites are mainly arborized in the boundary of the LH (Fig. 7) and in the satellite neuropil around the VL. The dendrites in the LH are branched off from the cell body stalks orienting medio-dorsally while those in the satellite neuropil around the VL from the primary dendritic trunks running antero-medially.

The three axonal branches, the anterior, central, and posterior branches are diverged from the cell body stalk at the fork point (indicated by a red circle, Figs. 3-6A). The axonal branches of individual CGs, ramify at the base of the MB calyces (Fig. 2F) and supply axon terminals to different peripheral-basal regions of the concentric calyces with some spatial overlap (Figs. 3-6A, 8). The anterior branch runs tangentially along calyces and gives rise to several branches that terminate in the peripheral (lip) region of the calyces. The central and posterior branches, bifurcated at the fork point, terminate primarily in the central region (base) and the postero-basal region of the calyces, respectively. The terminal specializations in the calyces are decorated with bead-like, often en route, varicosities (Nishikawa et al., 1998; Strausfeld and Li, 1999a).

## Morphological features of individual CGs

Despite a large overlap of primary neurites, the four CGs had unique morphological and physiological characteristics conserved across individuals. These were therefore assigned to different types as follows, although each type contained only one neuron. Most important differences in innervation patterns in the input and output regions are summarized in Table 3 at the last of this chapter.

***Type 1 CG*** The mean cell body diameter is 43.9 µm (n = 4, Table 3), the largest among the four types of CGs (Fig. 3A,B,D–F). Immediately after leaving the cell body, the medially oriented branches (a, Fig. 7B), unique to the type 1 CG, run postero-medially and supply dense dendritic processes in the ventral to medial boundaries of the triangular-shaped p LH. The ventrally oriented thick branch (b, Fig. 7A) provides dendritic processes profusely along the medial boundary of the a-v LH and p LH, and distal fibers penetrate into the posterior slope (Figs. 3A, 7B). The two laterally oriented branches (c and d, Fig. 7A) arborize along the lateral boundary of the a-v LH. The dorsally oriented branch (e, Fig. 7A,B) arborizes in the a-d LH and the dorsal region of the p LH. The medially oriented thin branch (f, Fig. 7B) arborizes in the medio-dorsal boundary of the p LH. The primary dendritic trunks arborize in the satellite neuropil antero-lateral and medial to the base of the VL (Fig. 3G,H). A small number of fine processes run anteriorly along the antero-lateral surface of the VL (Fig. 9A). Dendritic processes diverging from the primary dendritic trunk loop along the posterior surface of the VL to innervate sparsely the surface of the "lobelet" made by axons of class III KCs (Fig. 9B; Farris and Strausfeld, 2003).

The anterior axonal branch does not innervate the peripheral-most region of the calyces (zone I) but innervates a more basal region (Figs. 3I,J, 8A). Thus, three axonal branches collectively innervate zones II-IIIA, where type 1 uniglomerular PNs provide axon terminals (Fig. 8I–K; Strausfeld and Li, 1999a). Some collaterals diverging from the central axonal branch sparsely innervate the accessory calyx (ACA, Fig. 9C,D) that contains dendrites of class III KCs (Farris and Strausfeld, 2003). The long processes of axon terminals across calycal layers provide numerous collaterals in the outer half layer (Figs. 3I, 8E) but provide only few in the inner half layer, resulting in denser terminal arborizations in the outer half layer (Fig. 3I, 8E). The distal axonal processes also sparsely cover dendritic bundles of

developmentally newer class 1 KCs (Figs 3I, 8E, 9E; Strausfeld and Li, 1999b; Farris and Strausfeld, 2001), also termed KC1 by Mizunami et al. (1998a,b). The terminal specializations contain only thick bead-like processes of 1~2 µm in width (inset, Fig, 8E).

***Nonspiking (NS) CG*** The mean cell body diameter is the second largest, 33.7 µm (n = 3, Table 3). The ventrally oriented dendritic branch is feeble and arborizes only sparsely in the medial boundary of the a-v LH (b, Fig. 7C). The two laterally oriented branches (c and d, Fig. 7C) provide dendritic processes in the lateral boundary of the a-v LH. The dorsally oriented branch (e, Fig. 7C,D) arborizes in the a-d LH and the dorsal region of the p LH. The medially oriented branch (f, Fig. 7D) arborizes sparsely in the medio-dorsal boundary of the p LH. The primary dendritic trunks around the VL are located more dorsally than those of other types of CGs (Fig. 4G,H).

The axonal branches just below the calyces are the thickest among the four types of CGs (14.2 µm in width, n = 3, Table 3), and they provide axon terminals profusely in zone I of the MB calyces (Figs. 4I,J, 8B), where type 2 uniglomerular PNs supply axon terminals (Fig. 8L; Strausfeld and Li, 1999a). Additional terminals sparsely innervate the inner half layer of zones II-IIIA (Fig. 8F), but there are few in the outer half layer of zones II-IIIA (shaded area, Fig. 8F). The axon terminals exhibit fine mesh-like arborizations (Fig. 8B,F), reminiscent of those in a GGN of *S. americana* (Papadopoulou et al., 2011). The axonal specializations comprise two distinct processes: thick, bead-like processes (1~2 µm in width) and thin, tapered (ca. 0.5 µm in width) processes (indicated by arrowheads in inset, Fig. 8F).

***Type 2a CG*** The mean cell body diameter is 30.2 µm (n = 4, Table 3). The ventrally oriented branch (b, in Fig. 7E,F) arborizes in the dorsal boundary of the a-v LH and the ventro-medial region of the p LH. The laterally oriented thin branch (d, Fig. 7E) provides dendritic processes along the lateral boundary of the a-v LH. The dorsally oriented branch (e, Fig. 7E) arborizes in the a-d LH. The medially oriented branch (f, Fig. 7E,F) arborizes in the lateral boundary of the p LH. The primary dendritic trunks arborize in the satellite neuropil anterior and lateral to the VL (Fig. 5G,H).

The axon terminals profusely innervate zone I of the calyces but less densely innervate the inner most layer of zones II-IIIA (Figs. 5I,J, 8C,G). The outer half layer of zones II-IIIA is almost devoid of innervation (shaded area, Fig. 8G). These characteristics are evident in cross sections at the central region of the calyces (Fig. 8G) but are not clear in the three-dimensional reconstruction of whole axonal branches (Fig. 5I,J) due to the profuse terminals covering the most peripheral region of the calyces (the zone I) (Fig. 8C). As in the NS CG, the axon terminals contain both thick and thin processes (indicated by arrowheads in inset, Fig. 8G), but the processes along layers are short and clawed-shaped, resulting in more sparse arbors compared to type 1 and NS CGs (Fig. 8C,G).

***Type 2b CG*** The mean cell body diameter is 31.9 µm (n = 4, Table 3). The dendritic branches (b-f, Fig. 7G,H) run closely to those of the type 2a CG and provide dendritic processes in the boundary of the LH and around the lobes (Figs. 6G,H, 7G,H). Despite similar thicknesses of primary dendritic trunks to those in type 2a, dendritic processes become immediately tapered after diverging from the trunks, resulting in finer arborizations (Figs. 6G,H, 7G,H). This is manifested by one of the thickest dendritic trunks in the anterior surface of the lateral protocerebrum (indicated by black arrows, Fig. 6G,H), which is the hallmark of type 2b CG. The axon terminals in the calyces contain both thick and thin processes (indicated by arrowheads in inset, Fig. 8H) but cover a slightly more basal region in zone I than those of type 2a CG (Figs. 6I,J, 8D,H). The outer half layer of the zones II-IIIA is almost devoid of innervation (shaded area, Fig. 8H).

## Double labeling of CGs and associated interneurons

***Different types of CGs*** Double labeling of CGs in the same individuals and subsequent three-dimensional reconstruction more clearly demonstrated subtle morphological differences of CGs (Fig. 10). In a specimen in which the type 1 CG (magenta) and the NS CG (green) were differentially labeled with Alexa Fluor 568 and LY, respectively (Fig. 10A), the two cell bodies abut from each other (Fig. 10A), although their relative locations in GABA-immunoreactive cell cluster 5 (Fig. 2C) differed between individuals. Dendrites of the type 1 CG arborize broadly in the medial and ventral boundaries

of the p LH, whereas those of the NS CG arborize primarily in the dorso-medial region (Fig. 10B,C). Around the VL, dendrites of the NS CG arborize in a more dorsal region than those of the type 1 CG (Fig. 10F,G). The axon terminals of the type 1 CG clearly occupy a more basal region than do those of the NS CG throughout the calyces (Fig. 10D,H,I). The inner half layer of calyces (zones II-IIIA) is co-innervated by the type 1 CG and NS CG (Fig. 10D,E) but more densely by the NS CG, while the outer half layer is innervated almost exclusively by the type 1 CG (Fig. 10D). Only the NS CG has thin spiny processes in calyces (Fig. 10E).

In a specimen in which type 2a and type 2b were simultaneously stained at different intensities (Fig. 10M), primary neurites were readily discernible using different threshold settings (Fig. 10J-L). Dendritic neurites of type 2a and type 2b CGs with similar thicknesses cover spatially similar regions around the VL (Fig. 10J,K) but occupy slightly different basal-proximal regions of the calycal neuropil (Fig. 10L).

***CG vs MBONs*** MBONs, which receive synaptic inputs from MB intrinsic neurons KCs (Fig. 1B), are one of the candidate neurons making synaptic inputs to CGs because they have axon terminals in the lateral protocerebrum where the dendrites of CGs innervate. In order to estimate potential synaptic connections between axon terminals of MBONs and dendrites of CGs, I performed differential labeling of MBONs with LY and type 1 CG with Alexa Fluor 568 (Fig. 11C–F). When one of the largest MBONs with dendrites in the ML tip (Fig. 11A; see Fig. 1 in Okada et al., 1999) was differentially stained with the type 1 CG (Fig. 11C,D), blebby axon terminals of the medial lobe output neuron (MLON, green) spatially overlapped largely with fine dendritic branches of the type 1 CG (magenta, Fig. 11C,D) suggesting synaptic contacts and supporting the putative MB feedback function of the CG. However, when an MBON with dendrites in the VL tip (Fig. 11B) was differentially stained with the type 1 CG, the extent of overlapping between axon terminals of the vertical output neuron (VLON) and dendrites of the type 1 CG was much less than that between the MLON and type 1 CG (Fig. 11E,F). The results suggest that a specific subset of MBONs makes synaptic connection to a given CG.

***CG vs PNs*** PNs transmitting olfactory information from the AL to the MB calyces (Fig. 1B) are also one of the candidates for the direct input source of CGs because they have axon terminals in the LH as well as the MB calyces. Intracellular labeling of the type 1 CG with LY combined with local injection of micro-Ruby into the antennal lobe revealed that dendrites of the type 1 CG have little overlap with termination fields made by uniglomerular PNs (Fig. 11G) but have significant overlap with termination fields made by a population of multiglomerular PNs (see inset for single neuron, Fig. 11H) with axons in the lateral antennal lobe tract (lALT) (previously referred to as the outer antenno-cerebral tract by Malun et al., 1993) in the p LH (Fig. 11H). Those potent synaptic inputs from a population of multiglomerular PNs to CGs suggest a possibility of MB feedforward inhibition made by CGs (see also Discussion).

## Physiological properties of the four types of CGs

Among the four types of CGs, three types (type 1, type 2a, and type 2b) exhibited endogenous activity comprising episodic bursts of action potentials of instantaneous frequencies at 10-15 Hz (Figs. 3K–R, 5K–R, 6K–R; Nishino and Mizunami, 1998; Strausfeld and Li, 1999a). Action potentials recorded at the junction of the MB calyces exhibited typical “axonal spikes” followed by prominent undershoots (Figs. 3M, 5M, 6M). On the other hand, the NS CG never produced action potentials even when the membrane potential was depolarized by a positive current injection (Fig. 4K) or by post inhibitory rebound followed by a negative current injection plus odor stimulation (Fig. 4L; Mizunami et al., 1987).

Every odor stimuli tested usually elicited excitatory responses (Figs. 3N–R, 4K,O–R, 5N–R, 6N–R) in all types of CGs. The response latencies between time the odor reached the antenna and the start of change in the membrane potential were estimated to be 145–165 ms for type 1 CGs, 85–115 ms for nonspiking CGs, 125–175 ms for type 2a CGs and 205–215 ms for type 2b CGs. Transient inhibition occasionally preceded the excitatory responses, which were more prominent when the odor stimuli were applied during large EPSPs or during bursts of action potentials (arrowheads, Figs. 3O,Q, 4-6O,R).

I also investigated responsiveness to other sensory modalities because there is evidence that

the MB also participates in multisensory processing (Li and Strausfeld, 1997; Mizunami et al., 1998c, 1998d; Okada et al., 1999). Tactile stimuli to the ipsilateral antenna occasionally elicited brief excitatory responses except for type 2a CGs (Figs. 3K, 4M, 5K, 6K), though the responses to tactile stimuli were weaker than those to the odor stimuli and sometimes indistinguishable from spontaneous activity. No prominent responses to light stimuli were detected in any type of CG (Figs. 3L, 4N, 5L, 6L). Thus, I concluded that CGs are mainly involved in olfactory processing of the MB.

***Type 1 CG*** The resting membrane potential was -60 to -70 mV. The excitatory responses to odor stimuli consisted of two phases: transient increase in firing rate and subsequent oscillatory firing interposed by inhibitory inputs (Fig. 3N–R). The instantaneous firing reached 150–180 Hz followed by fluctuating rates (Fig. 12A–E). Tactile stimuli to the ipsilateral antenna elicited brief bursts of action potentials (Fig. 3K).

***NS CG*** The resting membrane potential was -30 to -40 mV. This type exhibited no action potentials. Only fluctuations of membrane potential composed of inhibitory postsynaptic potential (IPSP) and EPSP were recorded from neurites in the LH, around the MB lobes, and the junction of the calyces. The nonspiking CG usually exhibited graded excitatory responses to all odor stimuli with a peak depolarization of 5–10 mV above rest even in the thick axonal branches at the junction of the calyces (Figs. 4O–R, 12P–T). The membrane potential sometimes hyperpolarized before returning to the resting level, being especially prominent in responses to apple odor or orange odor. Tactile stimuli to the ipsilateral antenna elicited a transient hyperpolarization and subsequent depolarization (Fig. 4M).

***Type 2a CG*** The resting membrane potential was -40 to -60 mV. Recordings of the type 2a CG made from neurites at the junction of the calyces exhibited large EPSPs (Fig. 5N–R). However, the amplitude of action potentials (Fig. 5M) were smaller than those of the type 1 CG ($P < 0.05$; type 2a, 45.7 ± 9.49 mV, N = 9; type 1, 67.6 ± 8.29 mV, N = 5). In response to odor stimuli, the instantaneous firing rate reached a plateau (70–90 Hz) and was sustained for 500–760 msec before returning to the pre-stimulus

level (from the first bin exceeding one third of the peak firing rate to the last bin of consecutive five bins below it in PSTHs; Figs. 5N–R, 12F–J). Responses to tactile stimuli were not detectable (Fig. 5K).

***Type 2b CG*** The resting membrane potential was -40 to -50 mV. The amplitudes of action potentials were similar to those of the type 2a CG (Fig. 6M). However, falling voltage change from the peak to the half value of action potentials were slightly smaller in type 2b CG than type 2a CG ($P < 0.05$; type 2a, 32.8 ± 11.7 mV/ms, N = 9; type 2b, 19.7 ± 9.3 mV/ms, N = 4; 17–20 action potentials per individual were used for analysis). That meant action potentials of type 2b CG were slightly blunt than those of type 2a CG. The difference was detectable on oscilloscope during recording. Both types of action potentials were often observed in the same individual. The excitatory responses to odor stimuli were also similar to those of the type 2a CG (Fig. 6N–R, 12K–O). The instantaneous firing rate reached a plateau (50–70 Hz) and was sustained for 480–590 msec (Fig. 12K–O). Tactile stimuli to the ipsilateral antenna elicited brief bursts of action potentials (Fig. 6K).

### Inhibitory responses of CGs

In some recording sessions from the type 1 CG (3 out of 22 recordings) and the NS CG (3 out of 25 recordings), I observed inhibitory responses to all of the odor and tactile stimuli to the ipsilateral antenna (Fig. 13). This inhibition was not due to different recording sites because recordings were made from calycal junctions of the MB as in other recordings. Without a positive current injection into the neuron, the type 1 CG in “inhibitory mode” showed spontaneous spike activity at relatively regular frequencies (15–30 Hz, Fig. 13 A–E), in contrast to episodic bursts in spontaneous activity of CGs in “excitatory mode”. The inhibition occurred in an individual-specific manner, and no transition from excitatory to inhibitory responses, and *vice versa*, was observed during the same recording session, suggesting that powerful IPSPs from other neurons predominate sensory responses in these cases. The membrane fluctuations in spontaneous activity were similar for NS CGs that exhibited inhibitory responses and excitatory responses. The membrane potentials of NS CGs were hyperpolarized 5–10 mV below the resting potential in response to odor and tactile stimuli (Fig. 13F–K). Neither type 1 CG and

NS CG in “inhibitory mode” showed a change from excitatory to inhibitory responses or *vice versa* by a steady depolarizing or hyperpolarizing current injection. Inhibitory responses in the type 2a CG and 2b CG were not detectable, though this may be due to the small sample sizes.

## Discussion

I demonstrated that four closely located calycal giant interneurons (CGs) show distinct but partly overlapping morphologies, suggesting that the four neurons are not redundant iteration of identical units but are functionally segregated. Four CGs projecting to the MB have been recognized for more than two decades by histological studies in cockroaches (Weiss, 1974) and have been assigned as the largest GABA-immunoreactive neurons in the brain (Yamazaki et al., 1998; Strausfeld and Li, 1999a). However, physiological and subsequent morphological characterization had been challenging because of the tight bundling of neurites of CGs.

It is very likely that samplings of CGs in previous studies were strongly biased toward type 1 CGs upon recording from the lateral protocerebrum (Nishino and Mizunami, 1998) because maneuvering of an electrode into thinner neurites of CGs closely attached to thick dendritic neurites of the type 1 CG was extremely difficult. By pinpointing the recording sites to the junction of two calyces where the four CGs neurites dissociate, I succeeded in recording from individual CGs. All of these CGs originate from a GABA-immunoreactive cluster located in the posterior base of the OL. Together with results of multiple labelings of CGs in the same individuals, I concluded that the four CGs have similar but different morphologies and physiologies and are therefore assigned to different types: type 1, NS, type 2a, and type 2b CGs, based partly on the definition by Strausfeld and Li (1999a).

As Strausfeld and Li (1999a) insightfully pointed out, MB calyces are subdivided into the peripheral region (zone I) and the basal region (zones II-IIIA) according to input from two populations of uniglomerular PNs: type 1 and type 2 uniglomerular PNs with dendrites in postero-ventral and antero-dorsal group glomeruli, respectively (Watanabe et al., 2012). Accordingly, the four CGs were classified into type 1 of which axon terminals cover all zones except zone I and type 2 of which axon terminals cover predominantly zone I. From morphological and physiological characteristics, I surmise that the type 1 calycal giant afferent and the type 2 calycal giant afferent (Strausfeld and Li, 1999a) are morphologically equivalent to the type 1 CG and type 2a CG, respectively, in my study.

### Properties of CGs as MB feedback neuron

Consistent with results of previous studies (Nishino and Mizunami, 1998; Strausfeld and Li, 1999a), all of the CGs possessed dendrites in the lateral protocerebrum and axon terminals almost exclusively in MB calyces. The four CGs had no dendritic processes in the MB lobes where KCs send axonal processes. Instead, the dendrites of CGs contacted axon terminals of MBONs, as exemplified by double labelings of these neurons. These results collectively support the previous view (Weiss, 1974; Nishino and Mizunami, 1998; Strausfeld and Li, 1999a) that CGs participate predominantly in feedback inhibition of the MB input site (calyces) by receiving synaptic input from MBONs. Two important questions, whether there are monosynaptic connections between MB output terminals and CG dendrites and whether CGs postsynaptically inhibit KC dendrites and/or presynaptically inhibit PN terminals, await further investigation. In honeybees (Ganeshina and Menzel, 2001) and fruit flies (Yasuyama et al., 2002), GABA-immunoreactive profiles are known to form synapses onto both KC dendrites and PN terminals.

Although morphological data suggest that feedback inhibition from CGs onto MB calyces is prevailing, the possibility of feed-forward inhibition mediated by CGs is also plausible. CGs have no dendrites in the center of the a-v LH and center of the p LH, where uniglomerular PNs supply abundant axon terminals, but axon terminals of multiglomerular PNs with primary axons in the lALT appeared to overlap largely with dendritic processes of type 1, type 2a and type 2b CGs in the medial and ventral boundary of the p LH. For having dendrites broadly in interglomerular regions and projecting directly to the inferior lateral protocerebrum (Malun et al., 1993), these PNs may be suited for transmitting olfactory signals to MB calyces via CGs before signals processed by uniglomerular PNs reach MB calyces.

Responses of CGs to sensory stimuli matched to previous reports on olfactory processing in the MB. All CGs responded to all kinds of odor stimuli used in this study; odor specificity was not observed. The broadly tuned odor responsiveness of CGs is consistent with previous views of inhibition in the higher-order center of locusts (Papadopoulou et al., 2011) and rats (Poo and Isaacson, 2009). I also investigated responses to other sensory modality, tactile and visual, because there is evidence that the MB also participates in multisensory processing (Li and Strausfeld, 1997; Mizunami et al., 1998c,

1998d; Okada et al., 1999) although the principal input to the MB is olfactory (Strausfeld and Li, 1999a; Nishino et al., 2012). Type 1 CG, NS CG, and type 2b CG occasionally showed excitatory responses to tactile stimuli to the ipsilateral antenna weaker than those to odor stimuli. Therefore, I concluded that inhibition provided by CGs is mainly involved in olfactory processing of the MB.

### Functional implication of individual CGs

The terminal organizations of CGs strongly reflect two parallel calycal inputs in which type 1 and type 2 uniglomerular PNs participate. The type 1 CG supplies axon terminals to the termination fields of type 1 PNs (zones II-IIIA). On the other hand, the other three types of CGs provide dense terminals in the termination fields of type 2 uniglomerular PNs (zone I) with additional terminals in the inner half layer of zones II-IIIA (Table 3). At a closer look, type 2b CG terminals are biased toward slightly more basal regions than are type 2a terminals. NS CGs evenly cover both regions (Table 3). Thus, the type 1 CG and NS CG/type 2a/type 2b CGs complement projection fields from each other to cover the whole calycal neuropil and, conversely, three calycal regions receive inhibitory control from different combinations of CGs: (i) zone I receives dense innervations from NS, type 2a and type 2b CGs, (ii) the inner half layer of zones II-IIA receives sparse innervations from the four CGs, and (iii) the outer half layer of zones II-IIIA receives dense innervations from the type 1 CG (Table 3). Therefore, fine gain control including graded transmitter (GABA) release by the NS CG according to the membrane potential (Burrows and Siegler, 1978; Papadopoulou et al., 2011) could occur primarily on synapses between type 2 uniglomerular PNs and KCs.

The calycal subdivision defined by CGs is intriguing considering the distinct physiological and anatomical properties of type 1 and type 2 uniglomerular PNs. Type 2 uniglomerular PNs generally exhibit on-phasic response to odors (Watanabe et al., 2012; Watanabe et al., 2017) and those from approximately 100 glomeruli provide convergent input to small zone I (Strausfeld and Li, 1999a; Watanabe et al., 2012). In contrast, type 1 PNs exhibit more odor specific response patterns interposed by IPSPs (Watanabe et al., 2012; Watanabe et al., 2017) and those from the other 100 glomeruli provide divergent input to specific layers and/or zones in broad zones II-IIIA (Strausfeld and Li, 1999a;

Watanabe et al., 2012). Some degree of inhibitory gain control of type 1 uniglomerular PNs therefore already occurs in the antennal lobe in which numerous monosynaptic connections are formed between PNs and GABA-immunoreactive local interneurons (Distler et al., 1998); hence, zones II-IIIA of the calyx appear to be more appropriate than zone I for fine discrimination of odors. The response differences between the type 1 CG and other CGs, the former exhibiting fast adapting responses to odors and the latter exhibiting slowly adapting responses that are sustained even after the stimulus offset, may reflect different odor coding strategies (see further discussion in General discussion).

The calyx projection patterns of CGs also provide an insight into the functional subdivision of KCs. In cockroaches, class I KCs are newly added over the course of nymphal development in the calycal cup (base) region, concurrent with axonal recruitment posterior to the pre-existing γ layer formed by class II KC axons (Farris and Strausfeld, 2001). Since the locations of KC axons strongly suggest that calycal zone I is formed in the early nymphal stage and other zones are formed in a later nymphal stage (Strausfeld and Li, 1999b; Farris and Strausfeld, 2001), my results lead to a straightforward assumption that the type 1 CG makes synaptic connections with developmentally newer class I KCs, while other CGs make synaptic connections with developmentally older class I KCs in addition to pre-existing class II KCs. The former assumption is supported by the type 1 CG's innervation to dendritic neurites of developmentally newer KCs (Mizunami et al., 1998b; Farris and Strausfeld, 2001). The type 1 CG's innervation to the accessory calyx, which processes gustatory signals from mouth parts (Farris, 2008), implies some functional link between olfactory input via type 1 PNs and gustatory processing. Since KCs receiving input from type 2 uniglomerular PNs comprise two wide layers in MB lobes (Strausfeld and Li, 1999b), it is tempting to speculate that type 2a,b CGs provide inhibitory feedback to distinct subpopulations of KCs, whereas the NS CG provides feedback to both subpopulations.

In contrast to the ordered subdivision of output sites of CGs, knowledge about the morphological subdivision of their input sites in relation to axon terminals to MBONs is fragmental (Li and Strausfeld, 1997, 1999). Type 1 CG dendrites were uniquely characterized by extensive dendritic processes in satellite neuropils anterior to the ML and antero-lateral to the VL. The dendrites of the other three CGs in the satellite neuropil are generally confined to the region antero-lateral to the VL. Taken

together with the finding that axon collaterals of MBONs tend to be localized closely to the region of dendrites possessed by given output neurons (Li and Strausfeld, 1997, 1999), I surmise that the type 1 CG receives input more preferentially from MLONs, while NS/type 2a/type 2b CGs may receive input more preferentially from VLONs.

### Global functions of CGs from comparative viewpoints

The anatomical feature of CGs suggests a global function of CGs not only for sparsening KC output in fine odor discrimination but also for long-term gain control depending on learning or on circadian rhythms. In this context, prominent inhibitory responses to any odor occasionally seen in CG recordings are important because such responses suggest excitatory control of the MB through inhibition of CG activity, broadening the dynamic range of the MB in a state-dependent fashion. The source of inhibitory input to CGs has not yet been identified, but MBONs are candidates because a certain number of MBONs exhibit GABA-immunoreactivity (Yamazaki et al., 1998). The possibility of artifacts such as injury activity due to electrode maneuvering or a circuitry deficit due to anesthetization cannot be entirely ruled out, though I never observed a change from excitatory to inhibitory responses or *vice versa* by a steady depolarizing or hyperpolarizing current injection.

Although I recorded neural activity from animals awake under subjective night, the active state characterized by locomotor activity in subjective night is occasionally interposed by resting states in naturally behaving cockroaches (Tobler, 1983). Thus, it would be intriguing if a non-episodic, constant spike discharge of CGs represents a “resting state” of cockroaches. I need to confirm whether the transition from episodic activity to constant spike activity naturally occurs during longer recordings from CGs and whether such a state change can be artificially reproduced by pharmacological applications.

It is also important that feedback neurons are not controlled solely by KCs but are influenced by other neurons via inhibitory connections, as reported in locusts (Papadopoulou et al., 2011). Physiological investigation of the connectivity between CGs and MBONs and between different CGs

will be an urgent subject to unravel the central mechanism underlying synaptic plasticity of the MB at the circuitry level.

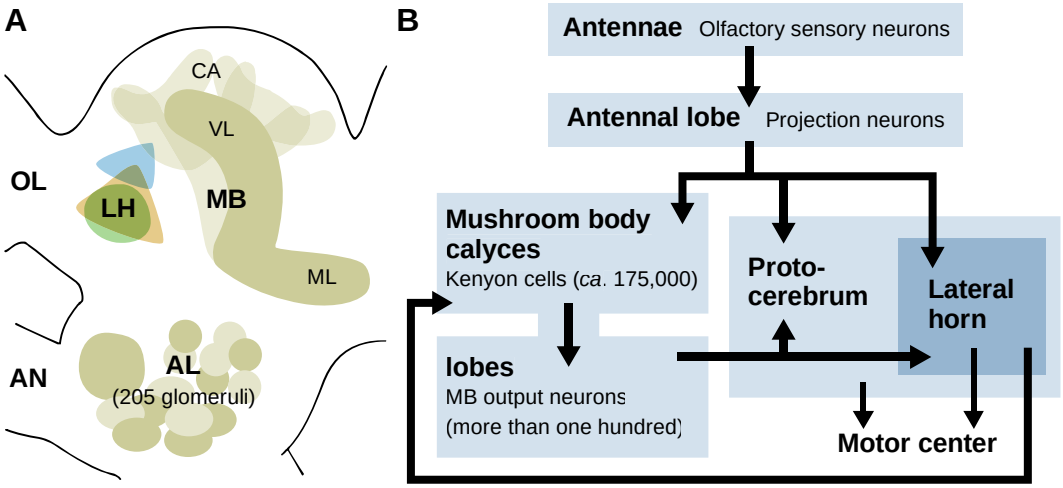



**Figure 1. A:** Schematic of the right hemisphere of the cockroach brain. The mushroom body (MB) consists of two calyces (lateral and medial calyces) as the input region and two lobes (vertical and medial lobes) as the output region. The lateral horn (LH) is compartmentalized into three regions: triangular-shaped antero-dorsal LH (blue), oval-shaped antero-ventral LH (green) and triangular-shaped posterior LH (yellow). **B:** The olfactory system of the cockroach. Olfactory pathways involved in this study are schematized. The pathway connecting the LH and the MB calyces includes calycal giants (CGs), putative MB-feedback inhibitory neurons. Protocerebrum includes the neuropils surrounding the mushroom body (MB). AN, antennal nerve; AL, antennal lobe; CA, calyx; LH, lateral horn; MB, mushroom body; ML, medial lobe; OL, optic lobe; VL, vertical lobe.

**Table 1.** Primary antibodies used.

| Antibody | Immunogen | Source, species, type, cat. no. | Dilution | RRID |
|---|---|---|---|---|
| GABA[1] | GABA linked to bovine serum albumin | Sigma, rabbit polyclonal, #A2052 | 1:1000 | AB_477652 |
| Synapsin "SYNORF1" | GST – synapsin fusion protein | DSHB[2], mouse monoclonal, #3C11 | 1:50 | AB_528479 |

[1] GABA: gamma-aminobutyric acid.

[2] Developmental Studies Hybridoma Bank

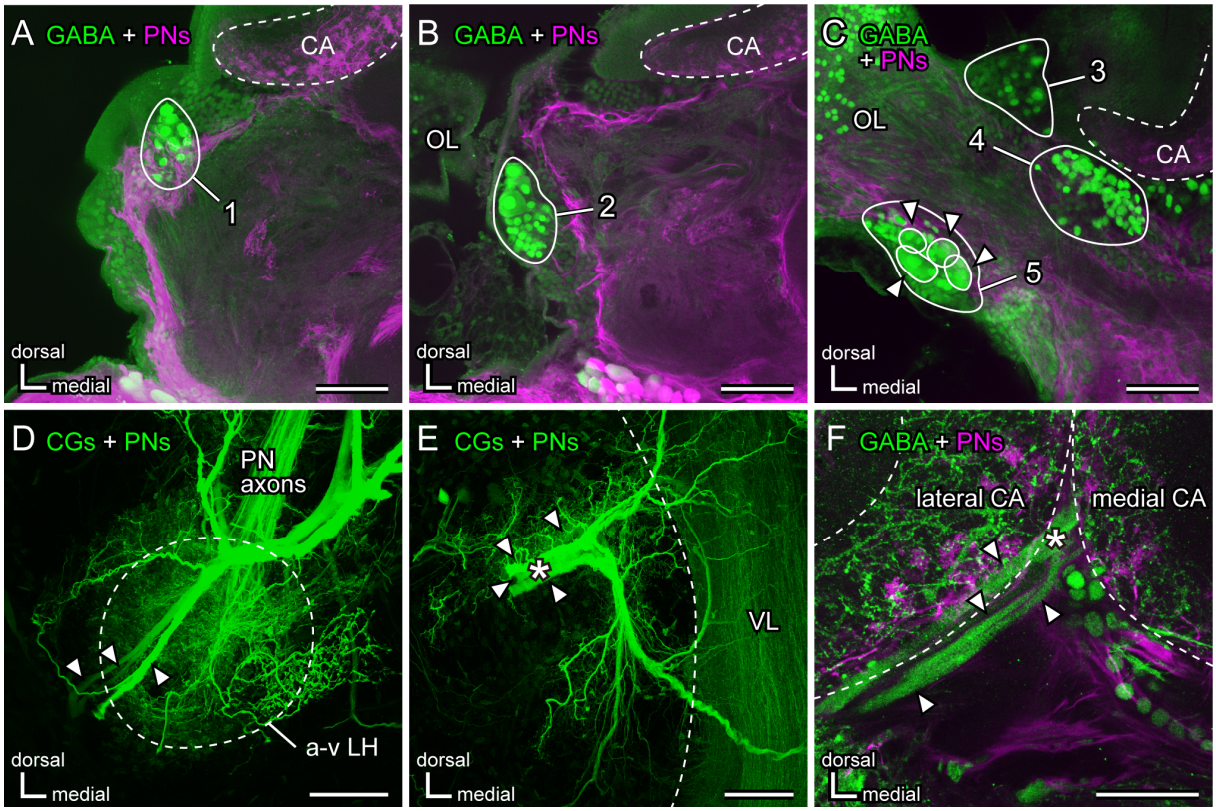

A GABA + PNs
CA
1
dorsal
medial
B GABA + PNs
CA
OL
2
dorsal
medial
C GABA + PNs
3
OL
4
CA
5
dorsal
medial
D CGs + PNs
PN axons
a-v LH
dorsal
medial
E CGs + PNs
VL
dorsal
medial
F GABA + PNs
lateral CA
medial CA
dorsal
medial

**Figure 2.** Distribution of GABA-immunoreactive neurons and primary neurites of CGs. **A–C:** Labeling of GABA-immunoreactive neurons (green) showing five GABA-immunoreactive cell clusters in the cell body rind of the anterior to posterior lateral protocerebrum (1-5, outlined by a white line). Projection neurons (PNs, magenta) were labeled at the same time to make the brain structures viewed clearly. Cell cluster 1 is located in the mid-anterior surface (A), cell cluster 2 is located in the antero-ventral region of the optic lobe (OL) base (B), cell cluster 3 is located in the antero-dorsal region of the OL base, cell cluster 4 is located in the posterior surface just beneath the lateral calyx, and cell cluster 5 is located in the postero-ventral region of the OL base (C). Cell cluster 5 contains four large cell bodies belonging to CGs (each encircled by a white line). **D–F:** Neurites of CGs running in the antero-ventral lateral horn (a-v LH) (D), satellite neuropils around the vertical lobe (VL) (E), and calyces (F). Other than CG neurites, bundles of PN axons were also stained because mass staining dye was injected from the MB calyces. Asterisks in D and F indicate locations where the widths of dendrites (D) and axons (F) were measured (see Table 3). Number and depth of confocal sections used for two-dimensional reconstructions are as follows. A: 16 sections in 45.0 μm; B: 4 sections in 3.0 μm; C: 23 sections in 66.0 μm; D: 131 sections in 130.0 μm; E: 130 sections in 129 μm; F: 7 sections in 6.0 μm. a-v LH, antero-ventral lateral horn; CA, calyx; OL, optic lobe; PNs, projection neurons; VL, vertical lobe. Scale bars = 100 μm in A–C; 50 μm in D–F. Immunolabeling images in A–C,F were generously provided by Dr. H. Watanabe.

| | small (< 15 μm) | Middle (15–30 μm) | large (> 30 μm) | total cell bodies |
|---|---|---|---|---|
| Cluster 1 | 46.7 ± 11.1 | 10.7 ± 2.6 | 2.3 ± 1.2 | 59.7 ± 10.7 |
| 2 | 109.0 ± 2.9 | 3.7 ± 0.9 | 1.0 ± 0.0 | 113.7 ± 2.1 |
| 3 | 78.0 ± 12.8 | 4.7 ± 0.5 | 0.0 ± 0.0 | 82.7 ± 12.6 |
| 4 | 60.0 ± 1.4 | 2.3 ± 1.2 | 0.0 ± 0.0 | 62.3 ± 2.1 |
| 5 | 31.7 ± 3.9 | 3.3 ± 0.5 | 4.0 ± 0.0 | 39.0 ± 4.3 |

**Table 2.** Cell bodies in five GABA-immunoreactive clusters shown in Fig. 2A–C. Number of cell bodies in each cluster is shown as means ± SD made in three wholemount preparations of the brain. Cell bodies were classified into small, middle, and large by diameter measured as the mean of major and minor axes. Four large cell bodies in cluster 5 were CGs.

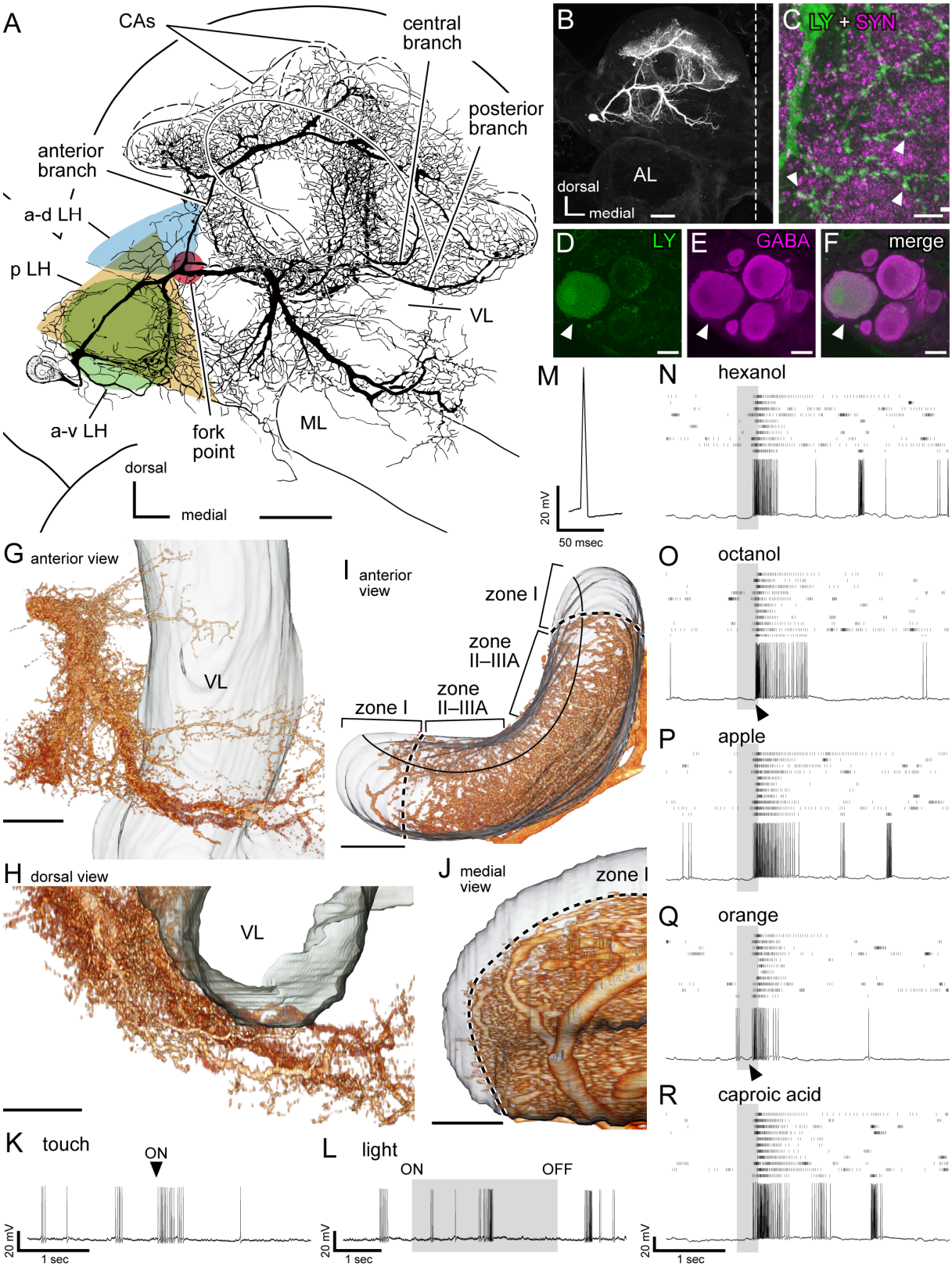

A
CAs
central branch
posterior branch
anterior branch
a-d LH
p LH
a-v LH
fork point
ML
VL
dorsal
medial
B
AL
dorsal
medial
C LY + SYN
D LY
E GABA
F merge
M
20 mV
50 msec
N hexanol
O octanol
P apple
Q orange
R caproic acid
G anterior view
VL
I anterior view
zone I
zone II–IIIA
zone I
zone II–IIIA
H dorsal view
VL
J medial view
zone I
K touch
ON
20 mV
1 sec
L light
ON
OFF
20 mV
1 sec
20 mV
1 sec

**Figure 3.** Morphology and physiology of the type 1 CG. **A,B:** Diagram of the type 1 CG (A), reconstructed from confocal sections (B), viewed anteriorly. In this figure and figures 4-6B, the white broken line indicates the midline of the brain. **C:** Double labeling of a type 1 CG and synapsin-immunoreactive vesicles, showing co-localizations of both signals (indicated by white arrowheads) in the MB calyces. **D–F:** Double labeling of a type 1 CG (D) and GABA-immunoreactive neurons (E). **G–J:** Three-dimensional reconstructions of primary dendritic trunks around the VL (G,H) and axon terminals in the lateral calyx (I,J). The axon terminals innervate the whole calyx except in zone I, where type 2 uniglomerular PNs supply axon terminals (Strausfeld and Li, 1999a). **K:** Response to a tactile stimulus to the ipsilateral antenna. **L:** Spike activity during lighting on compound eyes. **M:** Time-stretched action potentials recorded at the junction of mushroom body (MB) calyces. **N–R:** Rastar plots of responses to various odor stimuli (n = 5). Number and depth of confocal sections used for two-dimensional reconstructions are as follows. Arrowheads indicate transient inhibitory potentials preceding excitatory responses. B: 41 sections in 416.0 μm; C: 15 sections in 14.0 μm. a-d LH, antero-dorsal lateral horn; a-v LH, antero-ventral lateral horn; CA, calyx; ML, medial lobe; p LH, posterior lateral horn; VL, vertical lobe. Scale bars = 100 μm in A,B; 10 μm in C; 20 μm in D–F; 50 μm in G–J. Immunolabeling images in C–F were generously provided by Dr. H. Watanabe.

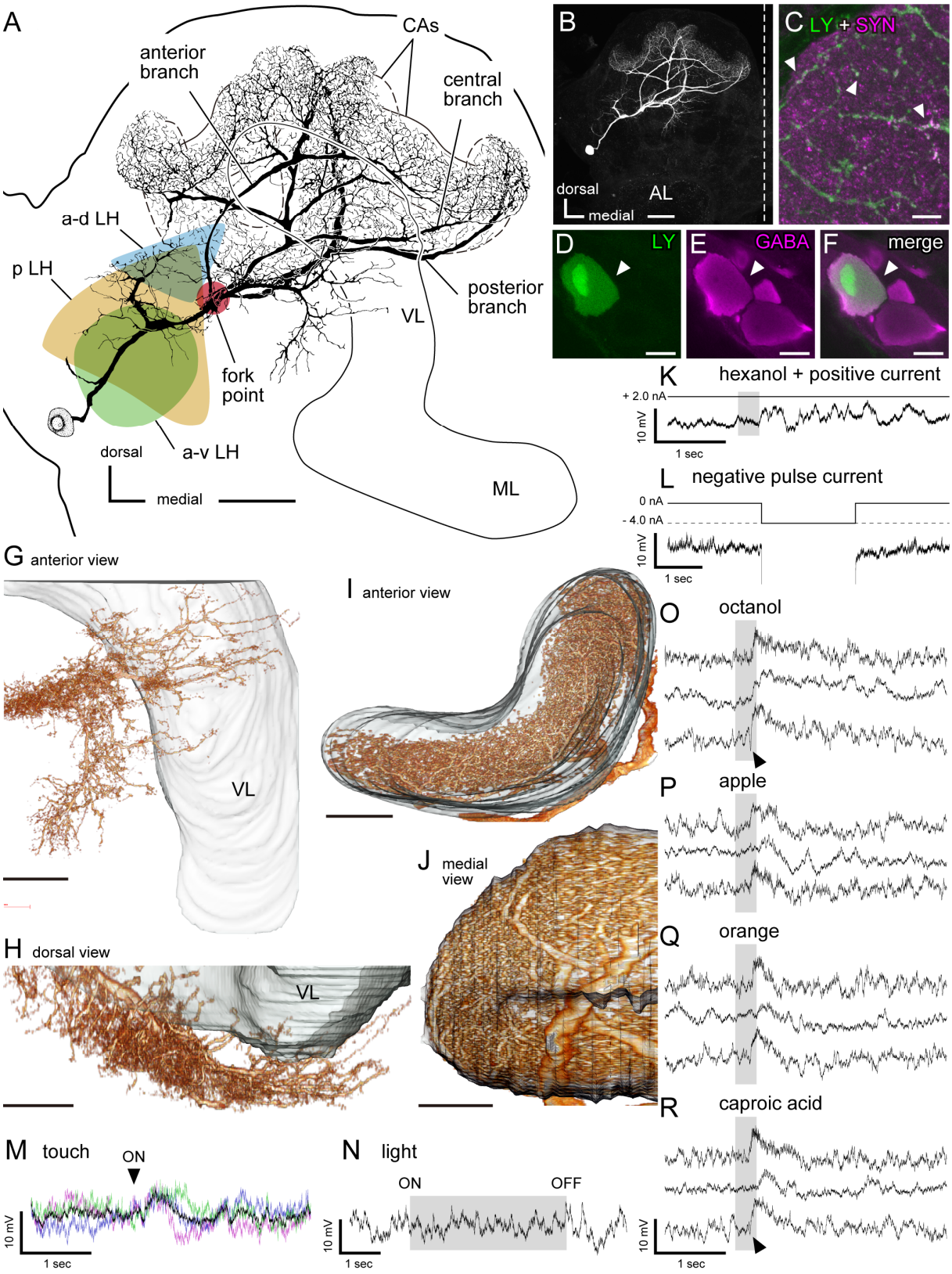

A
CAs
anterior branch
central branch
a-d LH
p LH
posterior branch
VL
fork point
dorsal
a-v LH
medial
ML
B
dorsal
medial
AL
C LY + SYN
D LY
E GABA
F merge
K hexanol + positive current
+ 2.0 nA
10 mV
1 sec
L negative pulse current
0 nA
- 4.0 nA
10 mV
1 sec
G anterior view
VL
I anterior view
J medial view
H dorsal view
VL
O octanol
P apple
Q orange
R caproic acid
M touch
ON
10 mV
1 sec
N light
ON
OFF
10 mV
1 sec
10 mV
1 sec

**Figure 4.** Morphology and physiology of the nonspiking (NS) CG. **A,B:** Diagram of the NS CG (A), reconstructed from confocal sections (B), viewed anteriorly. **C:** Double labeling of an NS CG and synapsin-immunoreactive vesicles (magenta), showing co-localizations of both signals (indicated by white arrowheads) in the MB calyces. **D–F:** Double labeling of an NS CG (D) and GABA-immunoreactive neurons (E). **G–J:** Three-dimensional reconstructions of primary dendritic trunks around the VL (G,H) and axon terminals in the lateral calyx (I,J). **K,L:** Current injections (+2.0 nA, K, –4.0 nA, L) failed to elicit action potentials in an NS CG. **M,N:** Membrane potentials to a tactile stimulus to the ipsilateral antenna (M) and lighting on compound eyes (N). **O–R:** Rastar plots of responses to various odor stimuli (n = 3). Arrowheads indicate transient inhibitory potentials preceding excitatory responses. Number and depth of confocal sections used for two-dimensional reconstructions are as follows. B: 178 sections in 389.4 µm; C: 16 sections in 12.0 µm. a-d LH, antero-dorsal lateral horn; a-v LH, antero-ventral lateral horn; CA, calyx; ML, medial lobe; p LH, posterior lateral horn; VL, vertical lobe. Scale bars = 100 µm in A,B; 10 µm in C; 20 µm in D–F; 50 µm in G–J. Immunolabeling images in C–F were generously provided by Dr. H. Watanabe.

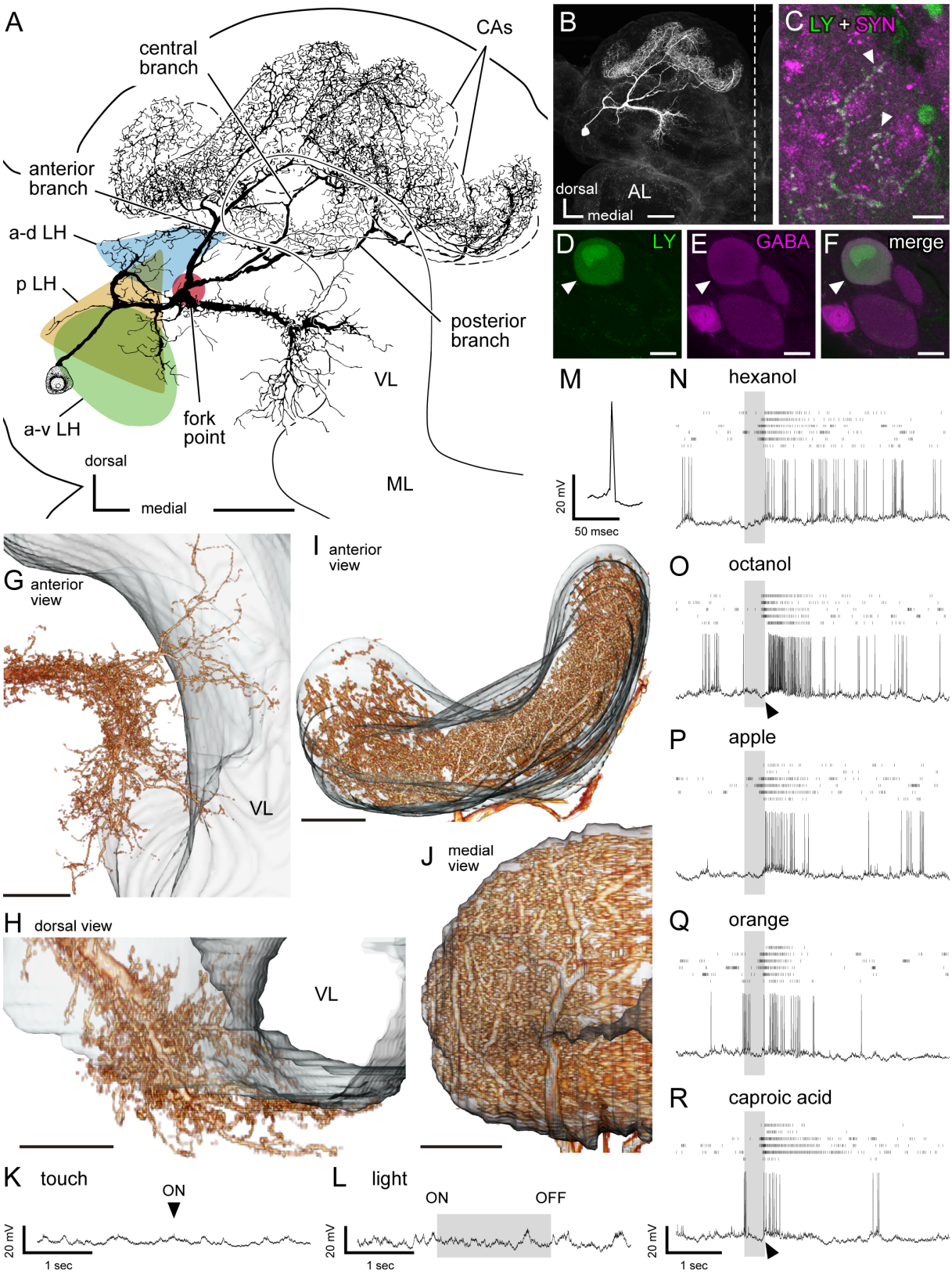

A
central branch
CAs
anterior branch
a-d LH
p LH
a-v LH
fork point
posterior branch
VL
ML
dorsal
medial
B
dorsal
AL
medial
C LY + SYN
D LY
E GABA
F merge
M
20 mV
50 msec
N hexanol
O octanol
P apple
Q orange
R caproic acid
G anterior view
VL
I anterior view
J medial view
H dorsal view
VL
K touch
ON
20 mV
1 sec
L light
ON
OFF
20 mV
1 sec
20 mV
1 sec

**Figure 5.** Morphology and physiology of the type 2a CG. **A,B:** Diagram of the type 2a CG (A), reconstructed from confocal sections (B), viewed anteriorly. **C:** Double labeling of a type 2a CG and synapsin-immunoreactive vesicles (magenta), showing co-localizations of both signals (indicated by white arrowheads) in the MB calyces. **D–F:** Double labeling of a type 2a CG (D) and GABA-immunoreactive neurons (E). **G–J:** Three-dimensional reconstructions of primary dendritic trunks lateral to the VL (G,H) and axon terminals in the lateral calyx (I,J). **K:** Response to a tactile stimulus to the ipsilateral antenna. **L:** Spiking activity during lighting on the compound eyes. **M:** Time-stretched action potentials recorded at the junction of MB calyces. **N–R:** Rastar plots of responses to various odor stimuli (n = 3). Arrowheads indicate transient inhibitory potentials preceding excitatory responses. Number and depth of confocal sections used for two-dimensional reconstructions are as follows. B: 178 sections in 371.7 μm; C: 12 sections in 11.0 μm. a-d LH, antero-dorsal lateral horn; a-v LH, antero-ventral lateral horn; CA, calyx; ML, medial lobe; p LH, posterior lateral horn; VL, vertical lobe. Scale bars = 100 μm in A,B; 10 μm in C; 20 μm in D–F; 50 μm in G–J. Immunolabeling images in C–F were generously provided by Dr. H. Watanabe.

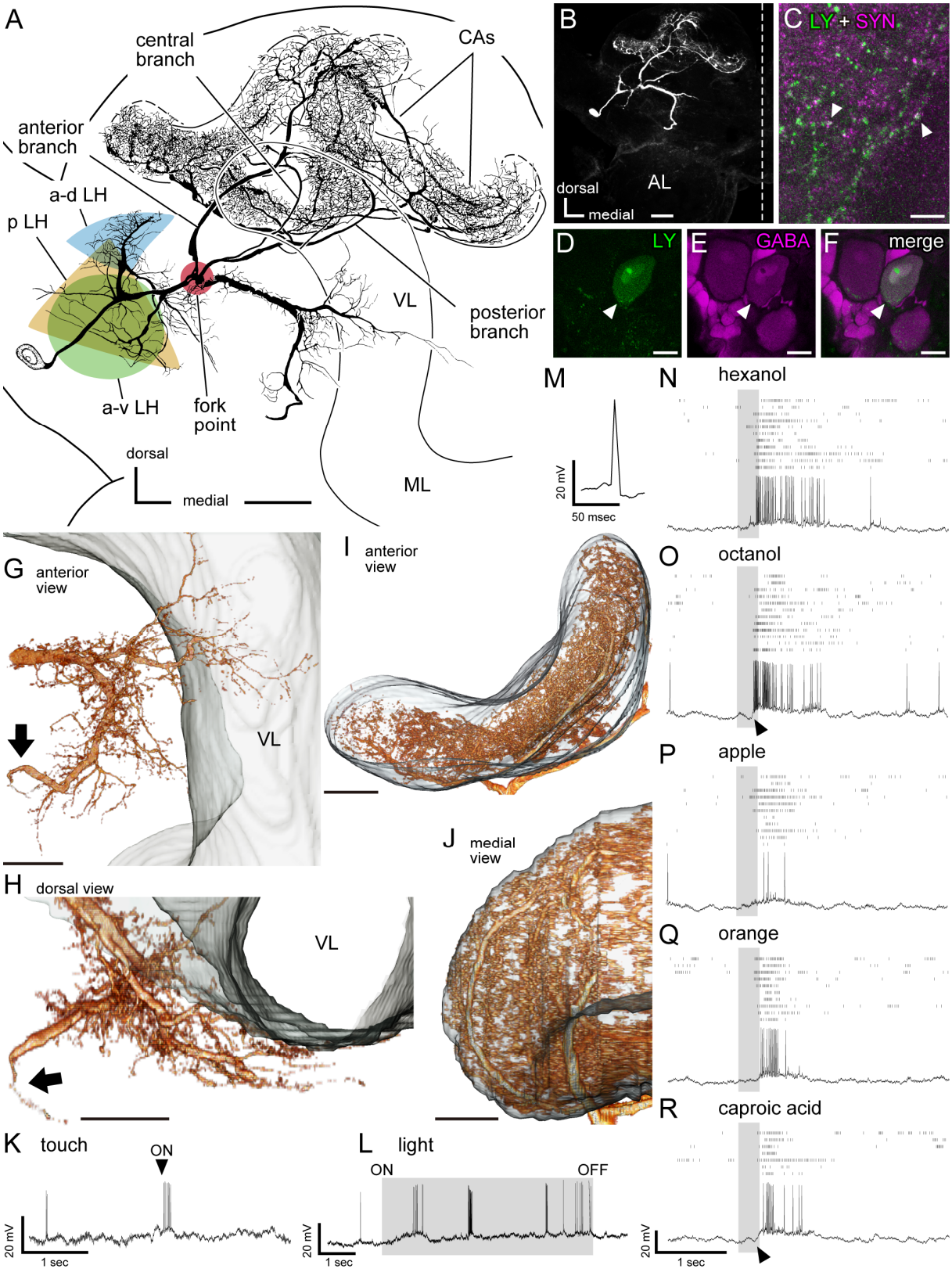

A
central branch
CAs
anterior branch
a-d LH
p LH
VL
posterior branch
a-v LH
fork point
dorsal
medial
ML
B
dorsal
AL
medial
C LY + SYN
D LY
E GABA
F merge
M
20 mV
50 msec
N hexanol
O octanol
P apple
Q orange
R caproic acid
G anterior view
VL
I anterior view
J medial view
H dorsal view
VL
K touch
ON
20 mV
1 sec
L light
ON
OFF
20 mV
1 sec
20 mV
1 sec

**Figure 6.** Morphological and physiological properties of the type 2b CG. **A,B:** Diagram of the type 2b CG (A), reconstructed from confocal sections (B), viewed anteriorly. The large cell body (about 30 µm in diameter) is situated in the postero-ventral base of the OL. **C:** Double labeling of a type 2b CG and synapsin-immunoreactive vesicles (magenta), showing co-localizations of both signals (indicated by white arrowheads) in the MB calyces. **D–F:** Double labeling of a type 2b CG (D) and GABA-immunoreactive neurons (E). **G–J:** Three-dimensional reconstructions of primary dendritic trunks around the VL (G,H) and axon terminals in the lateral calyx (I,J). One of the thickest branches ends close to the anterior surface of the lateral protocerebrum (indicated by a black arrow, G,H), characteristic to type 2b CG. **K:** Response to a tactile stimulus to the ipsilateral antenna. **L:** Spiking activity during lighting on the compound eyes. **M:** Time-stretched action potentials recorded at the junction of MB calyces. **N–R:** Rastar plots of responses to various odor stimuli (n = 4). Arrowheads indicate transient inhibitory potentials preceding excitatory responses. Number and depth of confocal sections used for two-dimensional reconstructions are as follows. B: 48 sections in 423.0 µm; C: 23 sections in 22.0 µm. a-d LH, antero-dorsal lateral horn; a-v LH, antero-ventral lateral horn; CA, calyx; ML, medial lobe; p LH, posterior lateral horn; VL, vertical lobe. Scale bars = 100 µm in A,B; 10 µm in C; 20 µm in D–F; 50 µm in G–J. Immunolabeling images in C–F were generously provided by Dr. H. Watanabe.

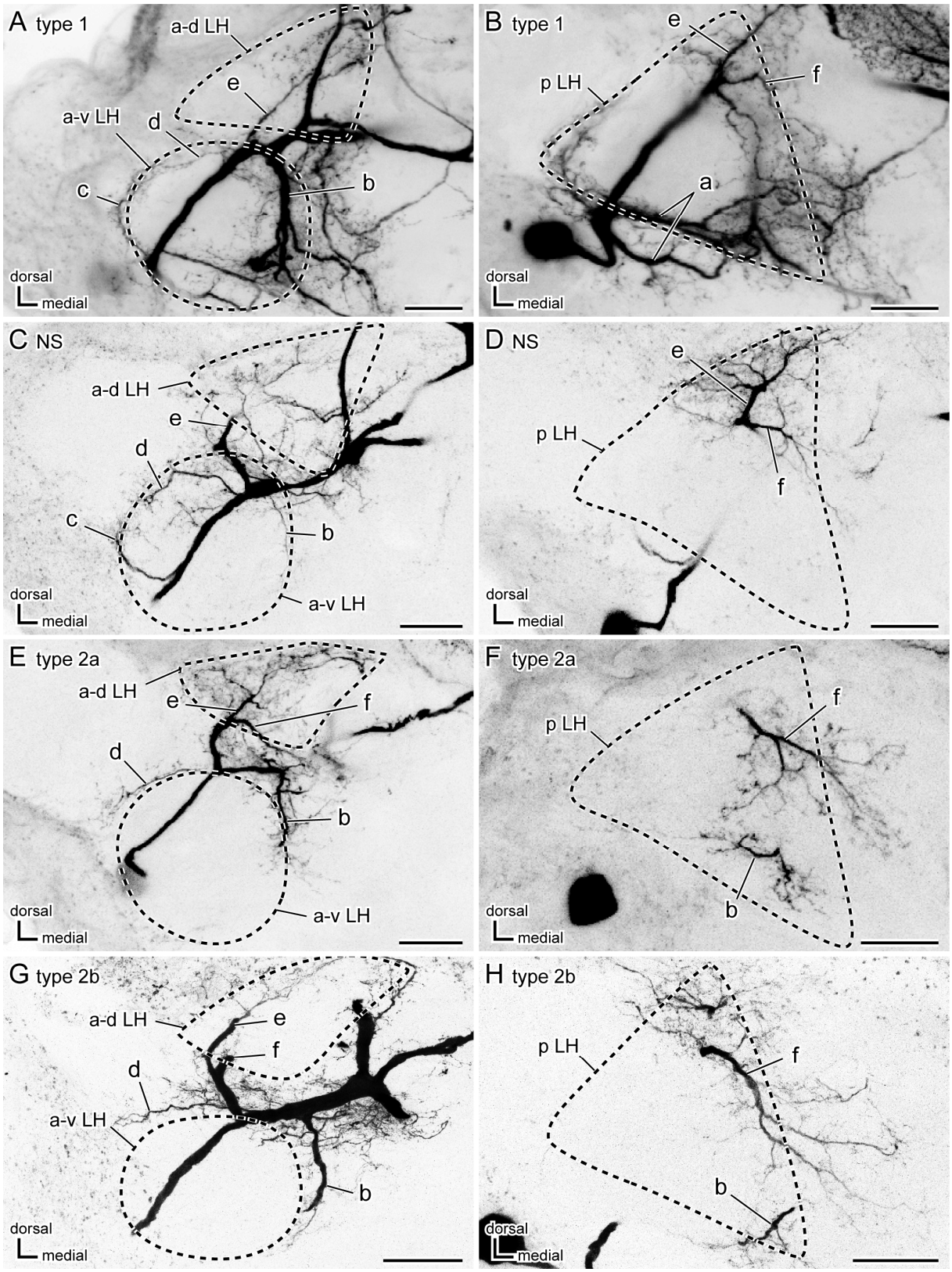

A type 1
a-d LH
e
a-v LH
d
c
b
dorsal
medial
B type 1
e
f
p LH
a
dorsal
medial
C NS
a-d LH
e
d
c
b
a-v LH
dorsal
medial
D NS
e
p LH
f
dorsal
medial
E type 2a
a-d LH
e
f
d
b
a-v LH
dorsal
medial
F type 2a
f
p LH
b
dorsal
medial
G type 2b
a-d LH
e
f
d
a-v LH
b
dorsal
medial
H type 2b
p LH
f
b
dorsal
medial

**Figure 7.** Dendritic arborizations of the four types of CGs in the anterior half (A,C,E,G) and posterior half (B,D,F,H) of the LH. The five dendritic branches (b-f) are conserved in all CGs except the branch possessed only by the type 1 CG (a). **A,B:** Type 1 CG. Arborizations are more abundant in the medial and ventral boundary of the a-v LH and posterior (p) LH. **C,D:** NS CG. Arborizations are abundant in the dorsal region of the a-v LH and p LH. **E,F:** Type 2a CG. Arborizations are primarily in the medial boundary of the a-v LH and p LH. **G,H:** Type 2b CG. Branching patterns in the LH are nearly identical to those of the type 2a CG, but dendritic processes are more slender than those of type 2a. Number and depth of confocal sections used for two-dimensional reconstructions are as follows. A: 6 sections in 52.0 µm; B: 7 sections in 62.4 µm; C: 35 sections in 71.4 µm; D: 26 sections in 52.5 µm; E: 8 sections in 63.7 µm; F: 5 sections in 36.4 µm; G: 100 sections in 118.8 µm; H: 68 sections in 88.4 µm. a-d LH, antero-dorsal lateral horn; a-v LH, antero-ventral lateral horn; p LH, posterior lateral horn. Scale bars = 50 µm.

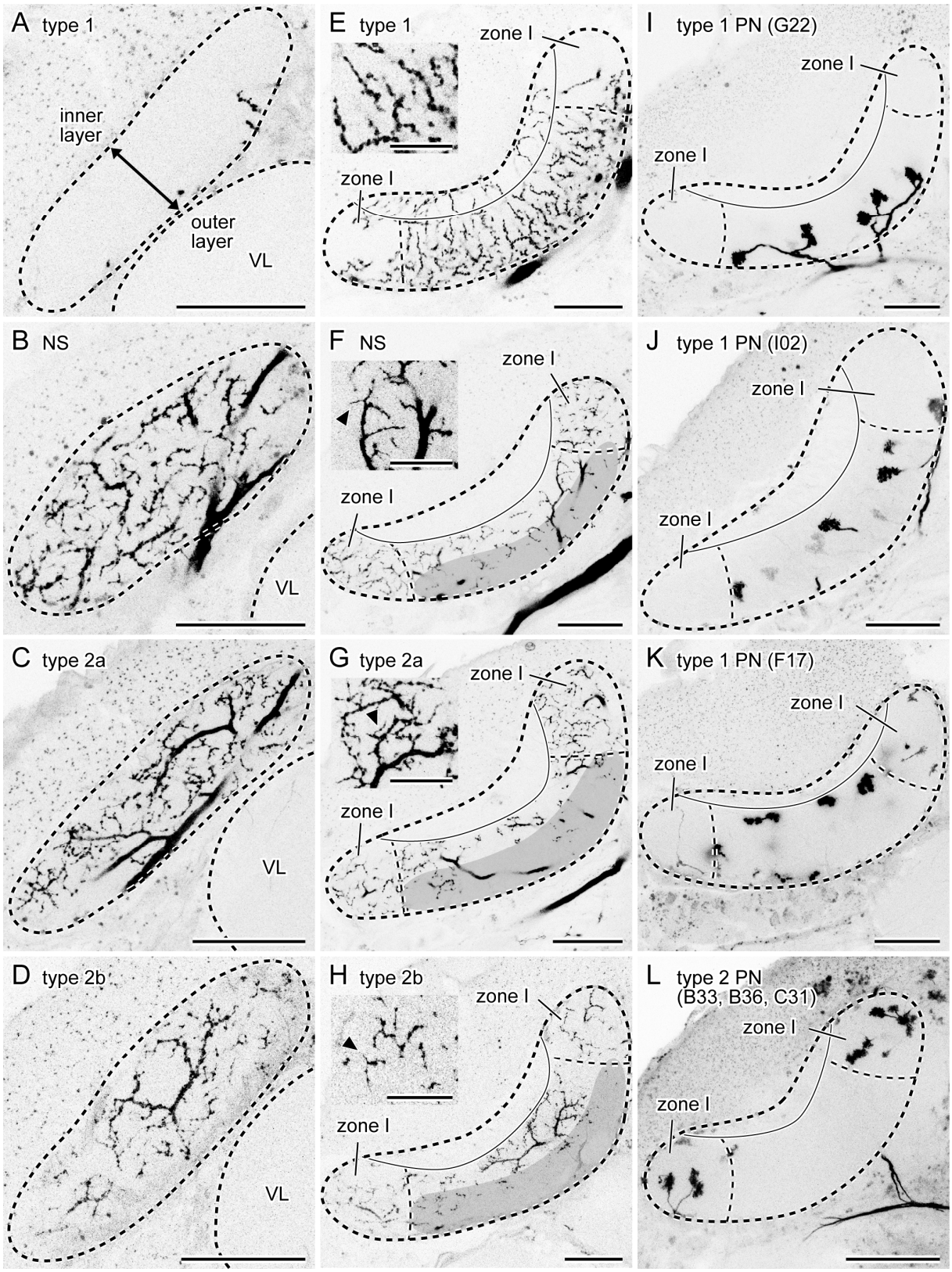

A type 1
inner layer
outer layer
VL
B NS
VL
C type 2a
VL
D type 2b
VL
E type 1
zone I
zone I
F NS
zone I
zone I
G type 2a
zone I
zone I
H type 2b
zone I
zone I
I type 1 PN (G22)
zone I
zone I
J type 1 PN (I02)
zone I
zone I
K type 1 PN (F17)
zone I
zone I
L type 2 PN
(B33, B36, C31)
zone I
zone I

**Figure 8.** Axon terminals of the four types of CGs (A-H) and uniglomerular PNs (I-L) in the anteriormost region (A-D) and the antero-central region (E-L) of the MB lateral calyx. **A,E:** Type 1 CG. Zone I of the calyx (Strausfeld and Li, 1999a) is devoid of axon terminals (A). Axonal branches are dense in the outer half layer of zones II-IIA (Strausfeld and Li, 1999a) but less dense in the inner half layer (E) and the axonal layer of KCs (outlined by solid line). **B,F:** NS CG. Axon terminals are abundant in the zone I (B), but there are few in the outer half layer of zones II-IIIA (shaded area, F). The arborizations are fine mesh-like. **C,G:** Type 2a CG. Axon terminals are abundant in the peripheral most region of zone I (C) but there are few in the outer half layer of zones II-IIIA (shaded area, G). **D,H:** Type 2b CG. The axon terminals are abundant in the basal region of zone I (D) but few in the outer half layer of zones II-IIIA (shaded area, H). Insets in F-H show fine, tapered processes (indicated by arrowheads) intermingled in thick blebby processes. **I–L:** Type 1 uniglomerular PNs with dendrites in the glomerulus G22 (I), I02 (J), F17 (K) and multiple type 2 PNs with dendrites in B33 B36 and C31 (L), showing that PN terminals occupy different basal-peripheral regions (I-K vs L) and inner-outer layers (I-K). Number and depth of confocal sections used for two-dimensional reconstructions are as follows. A–D: 5 sections in 4.8 μm; E–H: 3 sections in 2.4 μm; I: 20 sections in 22.8 μm; J: 14 sections in 15.6 μm;. K: 10 sections in 10.8 μm; L: 29 sections in 33.6 μm. VL, vertical lobe. Scale bars = 50 μm; 20 μm in insets.

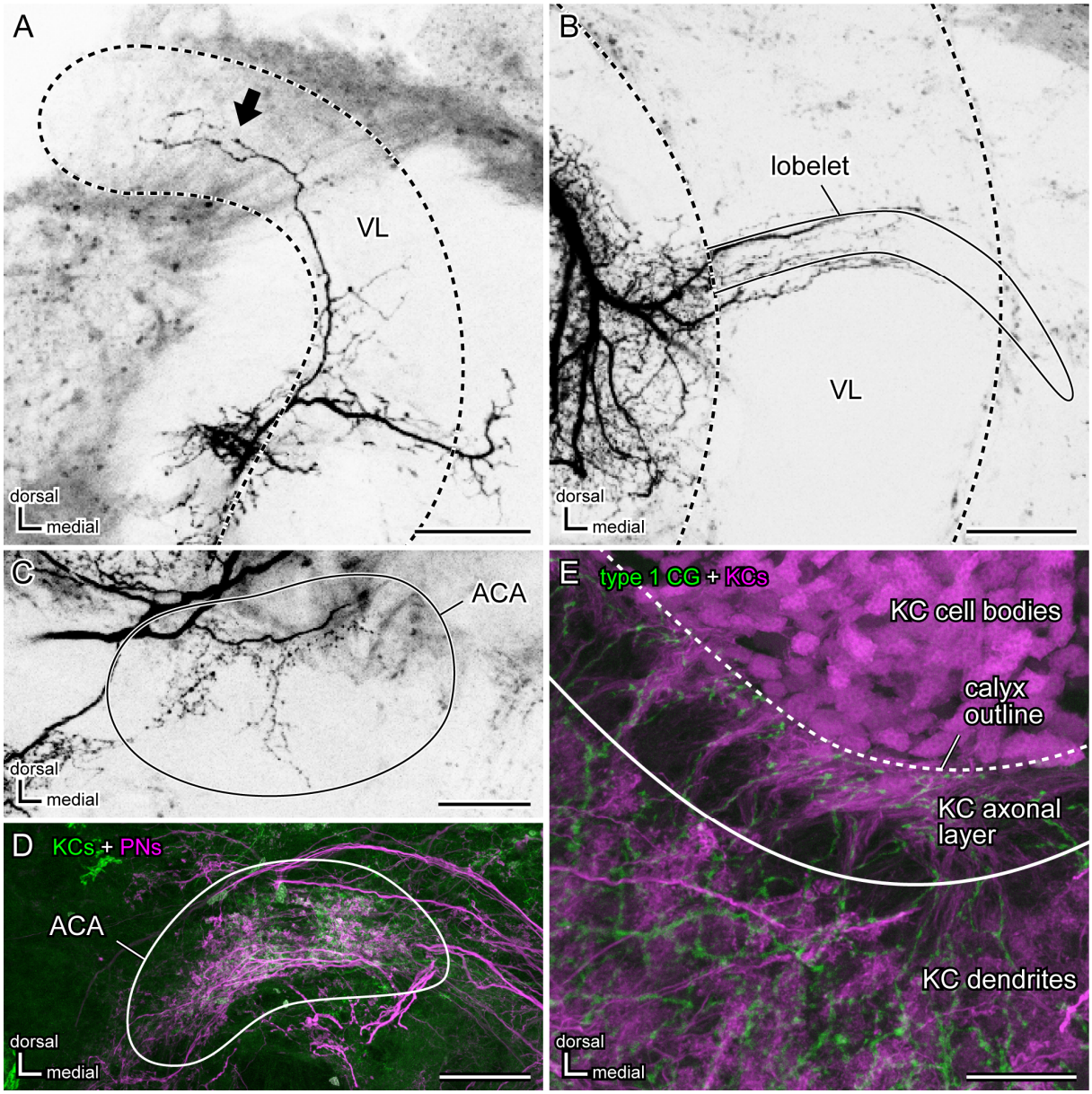

A
VL
dorsal
medial
B
lobelet
VL
dorsal
medial
C
ACA
dorsal
medial
D
KCs + PNs
ACA
dorsal
medial
E
type 1 CG + KCs
KC cell bodies
calyx
outline
KC axonal
layer
KC dendrites
dorsal
medial

**Figure 9.** Extensive dendritic and axonal innervations unique to the type 1 CG. **A:** Dendritic collaterals ascending along the antero-lateral surface of the VL (arrow). **B:** Dendritic collaterals that loop posteriorly and innervate the surface of the "lobelet" formed by axons of class III KCs (Farris and Strausfeld, 2003). **C,D:** Axon collaterals decorated with bead-like varicosities (C) sparsely innervate the accessory calyx (ACA, Farris and Strausfeld, 2003), defined by double labeling of KCs and PNs from the tritocerebrum (D). **E:** Double labeling of the type 1 CG and KCs showing that axon terminals of the type 1 CG specifically cover the dendritic bundles formed by developmentally newer KC1 (Mizunami et al., 1998b; Farris and Strausfeld, 2001). Number and depth of confocal sections used for two-dimensional reconstructions are as follows. A: 6 sections in 15 µm; B: 24 sections in 66 µm; C: 11 sections in 10 µm; D: 11 sections in 30 µm; E 33 sections in 38 µm. Scale bars = 50 µm in A,B,D,E; 20 µm in C.

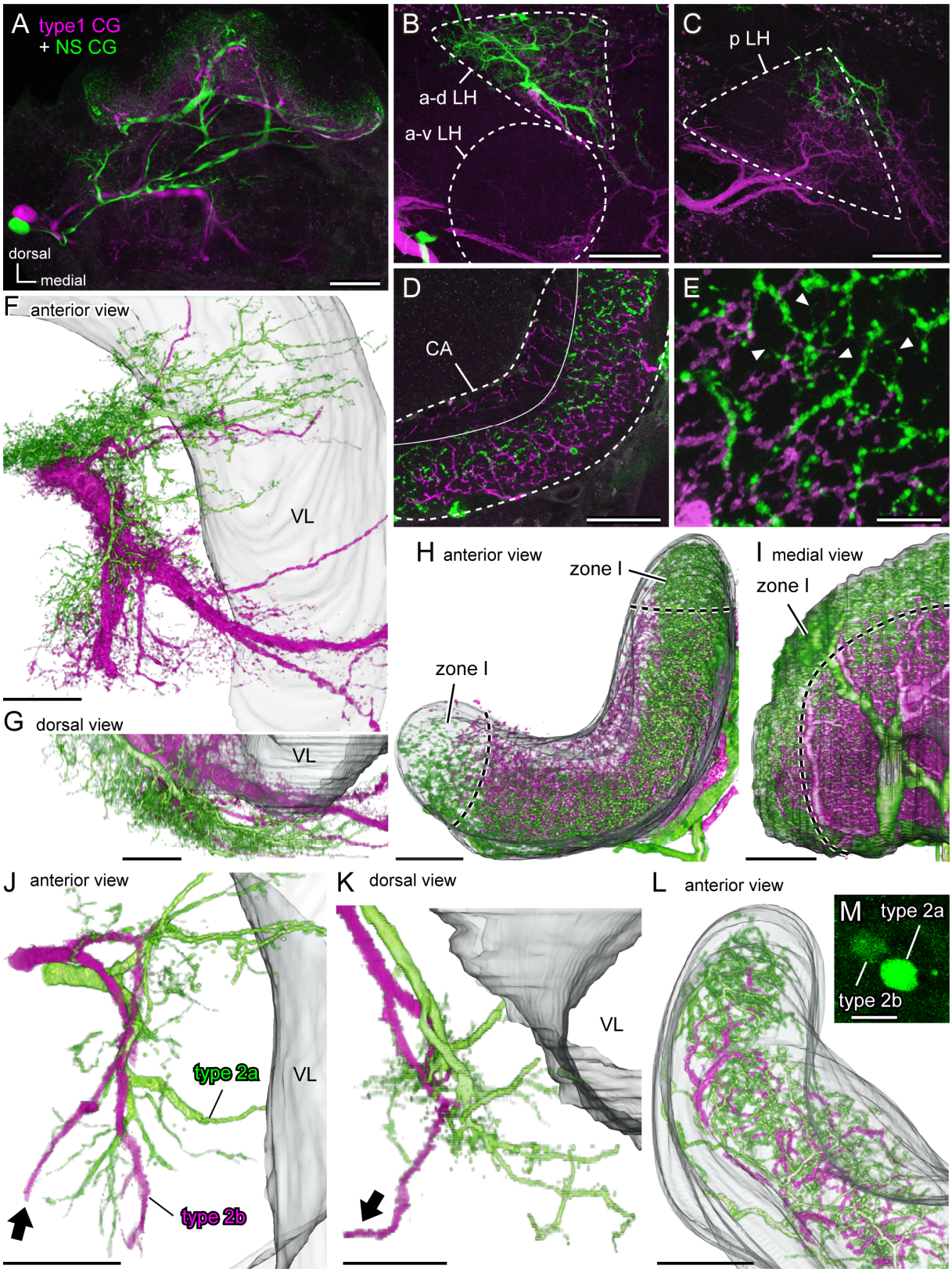

A type1 CG
+ NS CG
dorsal
medial
B
a-d LH
a-v LH
C
p LH
D
CA
E
F anterior view
VL
G dorsal view
VL
H anterior view
zone I
zone I
I medial view
zone I
J anterior view
type 2a
VL
type 2b
K dorsal view
VL
L anterior view
M
type 2a
type 2b

**Figure 10.** Two types of CGs labeled in the same brain. **A:** Confocal image of the type 1 CG (magenta) labeled with Alexa568 and the NS CG (green) labeled with LY. **B,C:** Dendritic arborizations in the anterior half (B) and posterior half (C) of the LH. **D,E:** Axon terminals in the central region of the lateral MB calyx at low magnification (D) and high magnification (E). Arrowheads in E indicate fine tapered processes possessed only by the NS CG. **F–I:** Three-dimensional reconstructions of primary dendritic trunks around the VL (F,G) and axon terminals in the lateral calyx (H,I). **J–M:** Type 2a (green) and type 2b (magenta) CGs stained at different intensities (see M for somata) showing largely overlapping but distinct branching patterns around the VL (J,K) and in the medial calyx (L). Only thick, clearly identifiable dendrites and axons were three-dimensionally reconstructed. Arrows in J and K indicate the dendritic branch uniquely possessed by the type 2b CC. Number and depth of confocal sections used for two-dimensional reconstructions are as follows. A: 15 sections in 350.0 μm; B: 61 sections in 72.0 μm; C: 40 sections in 46.8 μm; D: 12 sections in 11.0 μm; E: 4 sections in 3.6 μm. a-d LH, antero-dorsal lateral horn; a-v LH, antero-ventral lateral horn; CA, calyx; ML, medial lobe; p LH, posterior lateral horn; VL, vertical lobe. Scale bars = 100 μm in A; 50 μm in B,C,E–L; 20 μm in D,M.

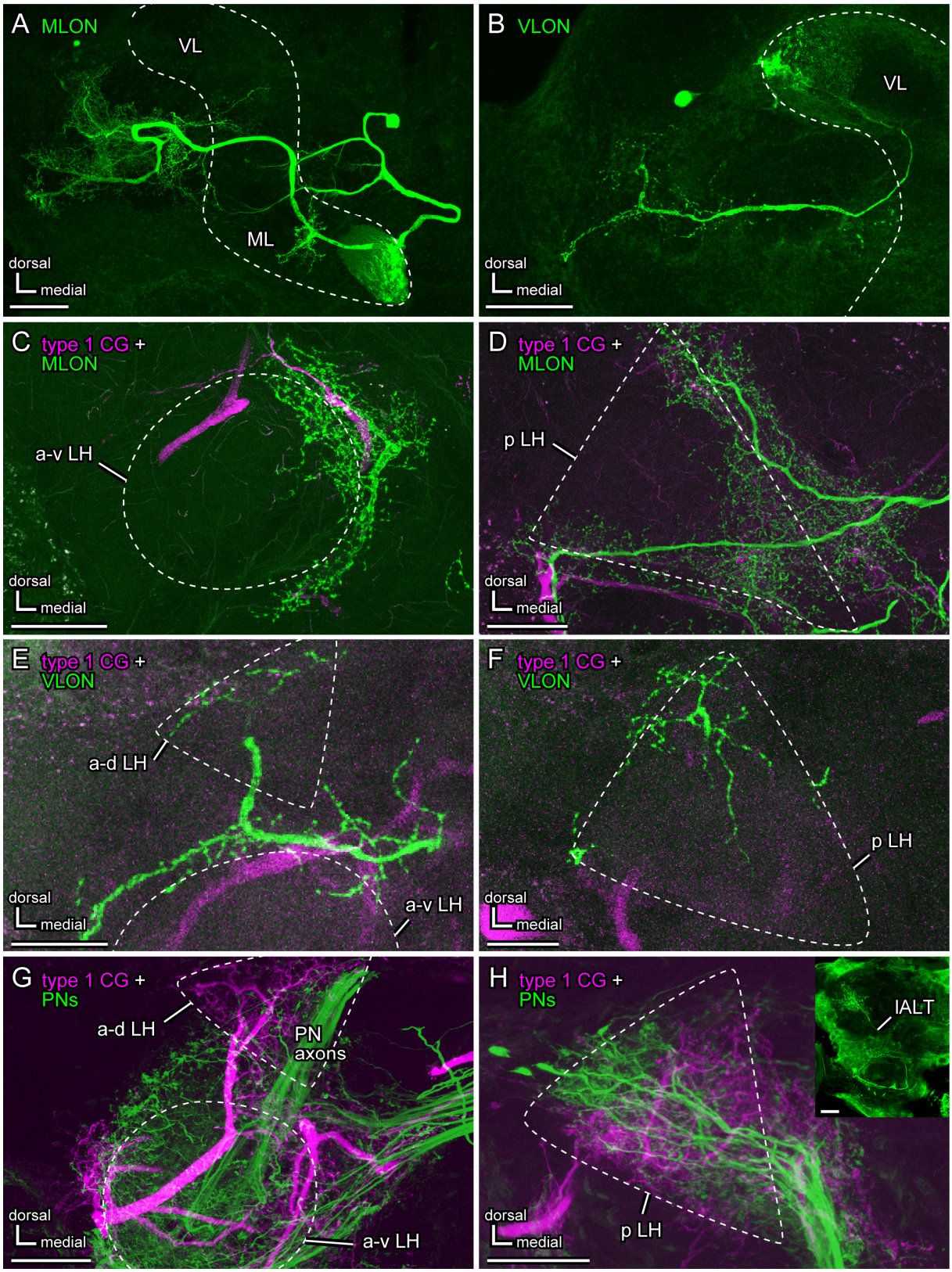

A MLON
VL
ML
dorsal
medial
B VLON
VL
dorsal
medial
C type 1 CG + MLON
a-v LH
dorsal
medial
D type 1 CG + MLON
p LH
dorsal
medial
E type 1 CG + VLON
a-d LH
a-v LH
dorsal
medial
F type 1 CG + VLON
p LH
dorsal
medial
G type 1 CG + PNs
a-d LH
PN axons
a-v LH
dorsal
medial
H type 1 CG + PNs
IALT
p LH
dorsal
medial

**Figure 11.** Differential labeling of the type 1 CG (magenta) and related neuron (s). **A,B:** Low-magnification confocal images of a medial lobe output neuron (MLON: C,D) and a vertical lobe output neuron (VLON: E,F) stained differentially with the type 1 CG. **C,D:** Large overlap of axon terminals of the MLON and dendrites of the type 1 CG. **E,F:** Little overlapping of axon terminals of the VLON and dendrites of the type 1 CG. **G,H:** Differential labeling of the type 1 CG and all presumed PNs showing that dendritic processes of the type 1 CG do not invade the center of the a-v LH, where uniglomerular PNs supply abundant terminals (G), but some overlapping is evident in the p LH, where multiglomerular PNs with axons in the lateral antennal lobe tract (lALT) supply axon terminals (see inset for a single lALT PN, H). Number and depth of confocal sections used for two-dimensional reconstructions are as follows. A: 11 sections in 60.0 µm; B: 17 sections in 90.0 µm; C: 91 sections in 90.0 µm; D: 55 sections in 54.0 µm E: 100 sections in 120 µm; F: 47 sections in 56.4 µm. a-d LH, antero-dorsal lateral horn; a-v LH, antero-ventral lateral horn; lALT, lateral antennal lobe tract; ML, medial lobe; p LH, posterior lateral horn; VL: vertical lobe. Scale bars = 100 µm in inset; 50 µm in A–F.

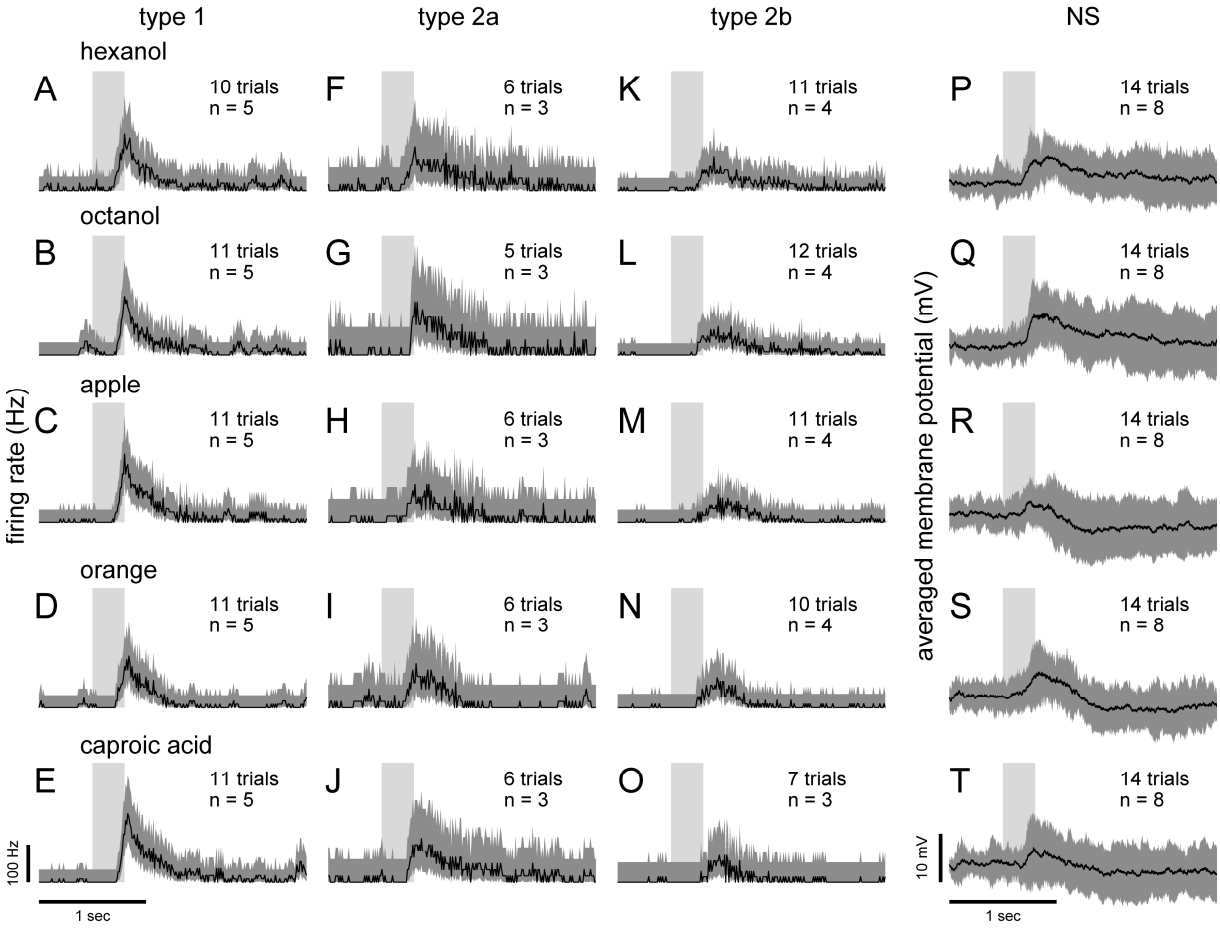



**Figure 12.** Typical excitatory responses during various odor stimuli. **A–O:** Averaged firing activities of spiking CGs (bin = 10 ms). **P–T:** Averaged membrane potentials of NS CGs (n = 8, 14 trials). Dark gray-shaded areas show the 95% confidence intervals.

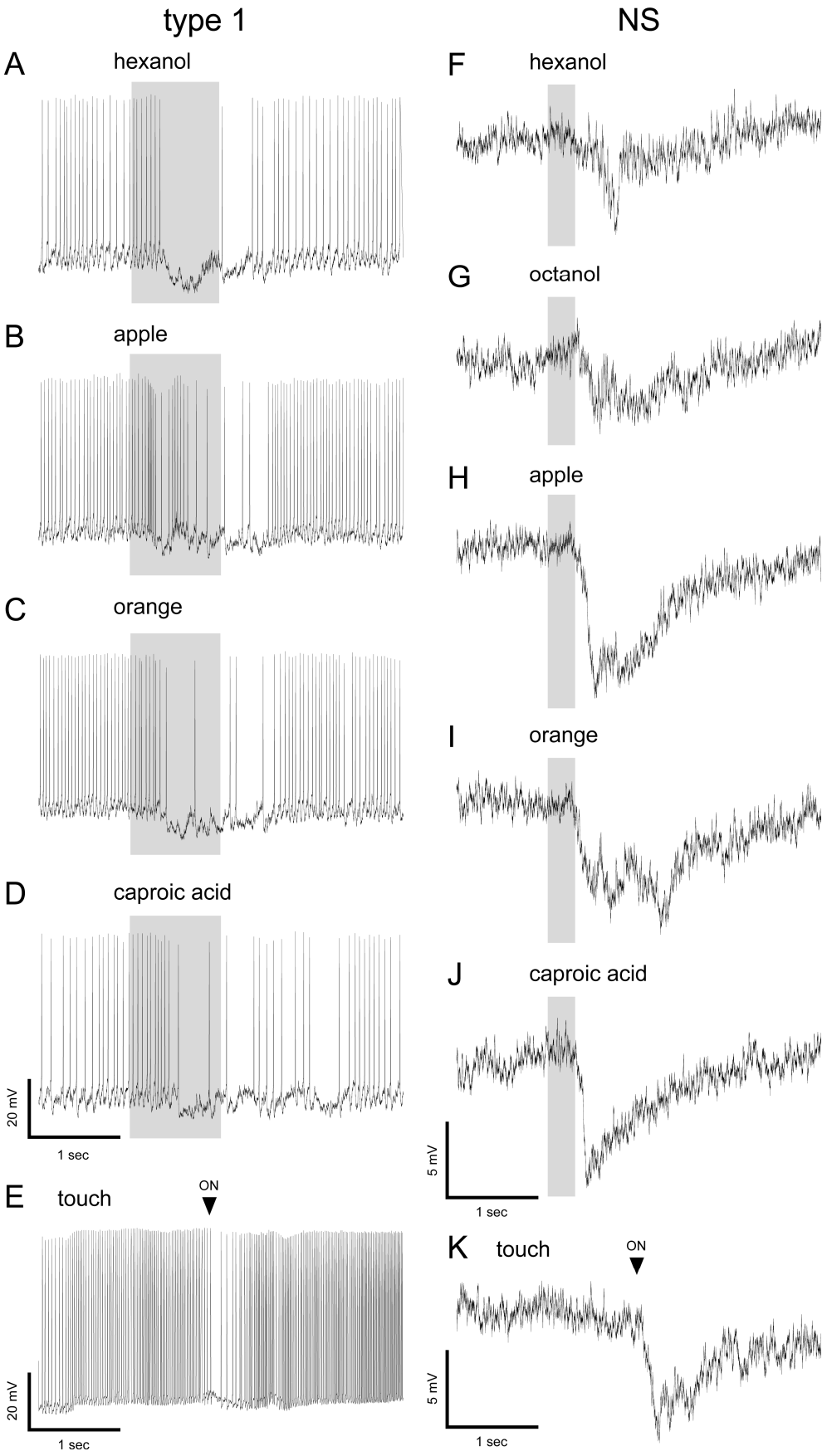

type 1
NS
A
hexanol
B
apple
C
orange
D
caproic acid
20 mV
1 sec
E
touch
ON
20 mV
1 sec
F
hexanol
G
octanol
H
apple
I
orange
J
caproic acid
5 mV
1 sec
K
touch
ON
5 mV
1 sec

**Figure 13.** Inhibitory responses to various odors (A–D; F–J) and tactile stimuli (E,K) in type 1 and NS CGs, which were not common but occurred in a few recording sessions.

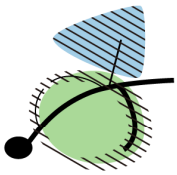
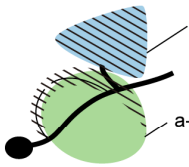
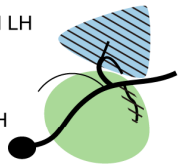
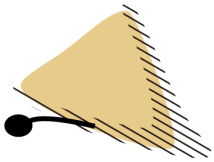
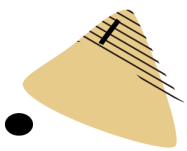
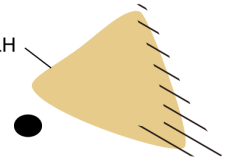
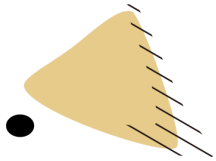
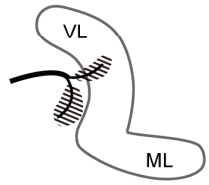
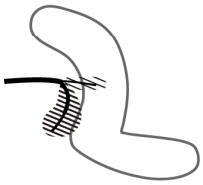
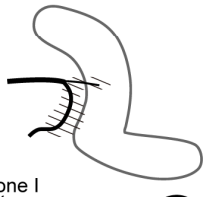
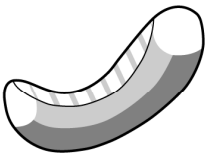
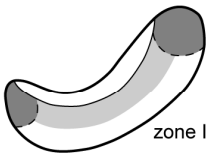
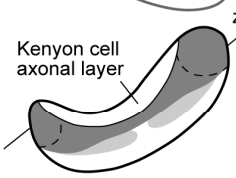
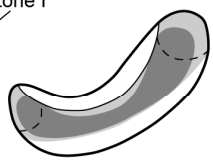
| CG types | type 1 | NS | type 2a | type 2b |
|---|---|---|---|---|
| **cell body diameter (μm)** | 43.9 ± 10.9 | 33.7 ± 1.5 | 30.2 ± 3.0 | 31.9 ± 2.8 |
| **branch width (μm)** | | | | |
| dendrites | 14.9 ± 2.3 | 6.8 ± 2.4 | 10.0 ± 2.4 | 9.6 ± 3.0 |
| axons | 8.3 ± 1.5 | 14.2 ± 1.0 | 5.8 ± 1.0 | 6.8 ± 1.2 |
| **arborization pattern** | | | | |
| a-d LH and a-v LH |  |  |  |  |
| p LH |  |  |  |  |
| lobes |  |  |  |  |
| calyx |  |  |  |  |
| **schematized waveform of synaptic potential** |  |  |  |  |

**Table 3.** Morphological and physiological characteristics of the four types of CGs. Morphological measurements expressed as means ± SD were made in four type 1 CGs, three NS CGs, four type 2a CGs, and four type 2b CGs. Cell body diameter is represented as the mean of major and minor axes. Dendritic width and axonal width were measured at the locations indicated by asterisks in Fig. 2D and in Fig. 2F, respectively.

# Chapter 2: Investigation of the mushroom body feedback circuit formed by calycal giants in the cockroach brain.

## Introduction

In Chapter 1, I succeeded in unambiguous identification of four tightly bundled gamma-aminobutyric acid (GABA)-immunoreactive giant interneurons, calycal giants (CGs). Consistent with putative feedback roles onto the mushroom body (MB), localization of synapsin-immunoreactive vesicles indicated that all CGs supply axon terminals almost exclusively to the input region of the MB, calyces. In the calyces, axon terminals of each CG innervate different peripheral-basal regions with some spatial overlap one another. Those terminal organizations of CGs correspond with the calycal zonation made by axon terminals of two populations of uniglomerular projection neurons (PNs): type 1 PNs and type 2 PNs. The four CGs, therefore, can be assigned to one type of type 1 CG, the largest spiking neuron, and other three types of type 2 CGs including a nospiking neuron (NS CG, type 2a CG, and type 2b CG) based on the definition by Strausfeld and Li (1999a). That suggests functional segregation among CGs to make different forms of inhibition on two parallel olfactory inputs to the MB. It needs investigation, however, whether axon terminals of each CG provide sufficient inhibition to a population of MB intrinsic neurons, Kenyon cells (KCs), during odor response.

Further investigation is also needed on input sites of CGs. Despite their putative roles of MB feedback inhibition, CGs have no dendrites in the MB and it remains unknown what kinds of neurons are intervened between CGs and the MB. One of the most-likely input sources of CGs is mushroom body output neurons (MBONs). Their dendrites in output region of the MB, lobes, are considered to receive convergent input from a population of KCs. Double labeling in Chapter 1 showed anatomical contacts between dendrites of type 1 CG and axon terminals of one type of MBON at the level of optical sections. Do those anatomical contacts mean synapses from the MBON to the type 1 CG? In addition, are there similar contacts between other combinations of a CG and a MBON?

In this Chapter, I performed paired intracellular recordings from a CG and a MBON and demonstrated CGs indeed comprise inhibitory feedback circuits. Each CG appears to receive excitatory synaptic inputs from a subset of MBONs and, conversely, activation of each CG inhibited activities of MBON by inhibiting activities of KCs.

## Materials and methods

### Animals

Total 218 adult male cockroaches were used for physiological experiment and morphological observation of CGs and/or MBONs. Animals were raised in the same manner as described in Chapter 1. I succeeded simultaneous recording from a CG and a MBON in 14 animals; Table 4 summarizes the recording details.

### Simultaneous recording

The procedures for animal preparation and intracellular recordings were almost the same as those described in Chapter 1. The neural sheath was softened by Actinase E (Kaken Seiyaku, Tokyo, Japan) and was removed mechanically with fine forceps if needed. The recording electrodes were inserted into the right hemisphere of the brain unless otherwise stated. Activities of CGs were recorded from the dendrites in the lateral horn (LH) or the axonal branches in the junction of the lateral and medial MB calyces while activities of MBONs were recorded from the dendrites in the MB lobes or the axonal branches running medio-laterally in the anterior surface of the brain. Neural activities were amplified and low-pass filtered at 30 kHz using amplifier, Axoclamp 2B (Axon Instruments Inc., Union City, CA, USA) in bridge mode or MEZ-8301 (Nihon Kohden, Tokyo, Japan), and then stored in a PC with a 10- or 20-kHz sampling rate using A/D converter, Micro1401-3 (Cambridge Electronic Design [CED], Cambridge, UK) and software, Spike2 ver. 6.18 (CED).

During recording, odor stimuli were delivered to the right antenna by continuous airflow system described in Chapter 1. A filter paper (5 × 40 mm) soaked with 15 µl of odorants, diluted 100 times by mineral oil (Wako, Osaka, Japan), were placed in a cartridge as an odor source. 1-hexanol, 1,8-cineol, 1-hexanal, and hexanoic acid were used as odorants (all odorants from Wako). The latency and the time-course of the odor delivery from the opening of solenoid valve wad measured by a photo-ionization detector (PID, Model 200B, Aurora Scientific Inc., ON, Canada) positioned in the center of the wind tunnel, at which the antenna is situated. It took approximately 71 ms from the onset of valve opening for PID voltage averaged over 3 trials exceeded 0 mV for 5 ms straight, so the value 71 ms was

added to the onset of valve opening when considering the latency of odor responses of neurons.

Some odor stimulations were accompanied by a hyper- or depolarized current injection into a CG through the recording electrode (duration: 1 s, amplitude: 10–15 nA). Injection was triggered by electric stimulator (SEN-8203; Nihon Kohden). Injection timing was stored in a PC with a 1-kHz sampling rate.

### Morphological observations

I used four types of dye for labeling recorded neurons: 1) 8% Lucifer Yellow (LY, Sigma-Aldrich, St. Louis, MO) in 1 M LiCl, 2) 2% Alexa Fluor 568 hydrazide (ThermoFisher Scientific, Pittsburgh, PA) in 1 M KCl, 3) 0.67% Alexa Fluor 555 hydrazide (ThermoFisher Scientific) in 1 M KCl and 4) 10% micro-Ruby (dextran, tetramethylrhodamine, and biotin, 3000 MW, ThermoFisher Scientific) in cockroach saline. Lucifer Yellow solution and Alexa Fluor 568 solution was used as described in chapter 1. Alexa Fluor 555 solution was injected by constant hyperpolarizing current (–1 to –5 nA) for 5–60 minutes while 10% micro-Ruby by depolarized current pulses (+ 10 to +20 nA) at 2 Hz for 10–20 minutes.

After experiments, the brain was incubated, dissected out, fixed, dehydrated, cleared, and observed under a confocal laser scanning microscope, LSM 5 Pascal (Carl Zeiss, Jena, Germany) in the same way as described in Chapter 1. Images were obtained using two objective lenses: Plan-Apochromat 10×/0.75 and oil-immersion Plan-Neofluar 40×/1.3 for high-magnification images. The laser and the filter set to visualize neurons filled with Alexa Fluor 568 was also applied for those filled with Alexa Fluor 555 or micro-Ruby. Optical sections were reconstructed two-dimensionally using image-processing software, LSM Image Browser (Carl Zeiss). In addition, highly-magnified optical sections were captured on LSM 880 with Airyscan Fast (Carl Zeiss) with a Plan-Apochromat 40×/1.3 objective lens. LY-labeled branches were visualized by 458-nm laser with a 495–550-nm bandpass filter while micro-Ruby-labeled branches by a 561-nm laser with a 570-nm longpass filter. The sections were three-dimensionally reconstructed using image processing software, Imaris ver. 9.0.0 (Bitplane AG, Zurich, Switzerland) to measure the distance between the branches. Two- or three-dimensionally reconstructed

images were processed in free photo-editing software, GNU Image Manipulation Program ver. 2.8.18 (GIMP Development Team, San Jose, CA), to adjust their brightness and contrast.

### Physiological data analysis

Spike timing was extracted from waveform data using a feature detection script on software Spike2 ver. 6.18. The following analysis were done on a free programming software R ver. 3.4.2 (R Foundation for Statistical Computing, Vienna, Austria)..

### Determination of odor responses

To determine whether a spiking neuron exhibits excitatory response to odor stimuli, I defined a response period as 300 ms from 200 + 71 ms after the solenoid valve opened, where the value 71 ms was added to correct the delay of the odor stimuli reaching the antenna (see Simultaneous recording section above). When [the averaged firing rate − standard deviation (SD)] during the response period exceeded the baseline rate, it was considered to be an excitatory odor response. The baseline rate was measured as the averaged firing rate over the continuous 20–35-s data. Odor response was evaluated without distinction of odor types because both CGs and MBONs showed similar responses to all odors used in this study. Odor stimuli accompanied by current injection into the CG were excluded from analysis. Following this criterion, MBONs in the left hemisphere (N = 3) had no excitatory responses to odor stimulation to the right antenna. In this study, odor response of a NS CG was not able to define because its activities varied among odors, trials, and animals. It was difficult to set a criterion of responses applicable to all data.

### Analysis of current injection experiment

To examine the effect of current injection into a CG on spike activities of a MBON, generalized linear models (GLMs) were constructed with Poisson distribution. The response variable was spike counts of a MBON during current injection to a CG while fixed effect was current types injected into the CG [no injection (0), hyperpolarizing (−) or depolarizing (+)]. The constructed model was compared

to the null model by likelihood ratio chi-square test with one degree of freedom. When the effect of current injection was considered to be significant ($P < 0.05$), Wald test was performed to coefficients estimated for each type of current (−, +) to examine which type of current had significant effect ($P < 0.05$). When the data were obtained from multiple individuals, generalized linear mixed models (GLMMs) with random effects of individual differences were constructed instead of GLMs.

In one paired recording of a type 1 CG and a medial lobe output neuron (MLON), depolarizing current was injected into the MLON, to examine whether action potentials of the MBON caused excitatory post synaptic potentials (EPSPs) in a dendritic branch of CG. It was not feasible to induce a single spike by injecting a brief depolarizing current into the MLON, so I injected 300-ms depolarizing current (+3 nA) to cause burst activities of the MLON. For the analysis, I used cases in which the action potentials of the MLON accompanied no immediately preceding or following action potentials (from −5 ms to +10 ms relative to the peak timing of the spike), and the membrane potential of CG generated no spikes. In paired recordings, action potentials in one neuron caused small cross-talk artifacts in the other. To cancel out the artifact, differentiated action potential of the MLON was subtracted from the averaged membrane potential of the CG.

### Cross-covariance analysis

The cross-covariance was measured based on binary spike sequences to quantify correlation levels between a type 1 CG and a MBON during their spontaneous and odor response activities. Continuous data without odor stimuli were used as spontaneous activity. The continuous data were divided into 1-s trials without no intervals for the analysis. As odor response activity, 1-s from 71 ms after the solenoid valve opened were used as one trial. Odor stimuli accompanied by current injection into a CG were excluded from analysis.

Each trial was divided into 1-ms bins representing 1 or 0 depending on whether it includes a spike or not. When $M$ represents the total trial number, and $t$ and $\tau$ represent time as number of 1-ms bins, the cross-covariance $C(\tau)$ was written as follows according to Brody (1999) and Bair et al. (2001);

$$C(\tau) = \frac{1}{M}\sum_{i}^{M}\sum_{t=1}^{1000} x_i(t)y_i(t+\tau) - \sum_{t=1}^{1000}\bar{x}\,(t)\bar{y}(t+\tau) \quad (1)$$

where $x_i(t)$ and $y_i(t)$ are the averaged firing rate at $t$th bin in $i$th trial while $\bar{x}$ and $\bar{y}$ are the averaged firing rate over the data. The first and second terms are the raw cross-correlation and the shuffle corrector, respectively. I divided $C(\tau)$ by the geometric mean firing rates (per sec) of neuron $x$ and neuron $y$ to obtain $COV(\tau)$, which is used to compare the cross-covariance among different recordings. For convenience, the term "covariance" is used for $COV(\tau)$ in this study. The correlation level between two neurons' activities was considered to be significant when $COV(\tau)$ exceeded more than two times of SD. When $\sigma(\tau)$ represent SD at $\tau$th bin, SD was written as follows according to Brody (1999).

$$\sigma(\tau) = \sqrt{\left(\sum_{t=1}^{1000}\sigma_x(t)^2\,\sigma_y(t+\tau)^2 + \sum_{t=1}^{1000}\bar{x}^2\,\sigma_y(t+\tau)^2 + \sum_{t=1}^{1000}\sigma_x(t)^2\bar{y}^2\right)/M} \quad (2)$$

where $\sigma_x(t)$ and $\sigma_y(t)$ represent SD of $x(t)$ and $y(t)$ among trials.

The auto-covariance was also measured in the same way as the cross-covariance assigning the same neuron to both neuron x and neuron y.

## Results

### Effect of CG activities on spike frequency of MBONs

Intracellular staining of individual CGs and subsequent synapsin-immunolabeling in Chapter 1 revealed localization of synapsin-immunoreactive vesicles in branches in the MB calyces but not in other areas, suggesting that the four CGs supply axon terminals almost exclusively to MB calyces. In addition, CGs responded to all odors used in Chapter 1 (organic alcohol, fatty alcohol, fatty acid, and food odors) usually with excitatory activities, i.e., an increase in the firing rate (type 1, 2a, and 2b CGs) or depolarization of the membrane potential (NS CG). Since CGs are GABA-immunoreactive, their excitatory responses to odors are considered to inhibit the activities of KCs, MB intrinsic neurons that are thought to play critical roles in odor discrimination and learning.

In order to obtain evidence that activation of a CGs indeed inhibit activities of KCs, I manipulated the activities of CGs by current injection through an intracellular electrode, simultaneously recording the activities of MBON, which are known to receive synapses from population of KCs (Fig. 14A). I injected a 1-s pulse current into a CG aligned to the onset of a 500-ms odor stimulation. The duration of the current injection completely covered the time range of the odor response (Fig. 14B,D). Spike frequency of the CG changed from 0 to 80 Hz during 10–15 nA hyperpolarizing or depolarizing current injection into a type 1 CG (Fig. 14C). The spike frequency of a simultaneously recorded MBON that innervate the tip of the medial lobe (ML) was well fitted by Poisson regression when spike frequency of type 1 CG during 1-s current injection was used as explanatory variable [Fig. 14C, $P < 0.05$ when it was compared to the model without explanatory variable (the null model) by likelihood ratio chi-square test]. It indicates that depolarization and hyperpolarization of the type 1 CG led to an excitation or inhibition of a population of KCs, and this effect was detected as an increase or decrease of spike frequency of the MLON.

Most of experiments in this chapter was performed on a MLON with the dendrites in the tip of the ML (ML tip ON) due to the following reasons. First, a ML tip ON had the thickest axons and the most characteristic overall morphology among MBONs (Fig. 15A,B), making it easier to identify among different individuals. In addition, when I injected dye into the ML for mass-staining of MBONs, I always

observed only one cell body of the ML tip ON that differs from surrounding cell bodies with different morphologies and with different axonal trajectories (Fig. 15C,D), suggesting one ML tip ON per hemisphere. Further, the ML tip ON exhibited responses to odor stimuli that were relatively consistent among different animals, allowing averaging of data from different animals.

Fig. 14E shows the spike activities of a ML tip ON during 1-s current injection into a type 1 CG in four animals including the one shown in Fig. 14C. Current injection into a CG significantly changed the spike frequency of the ML tip ON (N = 4, $P < 0.05$). Type 1 CG of one animal (grey symbol) and ML tip ON of two animals (open symbol) did not show excitatory odor responses, according to the criteria of this study described in Materials and methods. Although what caused the different odor response was unknown, whether or not to include neurons with no odor responses into the data did not change the statistical results. A CG depolarization (+) significantly decreased the spike frequency of the ML tip ON ($P < 0.05$) while CG hyperpolarization (−) did not significantly increased it ($P > 0.05$, table 5). However, when the neurons with no odor responses were excluded from the analysis, significant effect of CG hyperpolarization on the spike frequency of the ML tip ON was detected ($P < 0.05$). Current injection into a type 1 CG also significantly affected the spike frequency of another type of MBONs, output neurons at the junction of the lobes (JON; Fig. 14F, N = 1, $P < 0.05$). In this pair, only CG depolarization had significant effect on the spike frequency of the JON ($P < 0.05$, table 5). Conversely, no significant effect was detected on spike frequency of a ML tip ON in the contralateral (left) hemisphere of the brain, which did not respond to odor stimuli to the right antenna (Fig. 14G, N = 1, $P > 0.05$), indicating that the effect of the CG is confined to KCs of ipsilateral MB, as predicted from its morphology.

I also manipulated the activities of another type of CGs, NS CG. Since NS CG does not generate spikes, it responds to odor with graded changes in the membrane potential. Its typical odor responses are excitatory, in other words, transient depolarization, which are sometimes followed by hyperpolarization. I noted that the amplitude and the duration of depolarization varied among individuals and in even within an individual. The current injection into a NS CG significantly affected the spike frequency of a vertical lobe output neuron (VLON; Fig. 14I, N = 1, $P < 0.05$). In this pair, only CG

hyperpolarization had significant effect on the spike frequency of VLON ($P < 0.05$, table 5). In contrast to the results of current injection into a type 1 CG, however, current injection into a NS CG induced no significant effect on spike frequency of a ML tip ON, regardless of whether or not to include ML tip ON with no excitatory odor responses (Fig. 14H, N = 3, $P > 0.05$). Current injection into a NS CG induced no significant effect on a ML tip ON in the contralateral hemisphere of the brain, either (Fig. 14J, N = 1, $P > 0.05$). The results suggest that a CG inhibits many, but not all, KCs and this effect is found as changes of spike frequency in many, but not all, MBONs.

### Double labeling of a CG and a MBON

So far, direct input source of the CGs has been unknown, but one of the most-likely candidates is MBONs. As shown in Chapter 1, blebby axon terminals of a ML tip ON spatially overlapped largely with fine dendritic branches of a type 1 CG in the LH. Here, I performed additional double labeling experiments to further examine such overlaps. Double labeling of a type 1 CG and a ML tip ON in another individual (Fig. 15E) showed those overlaps in the LH (Fig. 15G) and the satellite neuropils anterior to the vertical lobe of MB (Fig. 15K). Remarkable extents of overlaps were observed in Fig. 15G,K despite of the thinness of stack (4 sections in 3.3μm for both). With higher magnification image captures and three-dimensional reconstructions, those overlaps in the LH were estimated as contact between branches of the two neurons, strongly suggesting synaptic connection (Fig. 15F, shaded points indicated by black arrowheads).

I also investigated the overlaps in the two-dimensionally reconstructed view in pairs of a type 2a or a 2b CG and a ML tip ON (Fig. 15I,J,M,N). I observed slight overlaps in those pairs, although extents of overlaps were slightly less than those of type 1 CG. Dendrites of a NS CG, on the other hand, had few overlaps with a ML tip ON (Fig. 15H,L) but tended to overlap with axonal branches of a VLON (Fig. 15Q,R). Together with much less extent of overlapping of type 1 CG to VLON than to a ML tip ON (chapter1, Fig. 15O,P), the observation indicates that the extent of contacts varies among types of CGs and MBONs.

### Depolarization of CG membrane potential follows the action potentials of a MBON

To examine whether action potentials of a MBON cause EPSPs in the membrane potential of a CG, a depolarizing current was injected into a ML tip ON thorough the recording electrode simultaneously recording the membrane potential of a type 1 CG from the dendrites (N = 1). Depolarizing current injection (300 ms; +3 nA) into the dendrites of the ML tip ON caused burst spike activities (Fig. 16A). EPSPs were not clearly observed in single traces of the type 1 CG membrane potential aligned to the peak of action potentials of the ML tip ON (Fig. 16B,C) due to large fluctuation of the CG membrane potential possibly by spontaneous EPSPs and inhibitory postsynaptic potentials (IPSPs). However, when 250 traces were averaged, a small amount of depolarization was observed following the cross-talk artifact caused by the action potential of the ML tip ON (Fig. 16D, black). To partially cancel out the artifact I subtracted the differentiated action potential of ML tip ON (Fig. 16D, red) from the averaged CG membrane potential. As a result, the depolarization of CG membrane potential was more remarkable (Fig. 16E). The peak amplitude of depolarization was +0.238 mV 3.6 ms after the peak of the action potential of the ML tip ON. This is no doubt EPSPs caused by action potential of the ML tip ON, indicating synaptic input from a MBON to a CG. Unfortunately, similar experiments were not feasible in other pairs of a CG and a MBON due to large membrane fluctuations and/or frequent spike bursts of the CG.

### Cross-covariance analysis

As shown in Chapter 1, type 1 CG usually exhibited endogenous activities comprising episodic bursts of spikes even without a specific stimulus externally and showed excitatory responses to odor stimuli. ML tip ON also exhibited endogenous activities and excitatory responses to every odor stimuli used in this study. Interestingly, timing of burst activities seemed well coincident between the two neurons recorded simultaneously, although some spike bursts and solitary spikes seen in ML tip ON were occasionally absent in type 1 CG. To quantify correlation levels of spike timings between the two neurons, cross-covariance was measured from 1-s binary spike sequence data divided into 1-ms bins. Cross-covariance represented shuffle-corrected cross-correlation, in which shuffling allows to remove

the effect of firing rate changes induced by external sensory stimuli (see Material and methods; Brody, 1999). One recording was excluded because only two trials of odor stimuli was done without current injection into a type 1 CG (Table 4).

During spontaneous spike activities where no odor stimuli were applied, cross-covariograms had broad peak, with significant level of covariance (> 2 SD, gray area in Fig. 17) being in the −80 to +30 ms time-lag range and with the peak at −27 ms or 0 ms. On the other hand, cross-covariograms measured during odor responses had an extremely sharp peak with significant level of covariance being in the −4 to 0 ms time-lag range and with the peak at −2or −1 ms. The occurrence of the peak at −1 ms delay time to the spikes of ML tip ONs from those of the CG support that the ML tip ONs makes monosynaptic connections with the type 1 CG, although the possibility of common synaptic input to both neurons should also be considered (see Discussion). Notice that the broad peak of cross-covariograms in the spontaneous activities did not disappear in those of odor responses. It was just obscured in the process of dividing $C(\tau)$ by the geometric mean firing rates of neurons (see Materials and methods). Cross-covariogramas not divided by the firing rate are shown in Fig. 18. Here, the sharp peak and the broad peak (half value of the sharp peak) coexisted during odor response although the broad one was difficult to see in the pairs with only a few trials available for the analysis.

In another pair (pair #3) of a type 1 CG and an ML tip ON, the type 1 CG fired less frequently during spontaneous activities than typical type 1 CG (inset in Fig. 17C). Its excitatory responses to odor stimuli consisted of spikes of less than ten. Infrequent spike bursts and occasional solitary spikes of CG, however, seemed to coincident with those of the ML tip ON. During spontaneous activities, the cross-covariance of spike counts occasionally exceeded the significant level in the −15 to +30 ms time-lag range, but a broad peak observed in pair #1 and #2 was absent. This may partly reflect the calculation method of this study, which tends to estimate low values of cross-covariance when the data consisted of very few spikes. During odor responses, these neurons produced only a few more spikes than during spontaneous activities. On account of this, the cross-covariogram had a sharp peak similar to those of pair #1 and #2. In pair #4, an ML tip ON showed injury-induced high-frequency spike activities, making odor responses undetectable (inset in Fig. 17D). In this pair, cross-covariogram fluctuated below the

non-significant level (Fig. 17I). In pair #5, a type 1 CG and a ML tip ON showed spontaneous activities typical of these neurons but showed no excitatory responses to odor stimuli (inset in Fig. 17E,J). As expected, cross-covariogram had a broad peak regardless of the presence or absence of odor stimulations (Fig. 17E,J) .

Another type of MBON, a JON was recorded simultaneously with a type 1 CG (pair #6). The JON had dendrites in the junction between the vertical and the medial lobes of the MB and axon terminals in the LH and the satellite neuropils anterior to the lobes. The JON exhibited spontaneous burst activities and excitatory responses to odor stimuli with transient increases in firing rate (insets in Fig. 19A,D) as a ML tip ON. Cross-covariogram of this pair was broad with significant level of covariance in the −70 to +60 ms time-lag range during spontaneous activities and sharp with significant covariance at the −3 ms time-lag point during odor responses (Fig. 19A,D). This was similar to those observed in pairs of a type 1 CG and an ML tip ON.

I happened to record from an ML tip ON in the contralateral (left) hemisphere of the brain simultaneously with a type 1 CG in two pairs (pairs #7 and #8), and examined cross-covariance between them as control (Fig. 19B,C,E,F). A ML tip ON in the left hemisphere had no dendrites of axon terminals in the right hemisphere and, as expected, it showed no excitatory response to odor stimuli to the right antenna (insets in Fig. 19E,F). The two neurons' activities did not seem to correlate with each other. In accordance with this, cross-covariance was below significant level in almost all time-lag range. Although there was a significant level of covariance peak, it was much smaller and far away from zero time-lag point, in contrast to robust cross-correlation with its peak near zero point found between a type 1 CG and a ML tip ON of the same side. The results indicate no physiological connections between a type 1 CG and a contralateral ML tip ON, providing a control to show that robust cross-correlations between a type 1 CG and an ipsilateral ML tip ON indeed reflects signal transmission in neural circuits in the same hemisphere.

In locusts, MB extrinsic neurons exhibit oscillatory spike activities (Gupta and Stopfer, 2012). If the same is the case in cockroaches, they should highly influence synaptic transmission from the MBONs to CGs. I thus measured auto-covariances of each neuron in pair #1. Both type 1 CG (Fig.

20A,C) and the ML tip ON (Fig. 20B,D) showed auto-covariance with an extremely sharp peak (> +0.8) at time-lag 0 typical of white noise, independently of presence or absence of odor stimuli but they exhibited no periodic covariance peaks, thus they indicate no evidence of oscillatory spike activities in both neurons.

## Discussion

In Chapter 1, I reported four types of CGs that are GABA-ergic and supply axon terminals to the calyces while dendrites to the LH and the lateral protocerebrum. Those dendrites appear to be overlapped with axon terminals of the MBONs. In this chapter, I performed paired intracellular recordings from CGs and MBONs and investigated whether it is feasible to show CGs are indeed feedback neurons of the MB, namely these neurons inhibit activities of MB intrinsic neurons KCs and receive synaptic inputs from MBONs.

### CGs inhibits KCs in the MB calyces during odor response

My paired recordings from a CG and a MBON showed depolarizing or hyperpolarizing current injection into a CG decrease or increase spike activities of some MBONs, demonstrating that axon terminals of CGs in the calyces make inhibitory synapses to control activities of KCs. Inhibitory effects of the CGs is confined to KCs of the ipsilateral MB as predicted from its morphology. It remains to be studied whether CGs provide inhibitory input to dendrites of KCs or to axon terminals of PNs. The former possibility is supported by the finding that cockroach KCs possess GABA receptors (Sattelle et al., 2000; Blankenburg et al., 2015) but the latter possibility cannot easily be denied because inhibitory synapses onto PN terminals have been observed in the honeybee (Ganeshina and Menzel, 2001) and the fruit fly (Yasuyama et al., 2002).

In other paired recordings, however, I observed no effect of current injection into the NS CG to spike activities of the ML tip ON, suggesting that each type of CGs inhibit not all KCs but a specific subset of KCs. This agrees with the morphological observation in Chapter 1; axon terminals of each type of CGs cover partly overlapped but different area of the calyces. Together with segregation of target

KCs, there may be redundancy to make up for the shortage of inhibition other CGs provide. Hyperpolarizing current injection into a type 1 CG had modest effect on spike activities of a ML tip ON compared to depolarizing current and had no significant effect on that of JON (Table 5, absolute value of estimated coefficient and the results of Wald test). This is best explained if a different level of inhibitory synaptic transmission is maintained from other CGs to KCs that make synaptic connections with the ML tip ON and JON. More studies are needed to clarify this.

In contrast to pairs of a type 1 CG and a ML tip ON/JON, only hyperpolarizing current injection to a NS CG had significant effect on spike activities of a VLON. Although I did not measure how much the membrane potential of the NS CG was hyperpolarized by current injection, the results suggest the importance of hyperpolarization sometimes following depolarization in odor responses of NS CGs (Fig. 12R,S in Chapter 1). This disinhibition allows the MB to transmit the olfactory input with a specific time interval (100~ ms) more effectively. Because the antennae receive odor with an intermittent pattern of odor filament (Huston et al., 2015), disinhibition with a specific time interval may be an efficient way to get close the odor source.

### Evidence to support direct synaptic inputs from MBONs to CGs

My anatomical investigation showed close proximity of axon terminals of MBONs and dendrites of the CGs both in the LH and the satellite neuropils anterior to the VL. (Fig. 15G,I–K,M,N,R). Three-dimensional reconstruction of high-magnification images of branches of a type 1 CG and those of a ML tip ON detected occasional contacts between them (Fig. 15F). I found that the possible contacts between a MBON and a CG are rather rare, possibly reflecting convergent input from many MBONs to a CG.

My physiological investigation provided a consistent view to those morphology. In one paired recording of a type 1 CG and a ML tip ON, I observed EPSPs in the type 1 CG following the action potentials of the ML tip ON (Fig. 16). The peak amplitude of post synaptic potential, however, was quite small (0.238 mV). It probably reflects (i) a high convergence ratio from MBONs to a given CG, (ii) CG membrane potentials continuously fluctuated by sub- and supra-threshold activities, and (iii) possibly

inputs from neurons other than MBONs. Although similar experiments should be done in more combinations of a CG and a MBON to confirm whether the same results are obtained from only specific pairs with anatomical overlaps, EPSPs observed in this experiment are strong evidence supporting synaptic inputs from MBONs to a CGs.

Cross-covariance analysis also supports synaptic connection between them. Significant cross-covariances of spike activities were observed between pairs of type 1 CG and a ML tip ON/a JON. Control experiment with paired recordings from a type 1 CG and a ML tip ON in the left hemisphere showed no observable covariances in their activities. In general, covariances between the activities of two neurons are considered to be caused by synaptic connections between them and/or common input source to them. It can be argued, however, that without assuming synaptic connections from MBONs to CGs, it is very difficult to account for a sharp peak in the cross-covariograms during olfactory stimuli (Figs. 17F,G,H, 19D). First, there have been no report of neurons with possible monosynaptic connections both to CGs and MBONs in the cockroach. Second, when we consider the possibility that PNs are common input source, it should be pointed that there are no PNs make direct synapses with both neurons (blue pathway in Fig. 20) and thus unlikely to produce sharp peak cross-covariance. For example, MBONs receive inputs from uniglomerular PNs and some types of multiglomerular PNs via MB intrinsic neurons KCs in the MB. Dendrites of CGs in the LH, though, do not invade the area where those type of PNs supply abundant terminals (Fig. 11G in Chapter 1), thus some interneurons need to be assumed to intervene between them. Another candidate is olfactory sensory neurons on the antenna further upstream of PNs, because potent synaptic connections are observed between CGs and multiglomerular neurons without axon terminals in the MB calyces (Fig. 11H in Chapter 1). It is almost unlikely that those segregated pathways could lead to the −3 to −1 ms time-lag range in the cross-covariogram between spike activities of CGs and those of MBONs during odor responses. Therefore, the sharp peak of cross-covariance observed in this study is a strong evidence supporting direct synaptic connection from MBONs to CGs together with other results.

**Synchronized spike activities at the onset of odor responses in a type 1 CG and a MBON**

Cross-covariograms of spike activities between a type 1 CG and a MBON had the peak broad in the delay-time range (−80 to +30 ms) during their spontaneous activities. During odor response, that broad peak was obscured by an extremely narrow peak (a few milliseconds in the time-lag range) at −3 to −1 ms. The amplitude of the peak during odor response was twice as large as that of spontaneous activities when the covariance was not corrected by the firing rate of the neurons. What caused different covariances between a type 1 CG and a MBON in spontaneous activities and odor response? In locusts, the follower neurons of KCs, including the giant GABAergic neuron GGN, exhibit activities phase-locked with those of MB oscillating synaptic activities of KCs at 15–30 Hz (Gupta and Stopfer, 2011). That is enough to make spike activities of multiple KCs synchronized (Gupta and Stopfer, 2012) but spike activities of type 1 CGs and MBONs recorded in this study in cockroaches did not show oscillation (see auto-covariograms typical of white noise in Fig. 20). Therefore, other neural mechanism is needed to describe the significant covariance observed in this study. There also remains to be studied whether spike activities of different MBONs are temporally synchronized with one another and whether activities of type 2 spiking CGs and NS CG also synchronized with those of MBONs.

| CG/MBON | firing rate (Hz) sponta-neous | odor | respon se | current injection to CG (Fig. 14) | to MBON | cross-covariance |
|---|---|---|---|---|---|---|
| type 1 | 7.2 | 16.3 | | – | Fig. 16 | pair #1 |
| ML tip | 9.7 | 21.5 | | | | |
| type 1 | 9.2 | 37.3 | | – | – | pair #2 |
| ML tip | 8.2 | 14.8 | | | | |
| type 1 | 0.3 | 5.7 | | C,D (red) | – | pair #3 |
| ML tip | 4.5 | 19.1 | | | | |
| type 1 | 9.7 | 26.5 | | D (purple) | – | pair #4 |
| ML tip | 54.5 | 44.3 | – | | | |
| type 1 | 4.0 | 6.2 | – | D (grey) | – | pair #5 |
| ML tip | 22.6 | 22.2 | – | | | |
| type 1 | 1.2 | 6.0 | | D (blue) | – | – (not enough trials) |
| ML tip | 14.8 | 22.8 | | | | |
| type 1 | 13.3 | 28.8 | | E (red) | – | pair #6 |
| J | 30.1 | 53.6 | | | | |
| type 1 | 3.5 | 18.4 | | F (red) | – | pair #7 |
| ML tip (left) | 18.8 | 16.3 | – | | | |
| type 1 | 1.3 | 19.3 | | F (blue) | – | pair #8 |
| ML tip (left) | 20.6 | 4.4 | – | | | |
| NS | – | – | | G (red) | – | – |
| ML tip | 21.4 | 28.7 | | | | |
| NS | – | – | | G (blue) | – | – |
| ML tip | 2.1 | 15.5 | | | | |
| NS | – | – | | G (purple) | – | – |
| ML tip | 50.9 | 40.7 | – | | | |
| NS | - | – | | H (red) | – | – |
| VL | 15.8 | 28.9 | | | | |
| NS | – | – | | I (red) | – | – |
| ML tip (left) | 18.9 | 23.7 | – | | | |

**Table 4.** Paired recordings used for the analysis. Firing rate was the averaged rate estimated from the data for cross-covariance analysis. The same procedure was performed for the neurons not used for cross-covariance analysis. –: impossible to calculate, no odor response, or not used for the analysis.

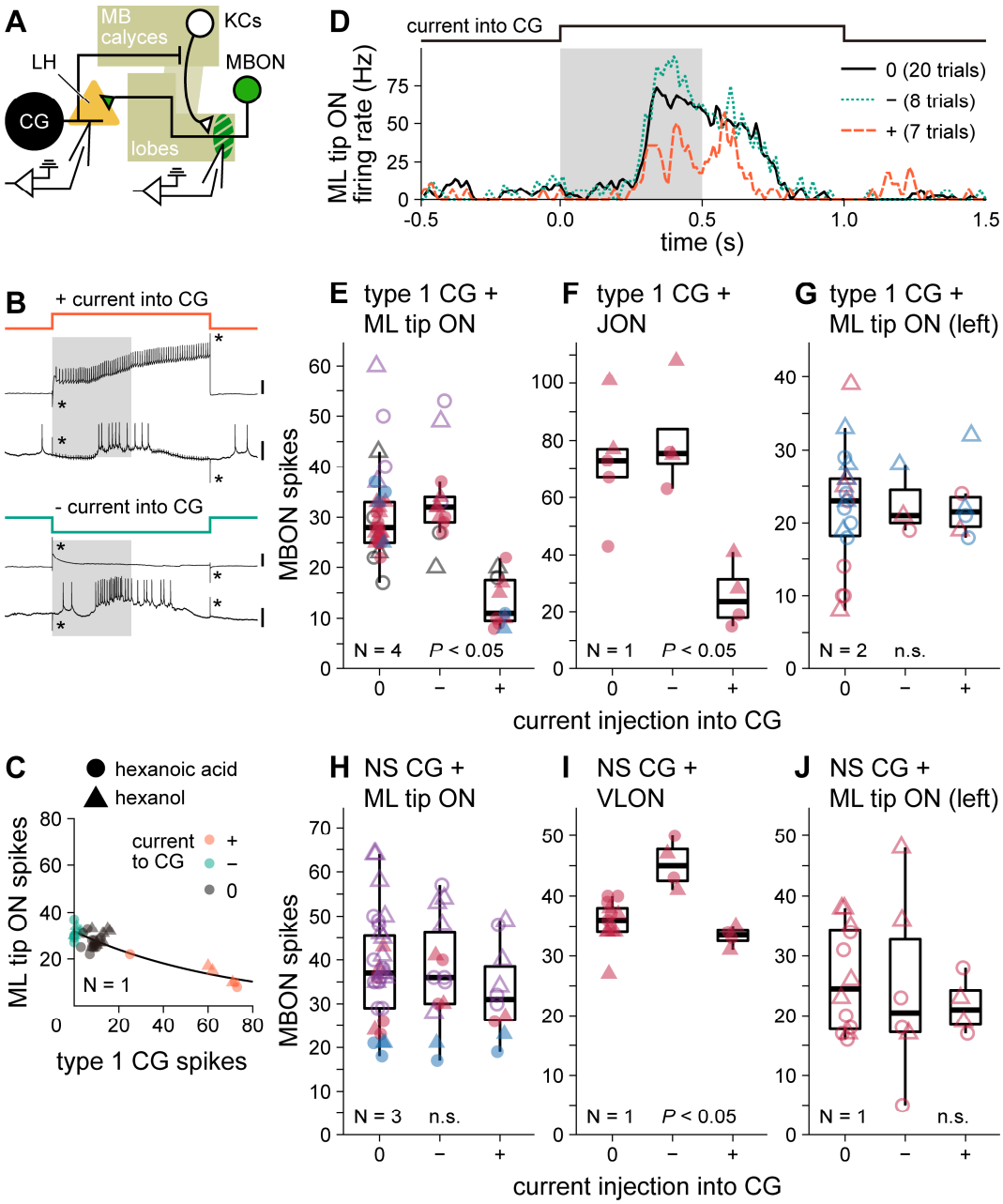

A
MB calyces
KCs
LH
MBON
CG
lobes
D
current into CG
ML tip ON firing rate (Hz)
0 (20 trials)
− (8 trials)
+ (7 trials)
time (s)
B
+ current into CG
- current into CG
E type 1 CG + ML tip ON
F type 1 CG + JON
G type 1 CG + ML tip ON (left)
MBON spikes
N = 4 P < 0.05
N = 1 P < 0.05
N = 2 n.s.
current injection into CG
C
hexanoic acid
hexanol
current to CG
ML tip ON spikes
N = 1
type 1 CG spikes
H NS CG + ML tip ON
I NS CG + VLON
J NS CG + ML tip ON (left)
MBON spikes
N = 3 n.s.
N = 1 P < 0.05
N = 1 n.s.
current injection into CG

**Figure 14.** Effects of current injection into a calycal giant neuron (CG) on spike activities of a mushroom body output neuron (MBON) during odor stimulation. **A:** Schematic diagram of paired recording. Electrodes were inserted in either the dendrites or the axonal branches of the neurons. **B:** Examples of 1-s depolarizing (top) or hyperpolarizing (bottom) current injection into a type 1 CG (upper traces, scale bars = 50 mV). A medial lobe output neuron (ML tip ON) was recorded simultaneously (lower traces, scale bars = 10 mV). Gray rectangles show 500-ms odor stimuli. Asterisks indicate artifacts caused by current injection. **C:** Spike frequency of a ML tip ON during the current injection into a type 1 CG is plotted against that of the type 1 CG in a paired recording. Differently colored symbols represent depolarizing (+: orange), hyperpolarizing (−: green), or no current (0: gray) was injected into the CG. The most-likely-fitting curve estimated by Poisson regression is shown ($P < 0.05$ when it was compared to the null model by likelihood ratio chi-square test). **D:** Firing rate change of a ML tip ON during current injection into a CG in the pair shown in C. Gray rectangles show 500-ms odor stimuli. Three lines represent firing rate during depolarizing (+: orange-dashed), hyperpolarizing (−: green-dotted), or no current (0: black-solid) injection into the CG. **E–J:** Spike frequency of a MBON during odor stimulation plus current injection into a type 1 CG (E–G) or a nonspiking (NS) CG (H–J). Differently colored symbols in each panel represent recordings from different individuals. Red symbols in E correspond to the data shown in C. MBONs and a type 1 CG without excitatory responsiveness to odors are represented by open and black symbols, respectively. Results of likelihood ratio test to examine the significant effect of current injection are shown at the bottom of each plot. See also table 5 summarizing the statistical results of current injection experiments.

| CG | MBON | pair | likelihood ratio test | + / − | coef | SE | z | Wald test |
|---|---|---|---|---|---|---|---|---|
| type 1 | ML tip | N = 4 | * | + | -0.760 | 0.089 | -8.564 | * |
| | | | | − | 0.040 | 0.059 | 0.674 | n.s. |
| | (odor-response pairs only) | N = 2 | * | + | -0.852 | 0.103 | -8.302 | * |
| | | | | − | 0.090 | 0.074 | 1.224 | * |
| | J | N = 1 | * | + | -1.031 | 0.112 | -9.229 | * |
| | | | | − | 0.109 | 0.077 | 1.420 | n.s. |
| | ML tip (left) | N = 2 | n.s. | | | | | |
| NS | ML tip | N = 3 | n.s. | | | | | |
| | (odor-response pairs only) | N = 2 | n.s. | | | | | |
| | VL | N = 1 | * | + | -0.073 | 0.098 | -0.743 | n.s. |
| | | | | − | 0.235 | 0.088 | 2.684 | * |
| | ML tip (left) | N = 1 | n.s. | | | | | |

**Table 5.** Effects of current injection into a CG on spike activities of a MBON. + / −, depolarizing- or hyperpolarizing current (10–20 nA), coef, coefficient; SE, standard error. * $P < 0.05$; n.s. not significant.

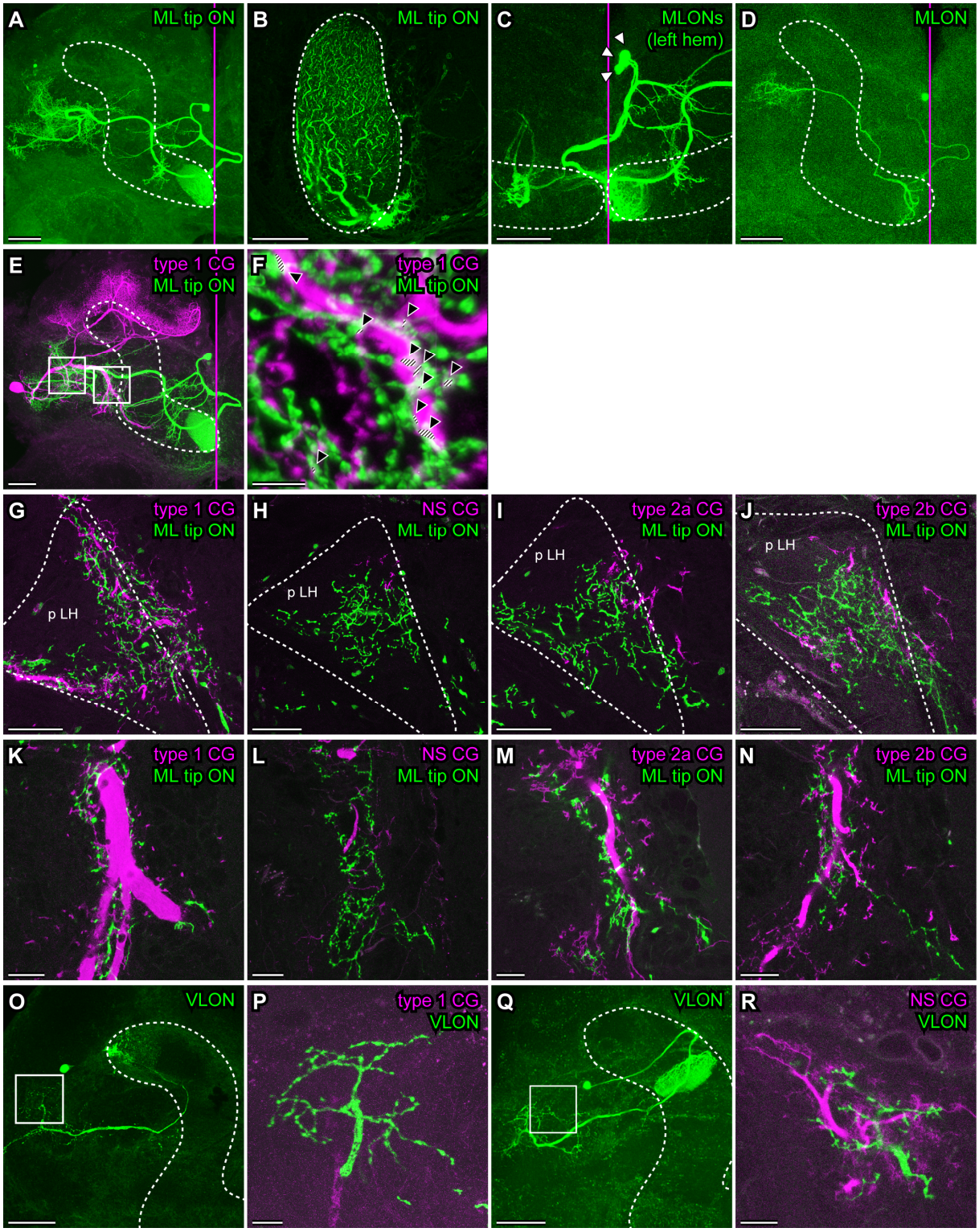

A
ML tip ON
B
ML tip ON
C
MLONs
(left hem)
D
MLON
E
type 1 CG
ML tip ON
F
type 1 CG
ML tip ON
G
type 1 CG
ML tip ON
p LH
H
NS CG
ML tip ON
p LH
I
type 2a CG
ML tip ON
p LH
J
type 2b CG
ML tip ON
p LH
K
type 1 CG
ML tip ON
L
NS CG
ML tip ON
M
type 2a CG
ML tip ON
N
type 2b CG
ML tip ON
O
VLON
P
type 1 CG
VLON
Q
VLON
R
NS CG
VLON

**Figure 15.** An occasional close apposition of axonal branches of MBONs and dendrites of CGs. **A–D:** All ML tip ONs recorded and stained in this study had the dendrites in the tip of the ML (A, whole morphology; B, sagittal section of the ML viewed medially). C, Dye injection into the ML revealed three cell bodies (white arrowhead), one of which is of one ML tip ON (C, ML tip ONs in the left hemisphere stained) the other is of a MBON with dendrites next to the tip of the ML (D, intracellularly stained in another individual) and the remaining is that of neurons with dendrites in contralateral ML. **E:** A low magnification confocal image of a type 1 CG (magenta) and a ML tip ON (green) labeled with different dyes. White rectangles represent the posterior lateral horn (p LH, left) and the satellite neuropils anterior to the vertical lobe (VL, right), which are magnified in the following panels. **F:** 3D view of branches of a ML tip ON (green) and a type 1 CG (magenta) in the p LH reconstructed from high-magnification optical sections. Shaded points indicated by black arrowheads show possible contacts between the branches of two neurons, overlapping images detected by image processing software, indicating possible contracts of branches between the two neurons. **G–H:** Differently labeled branches of a largest ML tip ON (green) and a CG (magenta) in the p LH (A–D) and the satellite neuropils anterior to the VL (E–H). The axonal branches of the ML tip ON overlapped more with the dendrites of type 1 CG than those of a NS CG. **O–R:** Differently labeled branches of a VLON (green) and a type 1 CG (magenta, P) or a NS CG (magenta, R). The overall morphologies of VLON in P and R are shown in O and Q, respectively. Unlike ML tip ON, axonal branches of the VLON have less overlap with dendrites of type 1 CG than those of NS CG. White dashed lines indicate the MB lobes in all panels except those in G–J indicating the p LH. Magenta vertical lines indicate the midline of the brain. Number and depth of confocal sections used for 2D or 3D reconstructions are as follows. A: 161 sections in 368 µm; B: 115 sections in 114 µm; C: 90 sections in 267 µm; D: 38 sections in 185 µm; E: 49 sections in 364 µm; F: 83 sections in 18.1 µm; G: 4 sections in 3.3µm; H: 6 sections in 5.5 µm; I: 4 sections in 3.3 µm; J: 6 sections in 5.5 µm; K: 4 sections in 3.3 µm; L: 7 sections in 6.6 µm; M: 4 sections in 3.3µm; N: 4 sections in 3.3 µm; O: 50 sections in 294 µm; P: 10 sections in 54 µm; Q: 11 sections in 200 µm; R: 7 sections in 7.2 µm. Scale bars = 100 µm in A,C–E,O,Q; 50 µm in B,G–J,P,R; 20 µm in K–N; 5 µm in F.

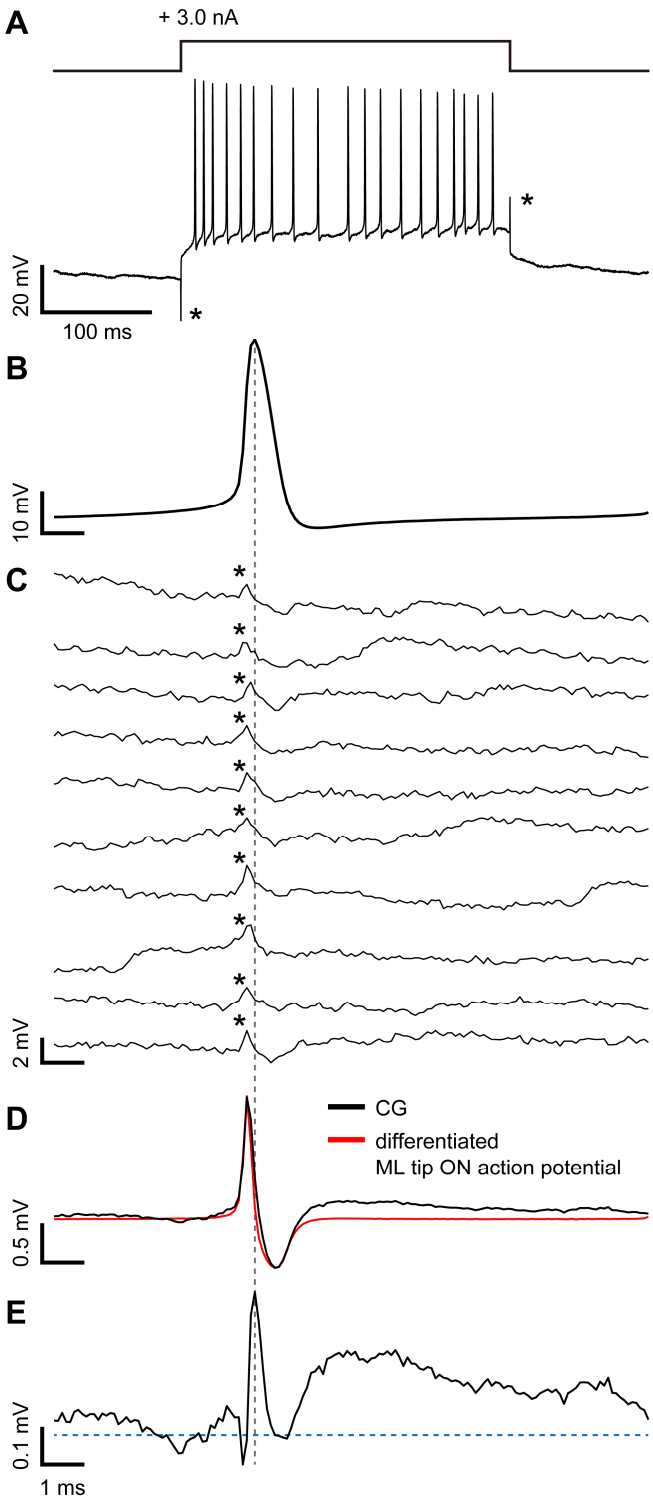

A
+ 3.0 nA
20 mV
100 ms
B
10 mV
C
2 mV
D
CG
differentiated
ML tip ON action potential
0.5 mV
E
0.1 mV
1 ms

**Figure 16.** Depolarization of a CG follows action potentials of a ML tip ON. Data were obtained from 250 events in one paired recording of a type 1 CG and a ML tip ON. **A:** A burst spike activity of the ML tip ON caused by depolarizing current injection. * shows artifacts caused by current injection. **B:** Averaged action potentials of the ML tip ON used for the analysis. Vertical dashed line shows the peak timing of action potential. **C:** Typical traces of membrane potential of a CG aligned to the peak of the action potentials of the ML tip ON. * shows artifacts caused by cross talk between the recording electrodes. **D:** Averaged membrane potential of the CG (black). To cancel out the artifact of the CG, the averaged action potential of the ML tip ON (A) was differentiated and subtracted from the artifact of the CG, with its amplitude fitted to the artifact (red). **E:** Remainder after subtracting the differentiated action potential of the ML tip ON from the averaged membrane potential of the CG. Although the artifact was not completely canceled out, a small amount of depolarization of CG (< 0.25 mV) was clearly detected; depolarization peak was 3.6 ms after the peak of action potential of the ML tip ON. Horizontal dashed line shows the baseline of the membrane potential of the CG.

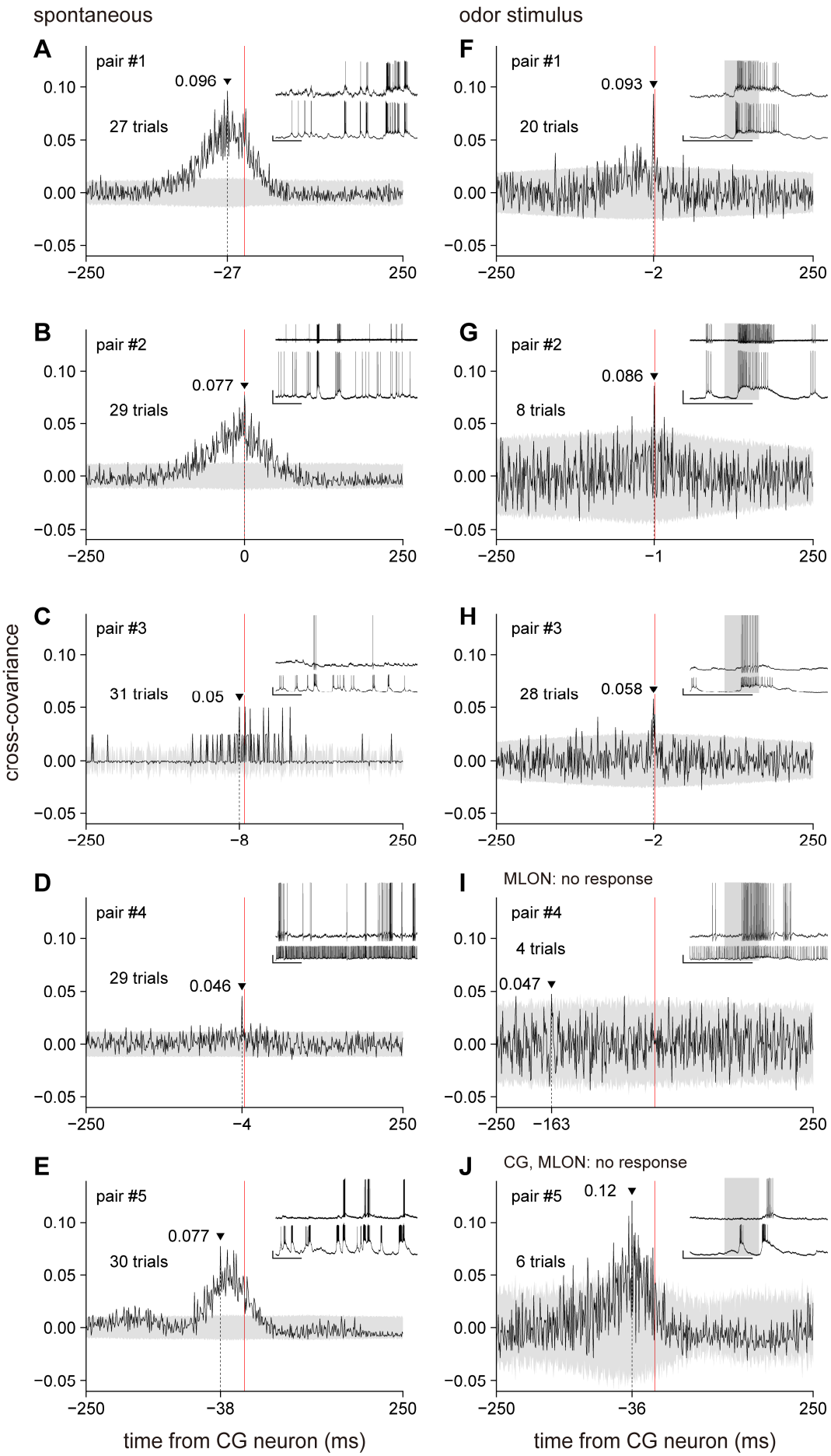

spontaneous
odor stimulus
A
pair #1
0.096
27 trials
F
pair #1
0.093
20 trials
B
pair #2
0.077
29 trials
G
pair #2
0.086
8 trials
C
pair #3
31 trials
0.05
H
pair #3
28 trials
0.058
D
pair #4
29 trials
0.046
I
MLON: no response
pair #4
4 trials
0.047
E
pair #5
0.077
30 trials
J
CG, MLON: no response
pair #5
0.12
6 trials
cross-covariance
0.10
0.05
0.00
−0.05
−250
−27
−2
0
−1
−8
−4
−163
−38
−36
250
time from CG neuron (ms)
time from CG neuron (ms)

**Figure 17.** Cross-covariograms between a type 1 CG and a ML tip ON. **A–E:** During spontaneous activities. **F–J:** During odor stimulation. Cross-covariance $COV(\tau)$ was measured by adding time lag to the activities of ML tip ON. Two cross-covariograms in each row show a single pair. In two pairs at the bottom, type 1 CG and/or ML tip ON had no excitatory responsiveness to odor. Gray area covers two times of standard deviation (SD) range. When $|COV(\tau)| > 2 \times$ SD, the maximum value and the time lag to obtain it were indicated in the cross-covariogram. Red vertical line shows time lag 0 ms. Insets are the part of neural activities used for analysis; top: CG, bottom: ML tip ON. Gray rectangles in insets in F–J represent 500-ms odor stimulation after being corrected the delay for the odor stimuli to reach the right antenna. Scale bars in insets are 10 mV (vertical) and 1 s (horizontal).

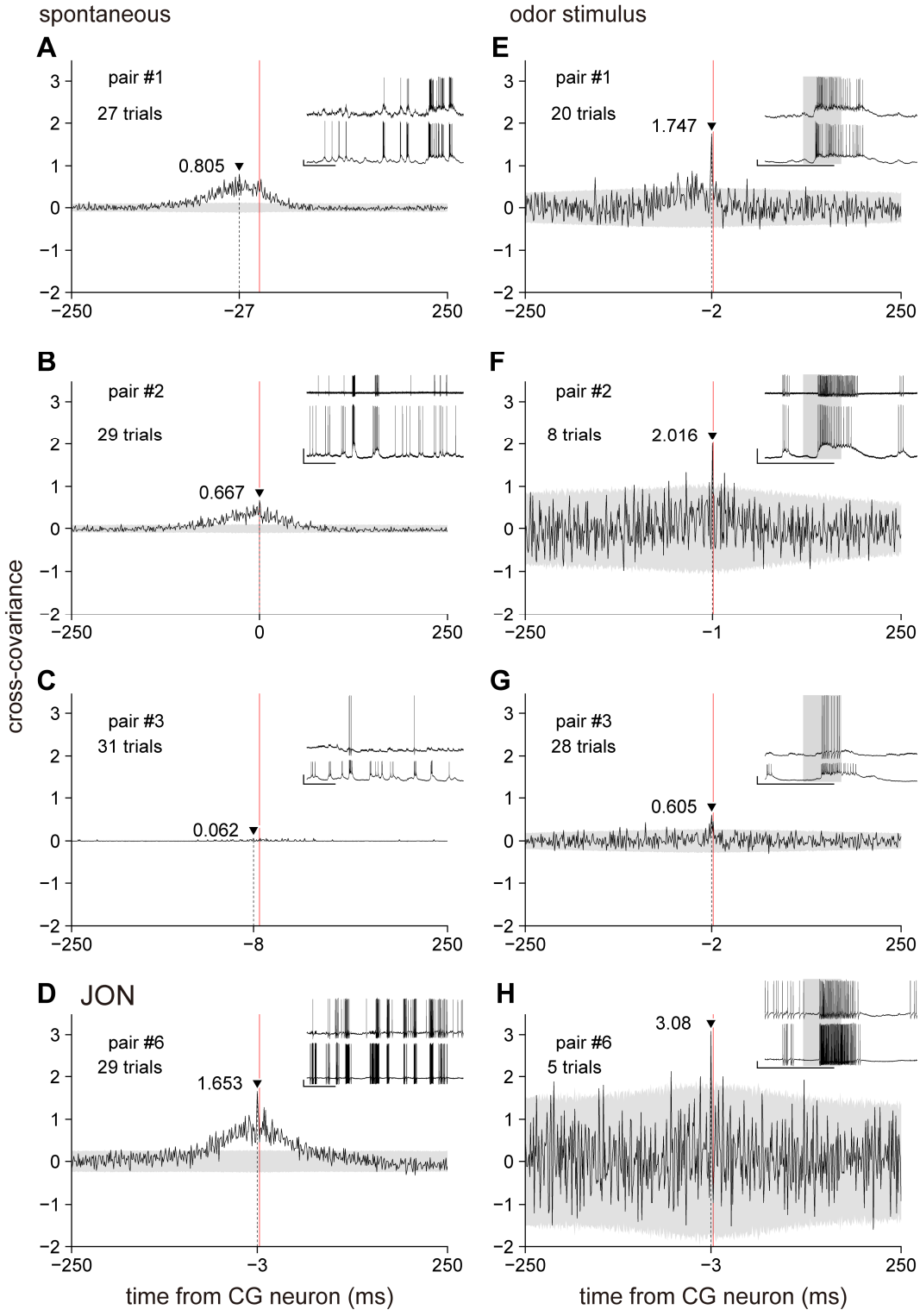



**Figure 18.** Cross-covariograms not divided by the geometric mean firing rates of neurons. **A–C,E–G:** ML tip ON. **D,H:** Junction output neuron (JON). Covariograms are shown in the same way as in Fig. 17. The higher the firing rate of neurons is, the larger cross-covariance of spike activities is.

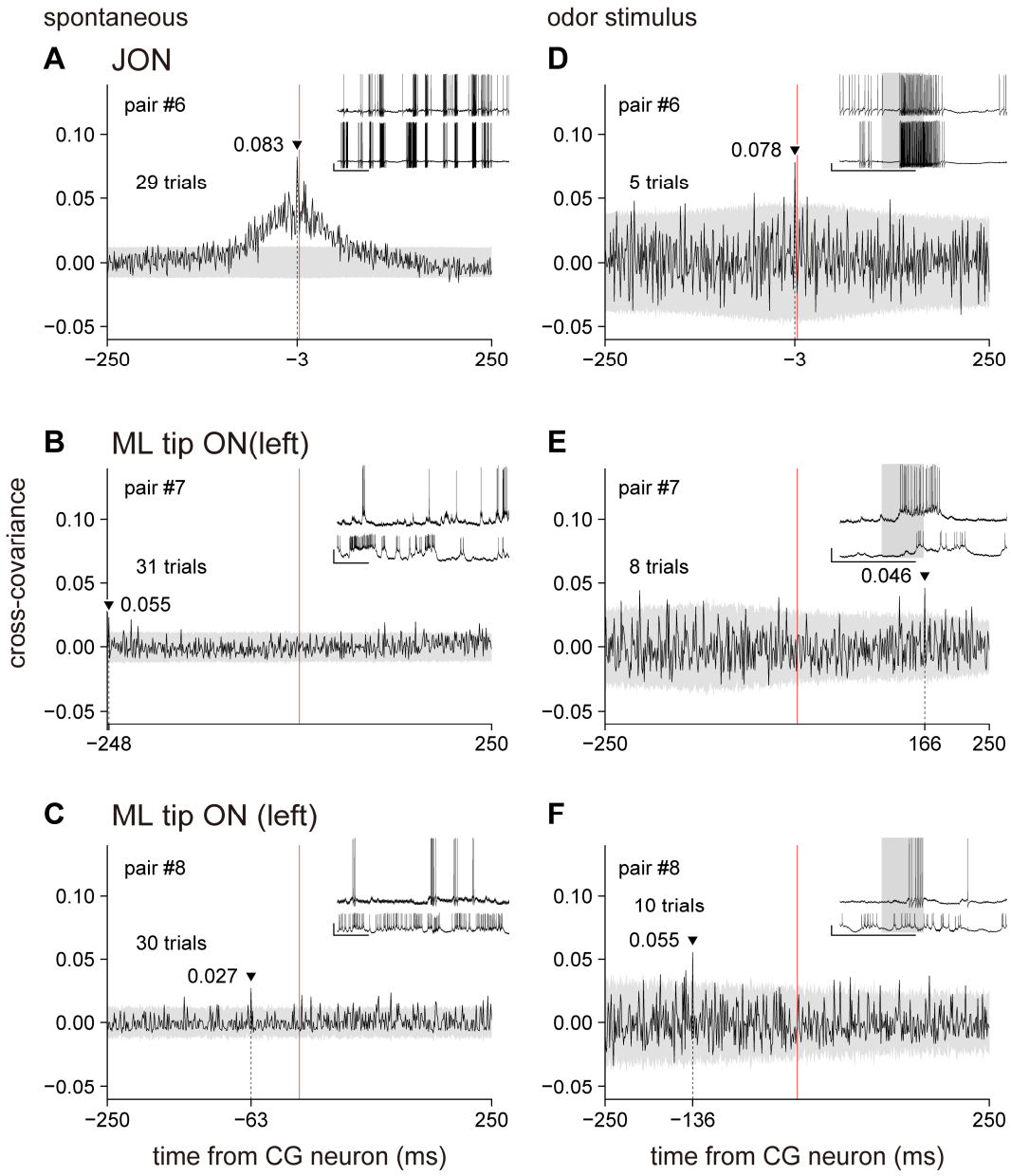



**Figure 19.** Cross-covariograms between type 1 CG and other MBONs. **A,D:** JON. **B,C,E,F:** ML tip ON in the left hemisphere. Covariograms are shown in the same way as in Fig. 17.

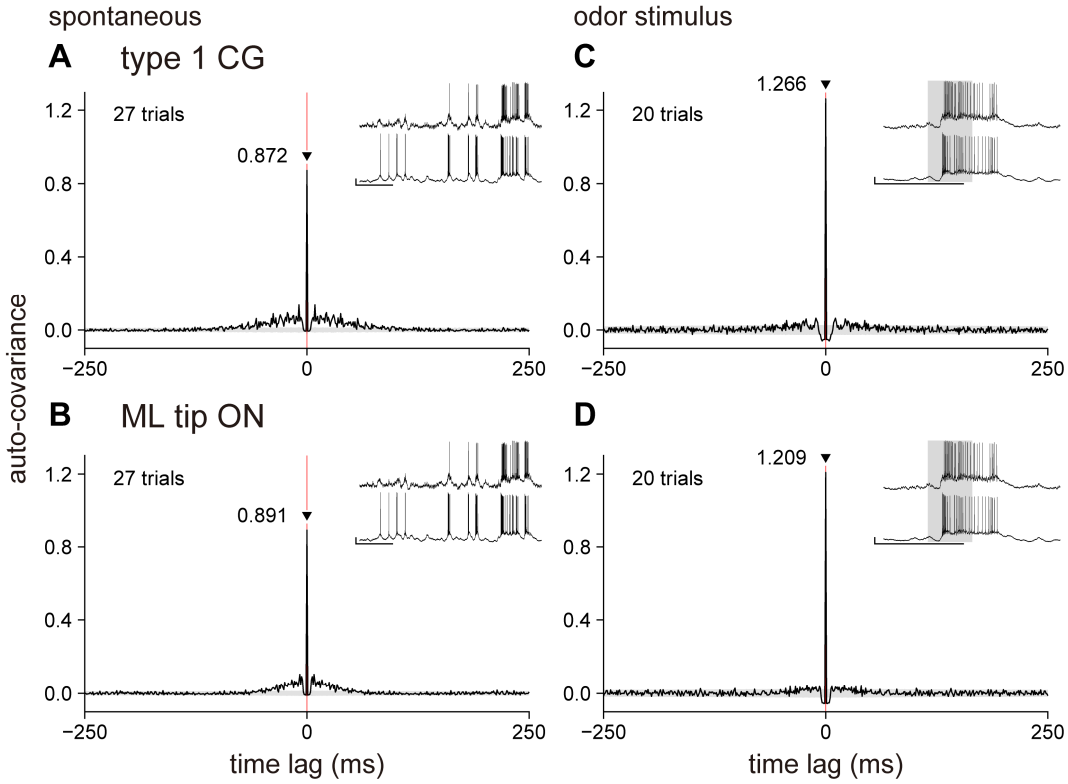



**Figure 20.** Typical examples of auto-covariograms obtained from the spike activities of type 1 CG (A,C) and ML tip ON (B,D). Covariograms are shown in the same way as in figure 17. The neurons belonged to pair #1. The auto-covariograms had an extremely sharp peak at time lag 0 typical of white noise. Auto-covariances were measured to all other paired-recorded neurons and showed similar results.

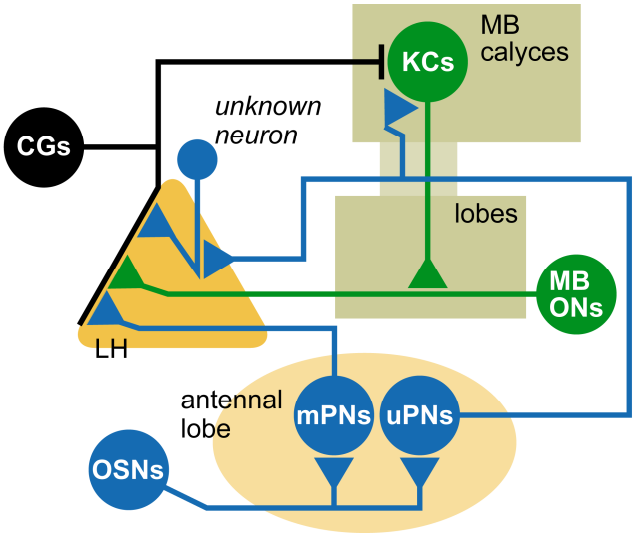



**Figure 21.** Possible in the cockroach pathways to account for a high covariance between the activities of CGs and the activities of MBONs during odor stimuli. Green pathway assumes synaptic connection from MBONs to CGs. In this case, the input source that produces a high covariance is KCs that make synaptic connection with MBONs. Alternatively, in blue pathway, it is assumed that MBONs have no synaptic connection with CGs and both neurons receive common synaptic input originated from (i) olfactory sensory neurons (OSNs) in the antennal lobe or (ii) uniglomerular PNs (uPNs) in case when some interneurons intervening between uniglomerular PNs and CGs (shown as unknown neuron in the diagram). In the blue pathway, different interneurons intervene between the common input source to CGs and MBONs and thus unlikely to account for a short (1–3ms) time range of cross-covariogram observed between the two neurons.

# General discussion

I succeeded in classifying four calycal giants (CGs) into four subtypes according to the results of my intracellular recording and staining (Chapter 1) and demonstrating that the mushroom body (MB) feedback circuits formed by CGs are intervened by MB output neurons (MBONs), which is unique to the cockroach MB circuit (Chapter 2). Because all CGs showed responses to all odor used in this study, functional segregation among CGs are not simple “processing of different odors” but should be more complicated.

## Arrangement of feedback loop

Results of paired intracellular recording in this study provide supporting evidence that a CG receive direct synaptic connections from some MBONs. The results confirm previous speculations that CGs, which are GABAergic and terminate in input region of the MB, might receive synapses from MBONs and thus serve as feedback neurons in the MB (Nishino and Mizunami, 1998; Yamazaki et al., 1998; Strausfeld and Li, 1999a). The arrangement of CGs differs from that of GABAegic feedback neurons of the MB of other insects, in which feedback neurons have dendrites in the lobes, where they receive synaptic connections with axon terminals of Kenyon cells (KCs), and they terminate in the calyces, where they make synapses with dendrites of KCs (locust: Papadopoulou et al., 2011; fly: Lin et al., 2014; honeybee: Grünewald, 1999a; b).

What is the possible functional meaning of the arrangement of feedback circuit unique to the cockroach MB? The arrangement would attribute to the reference level for adjusting the activities of KCs. In MB feedback circuits previously reported in other insects, an inhibitory neuron receives synaptic inputs from output sites of KCs as mentioned above (black neuron in Fig. 22) and thus the feedback is considered to inhibit the excessive activities of KCs and maintain the sparse representation of KCs (Gupta and Stopfer, 2011). In the MB feedback circuit of the cockroach, on the other hand, CGs inhibit the activities of KCs according with those of MBONs. Mizunami et al. (1998c) and Okada et al. (1999) reported movement-related activities of some of MBONs, demonstrating their contribution to behavioral control. Together with that MBONs project into neuropils surrounding the lateral horn (LH) in the lateral

protocerebrum, which are thought to participate in the formation of control signals for innately-induced behavior (Li and Strausfeld, 1997, 1999), CGs are likely to adjust the activities of KCs to the level more suitable for orientation behavior toward odor sources.

### Parallel pathways in the MB

Four CGs are classified into two subtypes, namely, type 1 class and type 2 class [nonspiking (NS), type 2a, and type 2b], according to their innervation patterns in the calyces, which well matches the calycal zonation formed by axon terminals of two populations of uniglomerular projection neurons (PNs): type 1 PNs and type 2 PNs. The results of this study also showed that distinction between the types extends to input sites of CGs, in other words, the dendrites of type 1 CG have more overlaps with the axonal branches of a medial lobe output neuron (MLON) than those of a vertical lobe output neuron (VLON) while the dendrites of NS CG have more overlaps with the axonal branches of a VLON than those of a MLON. Inhibition of a type 1 CG by current injection affected the MLON but that of NS CG did not, which matches the idea that type 1 CG and type 2 CGs form two parallel feedback pathways.

What are the possible functional roles of parallel feedback pathways? Type 1 PNs show more odor-specific activities than type 2 PNs and thus, are suitable for coding odor identity (Watanabe et al., 2017). Strong inhibition from type 1 CG (see the highest peak of firing rate during odor response in Fig. 12 in Chapter 1) may inhibit excessive activities of the KCs and help to improve odor identification and odor discrimination, which are critical for decision-making for behavioral response to the odor. In addition, as described in Chapter 1, a type 1 CG innervates the accessory calyx, which processes gustatory signals from mouth parts (Farris, 2008). It implies that a type 1 CG modulates inhibition level based on gustatory input. In this situation, parallel feedback pathways enable control of odor identify not interrupting processing of other aspects of odor stimuli.

I observed no inhibitory effect of type 1 CG on VLONs as discussed in Chapter 2. Future investigation of the plasticity of CGs and MBONs during olfactory learning will also be needed to clarify the validity of the hypothesis about two parallel feedback pathways in the MB.

## Conclusion

Roles of MB feedback circuits consisting of multiple inhibitory neurons appear not confined to maintain sparse activities of KCs but are related to parallel processing of different aspects of odor information such as odor identity and spatio-temporal distribution of odors. Since CGs are sufficiently large to endure long-time intracellular recordings, they will be useful for probing the dynamic functions of the higher olfactory center for olfactory learning and odor tracking behavior.

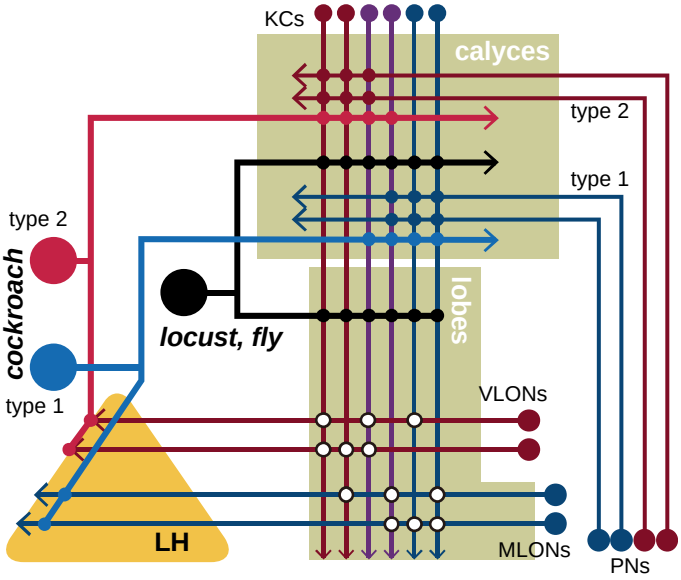



**Figure 22.** Mushroom body (MB) feedback circuits in insect brains. Schematic shows two types of MB feedback circuits at the same time in one hemisphere of the brain. Colors of Kenyon cells (KCs), projection neurons (PNs), and mushroom body output neurons (MBONs) corresponding with the cockroach circuits and should be disregarded when considering the circuits in other insects. In the locust and fly, a giant GABAergic neuron (black) feedback the activities of KC populations into input region of KCs. That inhibits excessive activities of KCs into the optimal level for odor representation. In the cockroach brain, on the other hand, giant GABAergic neurons (light blue/red) receive the activities of MBONs in the LH and give them back into input sites of KCs. That makes the level of MB activities optimal for orientation behavior toward odor sources.

## Acknowledgments

I am deeply grateful to Prof. Makoto Mizunami for his helpful discussion, technical advice, encouragement and criticism in course of my study. I am also grateful Prof. Toshiya Matsushima and Prof. Hiroto Ogawa for their constructive comments on my dissertation. I would like to thank Dr. Hiroshi Nishino for his technical advice and thank Dr. Hidehiro Watanabe at Fukuoka University for providing immunolabeling images in Chapter 1. I also would like to thank the member of the Laboratory of Animal Behavior and System Control. Finally, this work was partly supported by the Sasakawa Scientific Research Grant from The Japan Science Society.

## Literature cited


Assisi C, Stopfer M, Laurent G, Bazhenov M. 2007. Adaptive regulation of sparseness by feedforward inhibition. Nat Neurosci 10:1176–84.

Bair W, Zohary E, Newsome WT. 2001. Correlated firing in macaque visual area MT: time scales and relationship to behavior. J Neurosci 21:1676–1697.

Balling, A., Technau, G.M., Heisenberg, M., 1987. Are the structural changes in adult *Drosophila* mushroom bodies memory traces? Studies on biochemical learning mutants. J Neurogen. 4:65–73.

Baumann O, Kühnel D, Dames P, Walz B. 2004. Dopaminergic and serotonergic innervation of cockroach salivary glands: distribution and morphology of synapses and release sites. J Exp Biol 207:2565–2575.

Bicker G, Schäfer S, Kingan TG. 1985. Mushroom body feedback interneurones in the honeybee show GABA-like immunoreactivity. Brain Res 360:394–397.

Blankenburg S, Balfanz S, Hayashi Y, Shigenobu S, Miura T, Baumann O, Baumann A, Blenau W. 2015. Cockroach $GABA_B$ receptor subtypes: molecular characterization, pharmacological properties and tissue distribution. Neuropharmacology 88:134–144.

Boeckh J, Ernst KD. 1987. Contribution of single unit analysis in insects to an understanding of olfactory function. J Comp Physiol A 161:549–565.

Boitard C, Devaud JM, Isabel G, Giurfa M. 2015. GABAergic feedback signaling into the calyces of the mushroom bodies enables olfactory reversal learning in honey bees. Front Behav Neurosci 9:198.

Brody CD. 1999. Correlations without synchrony. Neural Comput 11:1537–1551.

Burrows M, Siegler MVS. 1978. Graded synaptic transmission between local interneurones and motor neurones in the metathoracic ganglion of the locust. J Physiol 285:231–255.

Demmer H, Kloppenburg P. 2009. Intrinsic membrane properties and inhibitory synaptic input of Kenyon cells as mechanisms for sparse coding? J Neurophysiol 102:1538–1550.

Distler P. 1990. GABA-immunohistochemistry as a label for identifying types of local interneurons and their synaptic contacts in the antennal lobes of the American cockroach. Histochemistry 93:617–626.

Distler PG, Cruber C, Boeckh J. 1998. Synaptic connections between GABA-immunoreactive neurons and uniglomerular projection neurons within the antennal lobe of the cockroach, *Periplaneta americana*. Synapse 29:1–13.

Ehmer B, Gronenberg W. 2002. Segregation of visual input to the mushroom bodies in the honeybee (*Apis mellifera*). J Comp Neurol 451:362–373.

Ehmer B, Gronenberg W. 2004. Mushroom body volumes and visual interneurons in ants: comparison between sexes and castes. J Comp Neurol 469:198–213.

Ernst KD, Boeckh J. 1983. A neuroanatomical study on the organization of the central antennal pathways in insects. III. Neuroanatomical characterization of physiologically defined response types of deutocerebral neurons in *Periplaneta americana*. Cell Tissue Res 229:1–22.

Farris SM. 2005. Evolution of insect mushroom bodies: old clues, new insights. Arthropod Struct Dev 34:211–234.

Farris SM. 2008. Tritocerebral tract input to the insect mushroom bodies. Arthropod Struct Dev 37:492–503.

Farris SM, Strausfeld NJ. 2001. Development of laminar organization in the mushroom bodies of the cockroach: Kenyon cell proliferation, outgrowth, and maturation. J Comp Neurol 439:331–351.

Farris SM, Strausfeld NJ. 2003. A unique mushroom body substructure common to basal cockroaches and to termites. J Comp Neurol 456:305–320.

Froese A, Szyszka P, Menzel R. 2014. Effect of GABAergic inhibition on odorant concentration coding in mushroom body intrinsic neurons of the honeybee. J Comp Physiol A 200:183–195.

Fusca D, Husch A, Baumann A, Kloppenburg P. 2013. Choline acetyltransferase-like immunoreactivity in a physiologically distinct subtype of olfactory nonspiking local interneurons in the cockroach (*Periplaneta americana*). J Comp Neurol 521:3556-3569.

Galizia CG, Rössler W. 2010. Parallel olfactory systems in insects: anatomy and function. Annu Rev Entomol 55:399–420.

Ganeshina O, Menzel R. 2001. GABA-immunoreactive neurons in the mushroom bodies of the honeybee: an electron microscopic study. J Comp Neurol 437:335–349.

Groh C, Rössler W. 2011. Comparison of microglomerular structures in the mushroom body calyx of neopteran insects. Arthropod Struct Dev 40:358–367.

Gronenberg W. 2001. Subdivisions of hymenopteran mushroom body calyces by their afferent supply. J Comp Neurol 435:474–489.

Grünewald B. 1999a. Morphology of feedback neurons in the mushroom body of the honeybee, *Apis mellifera*. J Comp Neurol 404:114–126.

Grünewald B. 1999b. Physiological properties and response modulations of mushroom body feedback neurons during olfactory learning in the honeybee, *Apis mellifera*. J Comp Physiol A 185:565–576.

Gupta N, Stopfer M. 2011. Insect olfactory coding and memory at multiple timescales. Curr Opin Neurobiol 21:768–773.

Gupta N, Stopfer M. 2012. Functional analysis of a higher olfactory center, the lateral horn. J Neurosci 32:8138–8148.

Gupta N, Stopfer M. 2014. A temporal channel for information in sparse sensory coding. Curr Biol 24:2247–2256.

Haehnel M, Menzel R. 2010. Sensory representation and learning-related plasticity in mushroom body extrinsic feedback neurons of the protocerebral tract. Front Syst Neurosci 4:161.

Hildebrand JG, Shepherd GM. 1997. Mechanisms of olfactory discrimination: converging evidence for common principles across phyla. Annu Rev Neurosci 20:595–631.

Homberg U, Kingan TG, Hildebrand JG. 1987. Immunocytochemistry of GABA in the brain and suboesophageal ganglion of *Manduca sexta*. Cell Tissue Res 248:1–24.

Huang J, Zhang W, Qiao W, Hu A, Wang Z. 2010. Functional connectivity and selective odor responses of excitatory local interneurons in *Drosophila* antennal lobe. Neuron 67:1021–1033.

Huston SJ, Stopfer M, Cassenaer S, Aldworth ZN, Laurent G. 2015. Neural encoding of odors during active sampling and in turbulent plumes. Neuron 88:403–418.

Ito I, Ong RCY, Raman B, Stopfer M. 2008. Sparse odor representation and olfactory learning. Nat Neurosci 11:1177–1184.

Ito K, Shinomiya K, Ito M, Armstrong JD, Boyan G, Hartenstein V, Harzsch S, Heisenberg M, Homberg U, Jenett A, Keshishian H, Restifo LL, Rössler W, Simpson JH, Strausfeld NJ, Strauss R, Vosshall LB. 2014. A systematic nomenclature for the insect brain. Neuron 81:755–765.

Jortner RA, Farivar SS, Laurent G. 2007. A simple connectivity scheme for sparse coding in an olfactory system. J Neurosci 27:1659–1669.

Kay LM, Stopfer M. 2006. Information processing in the olfactory systems of insects and vertebrates. Semin Cell Dev Biol 17:433–442.

Kee T, Sanda P, Gupta N, Stopfer M, Bazhenov M. 2015. Feed-forward versus feedback inhibition in a basic olfactory circuit. PLoS Comput Biol 11:e1004531.

Kinoshita M, Shimohigasshi M, Tominaga Y, Arikawa K, Homberg U. 2015. Topographically distinct visual and olfactory inputs to the mushroom body in the swallowtail butterfly, *Papilio xuthus*. J Comp Neurol 523:162–182.

Leitch B, Laurent G. 1996. GABAergic synapses in the antennal lobe and mushroom body of the locust olfactory system. J Comp Neurol 372:487–514.

Li Y, Strausfeld NJ. 1997. Morphology and sensory modality of mushroom body extrinsic neurons in the brain of the cockroach, *Periplaneta americana*. J Comp Neurol 387:631–650.

Li Y, Strausfeld NJ. 1999. Multimodal efferent and recurrent neurons in the medial lobes of cockroach mushroom bodies. J Comp Neurol 409:647–663.

Lin AC, Bygrave AM, de Calignon A, Lee T, Miesenböck G. 2014. Sparse, decorrelated odor coding in the mushroom body enhances learned odor discrimination. Nat Neurosci 17:559–568.

Liu X, Davis RL. 2009. The GABAergic anterior paired lateral neuron suppresses and is suppressed by olfactory learning. Nat Neurosci 12:53–59.

Malun D, Waldow U, Kraus D, Boeckh J. 1993. Connections between the deutocerebrum and the protocerebrum, and neuroanatomy of several classes of deutocerebral projection neurons in the brain of male *Periplaneta americana*. J Comp Neurol 329:143–62.

Martin JP, Beyerlein A, Dacks AM, Reisenman CE, Riffel JA, Lei H, Hildebrand JG. 2011. The neurobiology of insect olfaction: sensory processing in a comparative context. Prog Neurobiol 95:427–447.

Menzel R, Galizia G, Müller D, Szyszka P. 2005. Odor coding in projection neurons of the honeybee brain. Chem Senses. 30:i301–i302.

Mizunami M, Yamashita S, Tateda H. 1987. Calcium-dependent action potentials in the second-order neurones of cockroach ocelli. J Exp Biol 130:259–274.

Mizunami M, Iwasaki M, Okada R, Nishikawa M. 1998a, Topography of modular subunits in the mushroom bodies of the cockroach. J Comp Neurol 399:153–161.

Mizunami M, Iwasaki M, Okada R, Nishikawa M. 1998b. Topography of four classes of Kenyon cells in the mushroom bodies of the cockroach. J Comp Neurol 399:162–175.

Mizunami M, Okada R, Li Y, Strausfeld N.J. 1998c. Mushroom bodies of the cockroach: the activity and identities of neurons recorded in freely moving animals. J Comp Neurol 402: 501–519.

Mizunami M, Weibrecht JM, Strausfeld NJ. 1998d. Mushroom bodies of the cockroach: their participation in place memory. J Comp Neurol 402: 520–537.

Neder R. 1959. Allometrisches Wachstum von Hirnteilen bei drei verschiede grossen Schabenarten. Zool Jahrb Abt Anat 77:411–464.

Nishikawa M, Nishino H, Mizunami M, Yokohari F. 1998. Function-specific distribution patterns of axon terminals of input neurons in the calyces of the mushroom body of the cockroach, *Periplaneta americana*. Neurosci Lett 245:33–36.

Nishino H, Mizunami M. 1998. Giant input neurons of the mushroom body: intracellular recording and staining in the cockroach. Neurosci Lett 246:57–60.

Nishino H, Yamashita S, Yamazaki Y, Nishikawa M, Yokohari F, Mizunami M. 2003. Projection neurons originating from thermo- and hygrosensory glomeruli in the antennal lobe of the cockroach. J Comp Neurol 455:40–55.

Nishino H, Iwasaki M, Yasuyama K, Hongo H, Watanabe H, Mizunami M. 2012. Visual and olfactory input segregation in the mushroom body calyces in a basal neopteran, the American cockroach. Arthropod Struct Dev 41:3–16.

Okada R, Ikeda J, Mizunami M. 1999. Sensory responses and movement-related activities in extrinsic neurons of the cockroach mushroom bodies. J Comp Physiol A 185:115–129.

Okada R, Sakura M, Mizunami M. 2003. Distribution of dendrites of descending neurons and its implications for the basic organization of the cockroach brain. J Comp Neurol 458:158–174.

Olsen SR, Bhandawat V, Wilson R. 2007. Excitatory interactions between olfactory processing channels in the *Drosophila* antennal lobe. Neuron 54: 89–103.

Olsen SR, Wilson RI. 2008. Lateral presynaptic inhibition mediates gain control in an olfactory circuit. Nature 452:956–960.

Olshausen BA, Field DJ. 2004. Sparse coding of sensory inputs. Curr Opin Neurobiol 14:481–487.

Papadopoulou M, Cassenaer S, Nowotny T, Laurent G. 2011. Normalization for sparse encoding of odors by a wide-field interneuron. Science 332:721–725.

Perez-Orive J, Mazor O, Turner GC, Cassenaer S, Wilson RI, Laurent G. 2002. Oscillations and sparsening of odor representations in the mushroom body. Science 297:359–365.

Perez-Orive J, Bazhenov M, Laurent G. 2004. Intrinsic and circuit properties favor coincidence detection for decoding oscillatory input. J Neuroci 24:6037–6047.

Pitman JL, Huetteroth W, Burke CJ, Krashes MJ, Lai SL, Lee T, Waddell S. 2011. A pair of inhibitory neurons are required to sustain labile memory in the *Drosophila* mushroom body. Curr Biol 21:855–861.

Poo C., Isaacson JS. 2009. Odor representations in olfactory cortex: “sparse coding”, global inhibition, and oscillations. Neuron 62:850–861.

Sakura M., Okada R., Mizunami M. 2002. Olfactory discrimination of structurally similar alcohols by cockroaches. J Comp Physiol A 188:787–797.

Sattelle DB, Harrison JB, Chen HH, Bai D, Takeda M. 2000. Immunocytochemical localization of putative gamma-aminobutyric acid receptor subunits in the head ganglia of *Periplaneta americana* using an anti-RDL C-terminal antibody. Neurosci Lett 289:197–200.

Shang Y, Claridge-Chang A, Sjulson L, Pyaert M, Miesenböck G. 2007. Excitatory local circuits and their implications for olfactory processing in the fly antennal lobe. Cell 128:601–612.

Strausfeld NJ, Li Y. 1999a. Organization of olfactory and multimodal afferent neurons supplying the calyx and pedunculus of the cockroach mushroom bodies. J Comp Neurol 409:603–625.

Strausfeld NJ, Li Y. 1999b. Representation of the calyces in the medial and vertical lobes of cockroach mushroom bodies. J Comp Neurol 409:626–646.

Strausfeld NJ, Sinakevitch I, Brown SM, Farris SM. 2009. Ground plan of the insect mushroom body: Functional and evolutionary implications. J Comp Neurol 513:265–291.

Szyszka P, Ditzen M, Galkin A, Galizia CG, Menzel R. 2005. Sparsening and temporal sharpening of olfactory representations in the honeybee mushroom bodies. J Neurophysiol 94:3303–3313.

Tanaka NK, Tanimoto H, Ito K. 2008. Neuronal assemblies of the *Drosophila* mushroom body. J Comp Neurol 508:711–755.

Tobler I. 1983. Effect of forced locomotion on the rest-activity cycle of the cockroach. Behav Brain Res 8:351-260.

Turner GC, Bazhenov M, Laurent G. 2008. Olfactory representations by *Drosophila* mushroom body neurons. J Neurophysiol. 99:734–746.

Watanabe H, Mizunami M. 2007. Pavlov's cockroach: classical conditioning of salivation in an insect. PLoS One 2:e529.

Watanabe H, Nishino H, Nishikawa M, Mizunami M, Yokohari F. 2010. Complete mapping of glomeruli based on sensory nerve branching pattern in the primary olfactory center of the cockroach *Periplaneta americana*. J Comp Neurol 518:3907–3930.

Watanabe H., Ai H., Yokohari F. 2012. Spatio-temporal activity patterns of odor-induced synchronized potentials revealed by voltage-sensitive dye imaging and intracellular recording in the antennal lobe of the cockroach. Front Neurosci 6:55.

Watanabe H, Shimohigashi M, Yokohari F. 2014. Serotonin-immunoreactive sensory neurons in the antenna of the cockroach *Periplaneta americana*. J Comp Neurol 522:414–434.

Watanabe H, Nishino H, Mizunami M, Yokohari F. 2017. Two parallel olfactory pathways for processing general odors in a cockroach. Front Neural Circuits 11:1–20.

Wei H, el Jundi B, Homberg U, Stengl M. 2010. Implementation of pigment-dispersing factor-immunoreactive neurons in a standardized atlas of the brain of the cockroach *Leucophaea maderae*. J Comp Neurol 518:4113–4133.

Weiss MJ. 1974. Neuronal connections and the function of the corpora pedunculata of the American cockroach, *Periplaneta americana*. J Morphol 142:21–69.

Wilson RI, Turner GC, Laurent G. 2004. Transformation of olfactory representations in the *Drosophila* antennal lobe. Science 303:366–370.

Wilson RI, Laurent G. 2005. Role of GABAergic inhibition in shaping odor-evoked spatiotemporal patterns in the *Drosophila* antennal lobe. J Neurosci 25:9069–9079.

Wilson RI, Mainen ZF. 2006. Early events in olfactory processing. Ann Rev Neurosci 29:163–201.

Witthöft, W., 1967. Absolute Anzahl und Verteilung der Zellen im Hirn der Honigbiene. Zeitschrift für Morphologie der Tiere 61:160–164.

Wu Y, Ren Q, Li H, Guo A. 2012. The GABAergic anterior paired lateral neurons facilitate olfactory reversal learning in *Drosophila*. Learn Mem 19:478–486.

Yamazaki Y, Nishikawa M, Mizunami M. 1998. Three classes of GABA-like immunoreactive neurons in the mushroom body of the cockroach. Brain Res 788:80–86.

Yasuyama K, Meinertzhagen IA, Schürmann FW. 2002. Synaptic organization of the mushroom body calyx in *Drosophila melanogaster*. J Comp Neurol 445:211–226.

## License Details

This Agreement between Miss. Naomi Takahashi ("You") and John Wiley and Sons ("John Wiley and Sons") consists of your license details and the terms and conditions provided by John Wiley and Sons and Copyright Clearance Center.

Print Copy

| | |
|---|---|
| License Number | 4262361023643 |
| License date | Jan 05, 2018 |
| Licensed Content Publisher | John Wiley and Sons |
| Licensed Content Publication | Journal of Comparative Neurology |
| Licensed Content Title | Complete identification of four giant interneurons supplying mushroom body calyces in the cockroach Periplaneta americana |
| Licensed Content Author | Naomi Takahashi,Ko Katoh,Hidehiro Watanabe,Yuta Nakayama,Masazumi Iwasaki,Makoto Mizunami,Hiroshi Nishino |
| Licensed Content Date | Sep 27, 2016 |
| Licensed Content Pages | 27 |
| Type of Use | Dissertation/Thesis |
| Requestor type | Author of this Wiley article |
| Format | Electronic |
| Portion | Full article |
| Will you be translating? | No |
| Title of your thesis / dissertation | Analysis of four giant inhibitory neurons projecting to the input sites of mushroom body in the cockroach brain |
| Expected completion date | Mar 2018 |
| Expected size (number of pages) | 101 |
| Attachment | |
| Requestor Location | Miss. Naomi Takahashi<br>Room#1010, Bldg.#5, Graduate School<br>of Life Science, Hokkaido University,<br>Kita 10, Nishi 8, Kita-ku<br>Sapporo, Hokkaido 060-0810<br>Japan<br>Attn: Miss. Naomi Takahashi |
| Publisher Tax ID | EU826007151 |
| Billing Type | Invoice |
| Billing address | Miss. Naomi Takahashi<br>Room#1010, Bldg.#5, Graduate School<br>of Life Science, Hokkaido University,<br>Kita 10, Nishi 8, Kita-ku<br>Sapporo, Japan 060-0810<br>Attn: Miss. Naomi Takahashi |
| Total | **0 JPY** |